Complex Coacervates and Microgels for Emulsions

Robust, Responsive, Reversible

Hélène Monteillet

Thesis committee

Promotor
Prof. Dr F. A. M. Leermakers
Personal chair, Physical Chemistry and Soft Matter
Wageningen University

Co-promotors
Dr J. M. Kleijn
Assistant professor, Physical Chemistry and Soft Matter
Wageningen University

Dr J. Sprakel
Assistant professor, Physical Chemistry and Soft Matter
Wageningen University

Other members
Prof. Dr M. H. M. Eppink, Wageningen University
Dr M. H. G. Duits, University of Twente
Dr D. J. Kraft, Leiden University
Prof. Dr C. G. P. H. Schroën, Wageningen University

Complex Coacervates and Microgels for Emulsions

Robust, Responsive, Reversible

Hélène Monteillet

To my husband
To my parents

Contents

Chapter 1

Introduction

1.1 Motivation

Extractions, processes of removing a substance or an impurity from a mixture or a solution, are among the most prevalent unit operations in industrial processes.[1,2] They are found in a wide variety of industrial situations, ranging from the separation of crude oils into fuels, lubricants and chemical building blocks, to the separation of active pharmaceutical ingredients from fermentation broths.[3] Amidst the variety of extraction methods, liquid-liquid extractions are among the most common.[4] In liquid-liquid extractions, a substance of interest is retrieved, or removed, from a solution by extracting it into a second immiscible phase. This is often done using organic solvents; however, due to their toxicity, volatility and flammability, their use is often undesired. Moreover, the high purity of the solvents, required to achieve good extractions, increases the costs of processing.[5] Therefore, designing sustainable processes for extracting valuable components from complex mixtures has become a major challenge of chemical engineering.

In recent years, ionic liquids (ILs) have been explored as potential candidates for the replacement of organic solvents in extraction processes;[6] they have shown promising performance in liquid phase extractions, even those of delicate and easily degradable biomolecules.[7–19] Ionic liquids are typically defined as salts that exhibit a melting point below 100 °C; when the melting point is close to or below room temperature, they are referred to as room temperature ILs (RTILs).[20] For ionic systems of small ions with symmetric interactions, such as sodium chloride, electrostatic interactions are strong as the ions can approach closely when packing in a regular and crystalline structure. This leads to relatively high melting temperatures. By contrast, ionic liquids are typically composed of bulky side groups with asymmetric interactions, preventing close approach between the charge centres, thereby weakening cohesive Coulomb interactions. In addition, the strong asymmetry size between the anion and cation causes geometric frustration in reaching a crystalline state. This results in ionic substances with melting points close to, or below room temperature.

ILs have interesting properties from a processability perspective, such as excellent thermal stability,[22] low vapor pressure[23] and very low flammability.[24] Additionally, ionic liquids have good solvation capabilities, which can be tailored to the extraction process of interest by adjusting the anion and cation chemistry. A typical selection of IL ions is shown in Figure 1.1; the ion pair together with the length of the aliphatic substituent groups allow precise tuning of the physical properties of these liquids such as their density, water solubility and solvation properties,[25–28] and even the incorporation of functionality such as paramagnetism.[29,30]
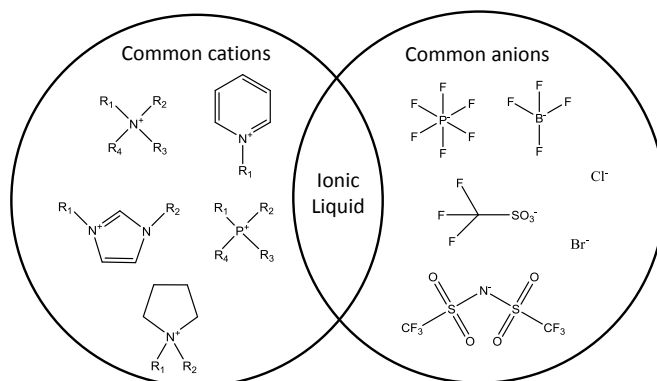
Figure 1.1: Common cations and anions of ionic liquids and room temperature ionic liquids. Reprinted from [21] with permission from The Royal Society of Chemistry.

It is this combination of features that makes ionic liquids interesting candidates to replace conventional organic solvents in a variety of industrial processes, overcoming environmental and safety issues.

One of the major drawbacks of ILs lies in their high viscosity, typically several orders of magnitude higher than that of water and conventional solvents, which slows down mass transport and increases energy expenditure during pumping and mixing. [31,32] When using ILs in a liquid phase extraction, the inherently low interfacial tension between the IL and water requires long incubation times to achieve a macroscopic phase separation between the water phase and the ionic liquid phase. [33] Moreover, commonly encountered water-immiscible ion pairs include fluorine moieties in the anion that are unstable towards hydrolysis. [34] Thus, despite their great promise in eradicating hazardous solvents in extraction processes, new strategies for the efficient application of these liquids are required to further increase their practical use.

One particular approach to overcome several of the mentioned drawbacks is the use of IL-in-water emulsions, where small droplets of ionic liquid are dispersed within a continuous water phase. The viscosity of emulsions is typically, for volume fractions of droplets below 0.40, only a few times that of water and they offer a large interfacial area, which enhances mass transport. Yet, the use of such emulsions in extractions imposes some requirements:

1. The emulsion should be stable at operating temperatures to enable the extraction to reach completion;

2. The emulsion must be broken to obtain the product; preferably, the emulsion

can be destabilized on-demand to facilitate this process, without the use of
co-solvents;

3. The stabilizer used to prepare the emulsion should be re-usable to increase
   the sustainability of the process.

Ideally, a strategy to formulate emulsions, which meet these requirements, should
be applicable to a wide variety of ILs and should not interact in a negative way
with the substance to be extracted; this is especially important for the extraction
of delicate biomolecules such as proteins and nucleic acids. So far, only few reports
have been published about the stabilization of IL-in-water emulsions [35–40] and
it seems that none of the presented strategies satisfies the requirements outlined
above. In this thesis we aim to explore new ways to formulate IL emulsions and
investigate their applicability for sustainable liquid phase extractions.

1.2   Emulsion stability

It is common wisdom that oil and water do not mix. However, oils can be dispersed
into a continuous water phase in the form of small micrometer-sized droplets. The
formation of these droplets requires the input of a significant amount of mechanical
energy, for example through vigorous stirring; this is due to the cost associated
with the creation of additional interface between oil and water. This energy cost is
characterized by the interfacial tension γ, which gives the free energy cost per unit
interfacial area. For common aliphatic oils the interfacial tension against water
is around 50 mN/m. However, for ionic liquids, due to the ionic nature of these
liquids, interfacial tensions against water are significantly lower, typically around
10 mN/m or below.

   As demixed systems of two immiscible fluids will tend to minimize their in-
terfacial area, emulsions are inherently thermodynamically unstable; as a result,
their characteristics may evolve over time. [41] Destabilization of any emulsion may
occur by a variety of mechanisms. While gravitational sedimentation or creaming,
and droplet aggregation may lead to spatial inhomogeneity in an emulsion, here we
consider only mechanisms that lead to a coarsening of the droplet population and
ultimately the demixing into two macroscopic phases.

   Ostwald ripening occurs due to the pressure difference between droplets of dif-
ferent sizes. [42,43] As a result of interfacial curvature, the phase inside a droplet will
exhibit an excess pressure with respect to the continuous phase. This is expressed
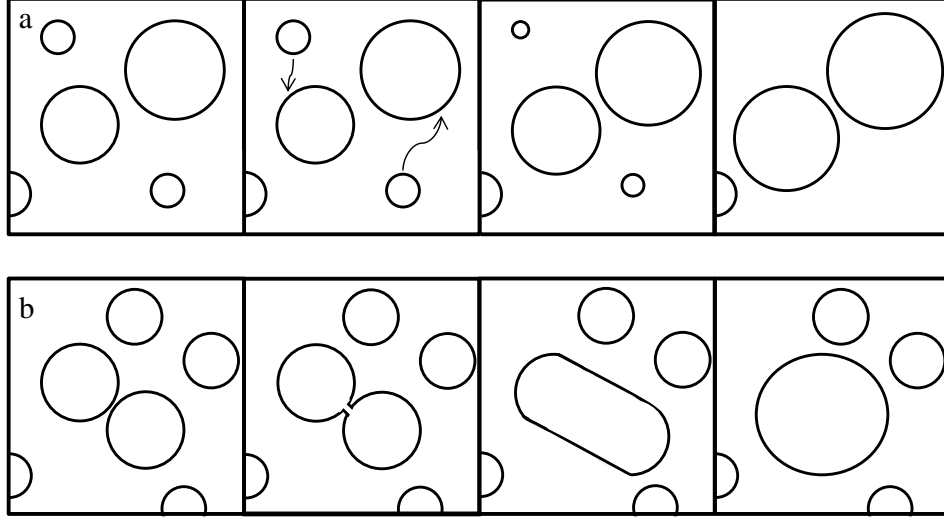
Figure 1.2: Schematics of the two main mechanisms of emulsion coarsening: (a) Ostwald ripening, (b) coalescence. In the Ostwald ripening process, the large droplets grow at the expense of the smaller ones, as indicated by the arrows. In the coalescence process, the thin film of fluid that separates two individual droplets drains and ruptures; the resulting neck grows in time and the two droplets merge.

by the Laplace pressure, which for spherical droplets of radius R is given by:

$$\Delta P = \frac{2\gamma}{R} \tag{1.1}$$

As the Laplace pressure is higher in smaller droplets, over time matter will migrate from small droplets to large droplets to equilibrate these pressure differences (Figure 1.2a). The rate at which this disproportionation occurs depends on the difference in Laplace pressure and the solubility of the oil in the water phase, which governs the mass transfer kinetics. For ionic liquids, the water solubility, and hence the rate of Ostwald ripening, can be tuned by the structure of the ions. Indeed, this phenomenon can in principle be slowed down by choosing ionic liquids with a large miscibility gap with water; nevertheless, ionic liquids are inherently soluble in water to some extent and typically coarsen rapidly. [44] Preventing this disproportionation is one of the major challenges in this field. One approach is to dissolve a substance in the ionic liquid that increases its osmotic pressure, which reduces partitioning of the ions into the aqueous phase. [45,46] A second approach consists of adsorbing at the interface surface active species, which lower the surface tension and the resulting Laplace pressure, and ideally solidify the interface, thereby

5

providing a mechanical resistance to droplet shrinking. [47]

Even when Ostwald ripening is completely suppressed, droplet coarsening may still occur by means of coalescence; [48–50] two droplets in close proximity merge when the thin liquid film of continuous phase that separates them ruptures (Figure 1.2b). The minimal pressure required to press two droplets together before film rupture may occur, the so-called critical disjoining pressure, depends strongly on the nature of the interfaces, the type of stabilizers and their concentration. [51] When this thermodynamic stability threshold is exceeded, kinetic effects come into play. The rupture of the thin film requires draining the fluid it contains, the rate of which depends strongly on the viscosity, or viscoelasticity, of the continuous phase, and the nucleation of a liquid bridge to connect the two droplets. Preventing coalescence can be achieved through the suitable choice of stabilizer, [52–54] and if necessary, the addition of a thickener to the continuous phase to slow down thin film drainage.

1.2.1   Stabilizers

Stabilizers serve to prolong the lifetime of an emulsion. While oil and vinegar separate into two macroscopic phases within seconds after mixing, the addition of a surface-active substance, such as egg yolk, allows the formation of an emulsion that can remain stable for months or years. Typically, stabilizers for emulsions are surfactants. These amphiphilic molecules are composed of distinct hydrophilic and hydrophobic segments, which therefore adsorb strongly at oil-water interfaces and can strongly reduce the oil-water interfacial tension. Owing to their molecular dimensions, surfactants show rapid diffusion-governed spontaneous adsorption at liquid interfaces. Once adsorbed at the interface, they provide steric and/or electrostatic repulsion between two droplets in close proximity, thereby effectively preventing coalescence. However, as their adsorption energy is typically on the order of the thermal energy, they are in dynamic equilibrium with the surfactants in solution. As a result, when a droplet shrinks, the excess adsorbed surfactant will re-enter the continuous phase. Thus, Ostwald ripening cannot be effectively prevented by surfactants.

Solid colloidal particles may also be used to stabilize liquid droplets; these emulsions are known as Pickering emulsions. [55,56] A wide variety of colloids has been shown to effectively stabilize liquid interfaces, with particle sizes ranging from few nanometers up to tens of micrometers, and of varying chemistry, such as proteins, [57] clays, [58] polymer lattices [59] or metal oxides such as silica. [60] The adsorption of solid particles is governed by Young's law, which describes the contact
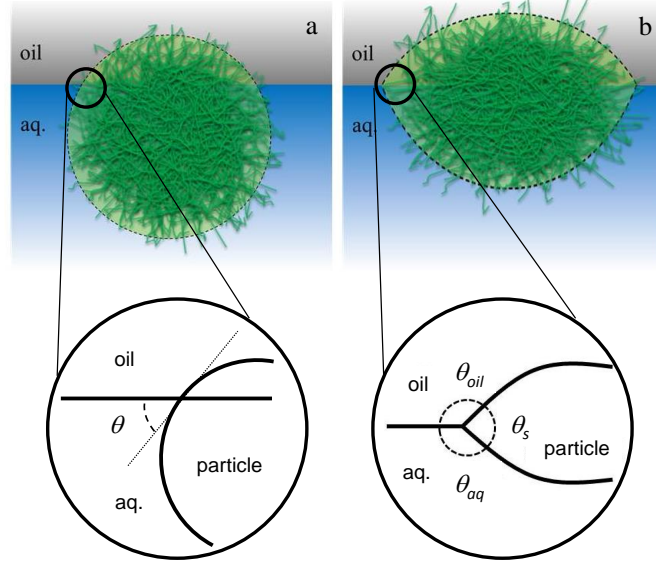
Figure 1.3: Illustration of (a) Young's law, (b) Neumann's law.

angle θ at the three phase contact line, determining the immersion depth of the colloid at the liquid-liquid interface (Figure 1.3a): [61,62]

$$\cos\theta = \frac{\gamma_{s-oil} - \gamma_{s-aq}}{\gamma_{oil-aq}} \qquad (1.2)$$

This law assumes that the tension at the contact line does not significantly deform the solid surface. When this assumption does not hold, for example when the particles themselves are deformable, such as for microgel colloids, a situation described by Neumann may be more appropriate (Figure 1.3b): [62,63]

$$\frac{\gamma_{s-oil}}{\sin\theta_{aq}} = \frac{\gamma_{s-aq}}{\sin\theta_{oil}} = \frac{\gamma_{aq-oil}}{\sin\theta_s} \qquad (1.3)$$

For particle adsorption to occur, partial wetting conditions $0 < \cos\theta < 180\,^\circ$, i.e. a finite immersion depth, are necessary. Even when these conditions are met, solid particles, especially of micrometer dimensions, do not adsorb spontaneously as there is a significant energy barrier to break the liquid film that separates the particles and the interface. Once the thin film is ruptured, equilibration of the particle at the interface may be very slow, for example due to the slow ageing of the contact line position. [64] Typically, the preparation of Pickering emulsions demands the input of a significant amount of mechanical energy to overcome these kinetic limitations. However, once adsorbed, colloids anchor irreversibly at the liquid interface due to a high adsorption energy E_{ad}:
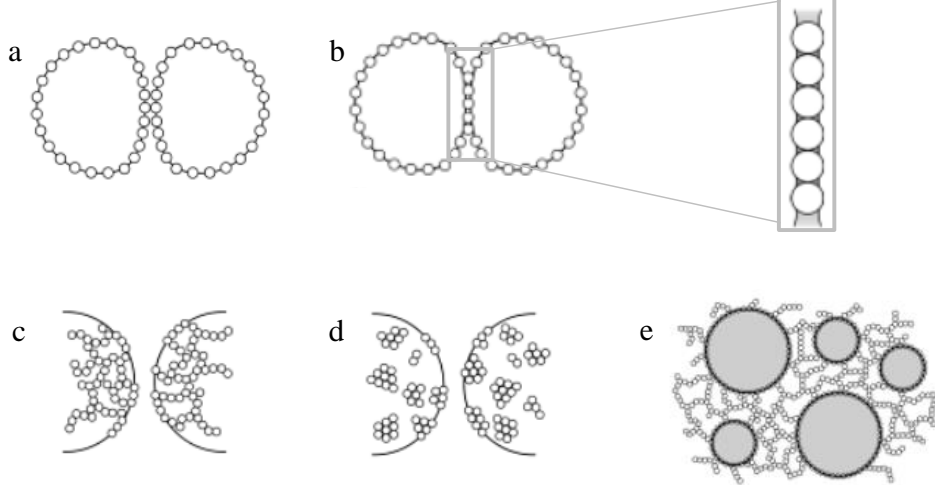
Figure 1.4: Different ways of particle organization at an oil-water interface: (a) monolayer, (b) bridging, (c) aggregation at the interface, (d) formation of domains, (e) 3D network around the droplets. Reprinted from [65] with permission.

$$E_{ad} = \pi R^2 \gamma_{oil-water}(1 - \cos\theta)^2 \tag{1.4}$$

The adsorption energy of a 10 nm particle with $\theta = 90\,^\circ$ at a standard oil-water interface is already more than 10^3 times the thermal energy and this value increases strongly with the particle size. Anchoring is strongest for $\theta = 90\,^\circ$, i.e. when the particle is half wetted by the oil and half wetted by the water. To achieve this condition, often chemical modification of the particle surface is required. The organization of particles at the surface depends not only on their immersion depth but also on the lateral interaction between the particles (Figure 1.4). The structures formed by solid colloidal particles provide significant rigidity to the interface of a Pickering emulsion; this improves their stability to both coalescence and Ostwald ripening. Even very large emulsion droplets, up to centimeters in diameter, have been shown to be effectively stabilized by solid particles. [66]

In this thesis we explore two different types of stabilizers for liquid interfaces as these may exhibit many of the features required for the effective application of emulsion-based extraction methods, as outlined above. Below we briefly describe these two types of stabilization methods: interfacial complex coacervation and microgel-based stabilization.

1.2.2 Complex coacervates

Complex coacervates, first studied by Bungenberg de Jong, [67] are insoluble phases resulting from associative phase separation upon mixing two solutions of oppositely charged polyelectrolytes. This phase separation is driven by both an enthalpic contribution due to ion pairing and solvency effects, and an entropic contribution, as the formation of a complex allows the counterions to be released into the bulk aqueous phase. [68] Complex coacervation between oppositely charged polyelectrolytes has been extensively studied in bulk and shown to be sensitive to parameters such as the charge density of the polyelectrolytes, [68] their chain length and flexibility, [69,70] the nature of the polymer backbone, the ionic strength and pH of the solutions. [68] Charged macroions typically strongly hydrate in aqueous solutions and as a result have a low surface activity towards oil-water interfaces. However, the electrostatic complexes, which demix from aqueous solution, tend to exhibit complete wetting at these interfaces due to their low interfacial tensions against the solution. As a consequence, the liquid coacervate droplets are strongly surface active and have therefore been used to stabilize liquid and solid interfaces. [71,72] The adsorption of coacervate layers at liquid interfaces has so far been accomplished either by adsorption of the coacervate itself or by layer-by-layer deposition. [73]

In the direct approach, coacervate droplets formed in the water phase, spontaneously adsorb to the interface where they wet the oil droplet surface and spread as envisaged by Neumann (Figure 1.3b). Once adsorbed, complexes provide elastic properties to the interface that can exceed by orders of magnitude the elasticity of interfaces prepared from either macroionic species alone. [74] To prepare a layer-by-layer structure at a liquid interface, a primary emulsion is stabilized by a polyelectrolyte or a charged surfactant, after which an oppositely charged polyelectrolyte is adsorbed onto the droplets. This sequence may be repeated many times, resulting in a layered structure. This approach is called a layer-by-layer (LbL) deposition, [75] and offers excellent control over the composition and the thickness of the adsorbed layer. However, its preparation is time consuming and requires careful tuning of the experimental conditions to avoid droplet aggregation when they pass through the isoelectric point during adsorption. Moreover, when insufficient polyelectrolyte is present to completely coat the surface of the droplets, bridging flocculation may result. [76–79] Similarly, if the polyelectrolyte is present in excess in the continuous phase, depletion flocculation can be induced. [77–79] Depending on the polyelectrolytes that compose this multilayer, the formation of the film as well as its properties vary. For LbL films composed of strong polyelectrolytes with hydrophobic backbones, the film thickness increases linearly with the number

of deposition layers.[80] By contrast, multilayer films composed of weak polyelectrolytes show an exponential growth and a strong degree of intermixing between the layers.[80–82]

1.2.3 Microgels

Microgels are solvent-swollen, cross-linked polymer gels of colloidal dimensions. First defined in 1949 by Baker to describe cross-linked polybutadiene latex particles,[83] Baker stated that microgel particles fulfill four criteria: 1) their size is between 10 and 1000 nm, 2) they are dispersed in a solvent, 3) they are swollen by that solvent and 4) their chemical structure is stable. In recent years, many studies have focussed on microgels composed of poly(N-isopropylacrylamide) (PNIPAm) or its copolymers.[84,85] These particles are of particular interest as this polymer exhibits a lower critical solution temperature (LCST) close to body temperature, i.e. a critical temperature below which the polymer mixes with water at all volume fractions. This allows the size, the functionality of the particles and the physical state of their suspensions to be tuned with a simple temperature trigger.[86] Amide groups in these polymers form hydrogen bonds with the water molecules. At low temperatures these hydrogen bonds are strong, which leaves PNIPAm strongly hydrated and under good solvency conditions. At higher temperatures these amide-water hydrogen bonds break and the polymer undergoes a coil to globule transition. The LCST can be tailored precisely by co-polymerizing NIPAm with other monomers.[87]

While microgels may be prepared by a variety of methods, such as mini emulsion polymerization[88] or droplet templating,[89] they are most commonly prepared by means of precipitation polymerization.[90] In precipitation polymerization, all monomers are soluble in the reaction mixture. The particles are formed by homogeneous nucleation upon initiating polymerization with a free radical initiator. This polymerization is carried out at elevated temperatures to allow both the formation of radicals from the initiator and the phase separation of the polymer from the aqueous solvent if the reaction temperature is higher than the LCST of the polymer. Microgels prepared in this way exhibit at their periphery charges, originating from the initiator, which stabilize the particles and allowing the formation of monodisperse colloids. To synthesize small microgels, nuclei are stabilized at earlier stages during the reaction using surfactants.

Recently, microgels have gained a lot of interest in emulsion stabilization owing to their responsivity to temperature, ionic strength, and the ability to tune particle deformability using the degree of crosslinking.[91–103] Much research has been done

by the groups of Richtering and Schmitt. These groups have reported that the stabilization of oil droplets appears to be independent of the charge sign and density of the microgels, which suggests that the stability is not provided by electrostatic interactions.[104] They have shown that it is rather the microgel deformability at the interface that plays a crucial role.[98,100] While microgels form monolayers at liquid interfaces when adsorbed spontaneously, strong mixing of a microgel solution with oil has been reported to induce severe droplet bridging (Figure 1.4b) resulting in stable emulsion gels.[105] Despite these extensive studies, many questions remain regarding the nature of microgel adsorption, their interfacial configuration and the arrangement of particles at the interface. This is exacerbated by the fact that, in contrast to solid particles, microgels do not have a defined interface with the surrounding medium. Since they are swollen by one of the two phases comprising the emulsion, it becomes difficult to define a contact line and associated contact angle. Some of these issues will be addressed in this thesis.

1.2.4 Emulsification

To prepare emulsions, mechanical energy is required to break the phase to be dispersed into small droplets, and for Pickering emulsions, to break the thin film that separates the particles from the interface. In many industrial processes, droplets are prepared by mechanical agitation such as intensive mixing, stirring or shearing.[106] Emulsions prepared with these techniques typically exhibit wide size distributions, lack of control of droplet size, and as a result have a large tendency towards Ostwald ripening. Emulsions can also be prepared using microtechnological devices, for example in microfluidic chips. These offer precise control of the droplet size and its distribution. Under the correct conditions, highly monodisperse emulsions, with complex structure, such as double or multiple emulsions,[107,108] can be prepared. Different microfluidic designs exist for the effective formation of well-defined droplets, as illustrated in Figure 1.5. One of the main challenges in the design of microfluidic devices for droplet generation is the throughput rate. Due to their small dimensions, yields are typically limited; however, scale-up approaches, for example based on the edge droplet generation (EDGE) method (Figure 1.5d), have been proposed, yet remain under development.[109]

1.3   Emulsion breaking

While the preparation of stable emulsions is challenging by itself, certain applications require destabilization of the droplets at a specific point during a process.
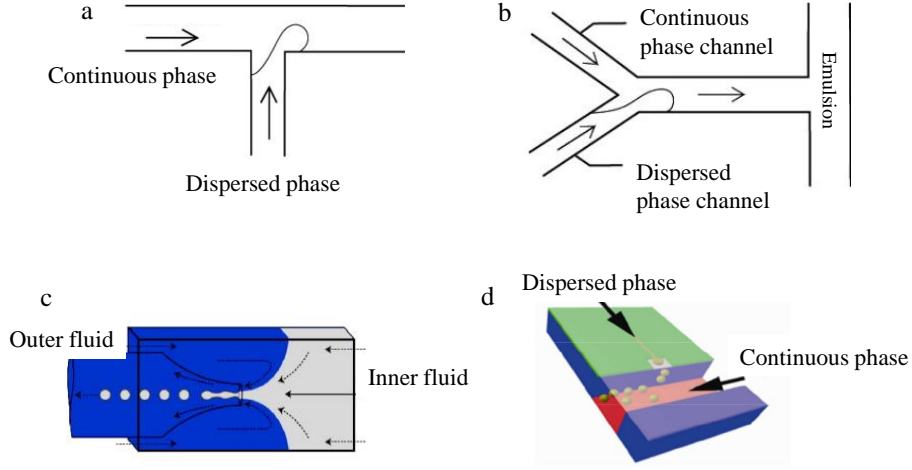
Figure 1.5: Example of microfluidic devices for emulsion droplet formation: (a) T-junction, (b) Y-junction, (c) Flow-focusing microcapillary device, (d) Edge Droplet Generation device. Reprinted from [110] with permission from Elsevier.

This is for example the case during film formation in paints, where a phase inversion process is required to form the final film, [111] or in extractions where the droplet phase needs to be collected to obtain the product of interest. Emulsion destabilization is commonly achieved by changing the conditions that provide stability, for example through heating or mechanical agitation, [50,112] or the addition of a destabilizer, [113] such as a co-solvent, which may remove surfactants from the interface, change the continuous phase viscosity, or reduce repulsive interactions between the droplets.

However, for the destabilization of oil droplets in the extraction of delicate biomolecules, the addition of extra components to the emulsion is often undesired. Ideally, the on-demand destabilization of the emulsion is a property inherent to the emulsion formulation itself, for example by the use of responsive stabilizers, whose interfacial activity can be switched on and off with a simple environmental trigger such as pH, temperature or magnetic or electric fields. Recently, a surfactant with a thermoresponsive block has been used to control emulsion stability; the emulsion prepared with this surfactant is stable for several months at room temperature but upon increasing the temperature above the collapse transition of the thermoresponsive block, coalescence of the droplets occurs within minutes. [50,112] In this thesis, we explore two different responsive systems, i.e. electrostatic polyelectrolyte complexes and thermoresponsive microgel colloids, for their ability to stabilize liquid

interfaces and the reversibility of the emulsification.

1.4 Towards sustainable emulsion processes

Sustainable development is often defined following the Brundtland Report: 'Development that meets the needs of the present generation without compromising the ability of future generations to meet their own needs'.[114] With a growing world population and an increasing demand for products and industrial processes, the transition towards a sustainable industry and society poses a major challenge for scientists and engineers. Indeed, scientists aim to provide solutions that minimize environmental impact for example through the reduction of energy consumption or the reusability of resources while maintaining the performance and quality of the process in question.

As discussed above, the preparation of emulsions involves energy input. In conventional high-shear mixing emulsification methods, more than 90% of the energy supplied to a two-phase system is not used to create interface but is lost through viscous dissipation, released as heat and causing the loss of functionality of delicate compounds.[115] The development of microstructured emulsification devices like membranes and microfluidic devices has allowed progress in reducing the energy expenditure during processing and minimizing viscous losses.[116] Interestingly, with some microfluidic methods mechanical energy input is minimized, using curvature effects to drive emulsification such as in the EDGE method developed by the Schroën group in Wageningen.[110]

Compared to organic solvents, ILs remain expensive and this limits their potential applicability at larger scales. From a sustainability perspective, one should ideally be able to recover and reuse the ILs and their stabilizers. Once an extraction has been performed using an IL-in-water emulsion, several steps are still required before another extraction can be done. These steps consist of collecting the droplets, breaking the droplets to obtain a macroscopic IL phase, retrieving the compound of interest from the IL and finally purifying the IL for its repeated use. This may be achieved through the use of paramagnetic ionic liquids,[29] which have paramagnetic properties due to their specific ion species, without the requirement of adding magnetic nanoparticles. The most common paramagnetic ionic liquids are those containing the anion $FeCl_4^-$. In principle, droplets formed from a paramagnetic ionic liquid can be collected in a magnetic field,[117] allowing the separation of IL from the continuous water phase. However, this still requires a back-extraction to obtain the final product, before the IL is purified for another

cycle of extraction. The purification procedure depends on the type of impurity. If it is volatile, the IL can be washed and dried before its use in a new extraction. [118] Nevertheless, using this technique may change the chemical composition of the IL as these liquids are very sensitive to ion exchange processes. Alternatively, one could use crystallization of ILs for their purification, ideally by designing the ionic liquid to solidify at temperatures just below the operating temperature, to reduce costs for refrigeration.

1.5   Outline of this thesis

In this thesis we explore the use of different responsive stabilization mechanisms for liquid-liquid interfaces in general, and IL-water interfaces in particular, for the creation of stable and responsive emulsions for extraction processes. This thesis is divided into two parts:

In **Part I: "Charge complexation at interfaces"**, we focus on the formation of electrostatic complexes across oil-water interfaces to extend the concept of interfacial stabilization by complex coacervates. In Chapter 2 we consider a system with oppositely charged polyelectrolytes; one polyelectrolyte is dissolved in the water phase and the oppositely charged polyelectrolyte in the oil phase. We show that, while either polyelectrolyte is not surface-active by itself, the presence of both species and their interactions at the interface result in the spontaneous formation of a stabilizing film, whose strength can be tuned using pH and salt concentration. This allows the formation of very stable emulsions, which can be broken on-demand using a pH trigger.

In Chapter 3, we use self-consistent field calculations to study this interfacial complexation in more detail. We investigate the thermodynamics and structures of these (inter)phases. We show that the theory reasonably accounts for the ion-release effect as our system contains two solvents. We also reveal that, under most conditions, the interfacial coacervate exhibits a pseudo-partial wetting scenario in which a microscopically thin coacervate film coexists with droplets of coacervate.

In **Part II: "Soft colloids at interfaces"**, we address some important issues associated with the adsorption of microgels to liquid and solid surfaces, in particular their application in stabilizing IL-in-water emulsions. We design composite microgels that consist of a dyed polystyrene core embedded in a microgel shell, which allow us to obtain new insights into the interfacial properties of microgels using imaging. In Chapter 4 we study the adsorption, organization and deformation of the composite microgels at oil-water interfaces. We demonstrate a

duality in the interfacial behaviour of these particles, which exhibit a spontaneous and barrier-free adsorption, yet a strong and irreversible anchoring, at a variety of liquid interfaces.

In Chapter 5, we use the same composite microgels to stabilize ionic liquid-water interfaces. Despite the presence of these particles, the IL-water interface remains permeable for molecules, allowing us to use these emulsions for extractions. Using the reversible thermosensitivity of the particles, we are able to break and reform the emulsion. This leads to the proof-of-principle for a completely sustainable process for IL-based extractions, in which energy input is minimized and all components can be efficiently reused.

Finally, we study how these microgels adsorb on solid surfaces in Chapter 6. We show how adsorption studies can be obscured by drying effects, thus requiring *in-situ* investigation to obtain high-quality data on adsorption density, which we show to depend strongly on pH, ionic strength and surface chemistry.

We conclude this thesis by a **general discussion** and a **summary**.

References

[1] *Separation processes in the Food and the Biotechnology Industries*, ed. A.S. Grandison and M.J. Lewis, 1996.

[2] J.F. Richardson, J.H. Harker, and J.R. Backhurst, *Book Chemical Engineering, Volume 2*, 2002.

[3] P. Bi, D. Li, and H. Dong, *Sep. Purif. Technol.*, 2009, **69**, 205–209.

[4] *Principles and Practices of Solvent Extraction*, ed. New York City Marcel Dekker, Inc, Tydberg, J. and Musikas, C. and Choppin, G.R., 1992.

[5] J.G. Huddleston and R.D. Rogers, *Chem. Commun.*, 1998, 1765–1766.

[6] R.D. Rogers and K.R. Seddon, *Science*, 2003, **302**, 792–793.

[7] A. Soto, A. Arce, and M.K. Khoshkbarchi, *Sep. Purif. Technol.*, 2005, **44**, 242–246.

[8] Q.F. Liu, J. Yu, W.L. Li, X.S. Hu, H.S. Xia, H.Z. Liu, and P. Yang, *Sep. Sci. Technol.*, 2006, **41**, 2849–2858.

[9] Z. Du, Y.L. Yu, and J.H. Wang, *Chem.-Eur. J.*, 2007, **13**, 2130–2137.

[10] C.-H. Li, J. Han, Y. Wang, Y.-S. Yan, X.-H. Xu, and J.-M. Pan, *Anal. Chim. Acta*, 2009, **653**, 178–183.

[11] Y.C. Pei, Y.Z. Wang, K. Wu, X.P. Xuan, and X.J. Lu, *Sep. Purif. Technol.*, 2009, **64**, 288–295.

[12] G. Young, F. Nippgen, S. Titterbrandt, and M.J. Cooney, *Sep. Purif. Technol.*, 2010, **72**, 118–121.

[13] E. Alvarez-Guerra and A. Irabien, *Sep. Purif. Technol.*, 2012, **98**, 432–440.

[14] Y.H. Kim, Y.K. Choi, J. Park, S. Lee, Y.H. Yang, H.J. Kim, T.J. Park, Y.H. Kim, and S.H. Lee, *Bioresour. Technol.*, 2012, **109**, 312–315.

REFERENCES

[15] X.W. Chen, Q.X. Mao, and J.H. Wang, *Prog. Chem.*, 2013, **25**, 661–668.

[16] X. Lin, Y. Wang, Q. Zeng, X. Ding, and J. Chen, *Analyst*, 2013, **138**, 6445–6453.

[17] Q. Zeng, Y. Z. Wang, N. Li, X. Huang, X.Q. Ding, X. Lin, S.Y. Huang, and X.J. Liu, *Talanta*, 2013, **116**, 409–416.

[18] S.A. Choi, Y.K. Oh, M.J. Jeong, S.W. Kim, J.S. Lee, and J.Y. Park, *Renew. Energy*, 2014, **65**, 169–174.

[19] R.K. Desai, M. Streefland, R.H. Wijffels, and M.H.M. Eppink, *Green Chem.*, 2014, **16**, 2670–2679.

[20] M. Freemantle, *An introduction to ionic liquids*, The Royal Society of Chemistry, 2010.

[21] M.D. Joshi and J.L. Anderson, *RSC Adv.*, 2012, **2**, 5470–5484.

[22] C.P. Fredlake, J.M. Crosthwaite, D.G. Hert, S.N.V.K. Aki, and J.P. Brennecke, *J. Chem. Eng. Data*, 2004, **49**, 954–964.

[23] O. Aschenbrenner, S. Supasitmongkol, M. Taylor, and P. Styring, *Green Chem.*, 2009, **11**, 1217–1221.

[24] H. Nakagawa, Y. Fujino, S. Kozonoa, Y. Katayama, T. Nukuda, H. Sakaebe, H. Matsumoto, and K. Tatsumi, *J. Power Sources*, 2007, **174**, 1021–1026.

[25] S.J. Zhang, N. Sun, X.Z. He, X.M. Lu, and X.P. Zhang, *J. Phys. Chem. Ref. Data*, 2006, **35**, 1475–1517.

[26] M.G. Freire, C. Neves, P.J. Carvalho, R.L. Gardas, A.M. Fernandes, I.M. Marrucho, L. Santos, and J.A.P. Coutinho, *J. Phys. Chem. B*, 2007, **111**, 13082–13089.

[27] M.G. Freire, L.M.N.B.F. Santos, A.M. Fernandes, J.A.P Coutinho, and I.M. Marrucho, *Fluid Phase Equilib.*, 2007, **261**, 449–454.

[28] M.G. Freire, P.J. Carvalho, R.L. Gardas, I.M. Marrucho, L. Santos, and J.A.P. Coutinho, *J. Phys. Chem. B*, 2008, **112**, 1604–1610.

[29] S. Hayashi and H.O. Hamaguchi, *Chem. Lett.*, 2004, **33**, 1590–1591.

[30] R.E. Del Sesto, T.M. McCleskey, A.K. Burrell, G.A. Baker, J.D. Thompson, B.L. Scott, J.S. Wilkes, and P. Williams, *Chem. Commun.*, 2008, 447–449.

[31] K.N. Marsh, J.A. Boxall, and R. Lichtenthaler, *Fluid Phase Equilib.*, 2004, **219**, 93–98.

[32] Y. Wang, T. Kakiuchi, Y. Yasui, and M.V. Mirkin, *J. Am. Chem. Soc.*, 2010, **132**, 16945–16952.

[33] A. Chaumont, R. Schurhammer, and G. Wipff, *J. Phys. Chem. B*, 2005, **109**, 18964–18973.

[34] R. Liu, J. Liu, Y. Yin, X. Hu, and G. Jiang, *Anal. Bioanal. Chem.*, 2009, **393**, 871–883.

[35] Y. N. Gao, S.B. Han, B.X. Han, G.Z. Li, D. Shen, Z.H. Li, J.M. Du, W.G. Hou, and G.Y. Zhang, *Langmuir*, 2005, **21**, 5681–5684.

[36] Y. Gao, N. Li, L.Q. Zheng, X.Y. Zhao, S.H. Zhang, B.X. Han, W.G. Hou, and G.Z. Li, *Green Chem.*, 2006, **8**, 43–49.

[37] J.H. Porada, M. Mansueto, S. Laschat, and C. Stubenrauch, *Soft Matter*, 2011, **7**, 6805–6810.

[38] A. Klee, S. Prevost, W. Kunz, R. Schweins, K. Kiefer, and M. Gradzielski, *Phys. Chem. Chem. Phys.*, 2012, **14**, 15355–15360.

[39] J. Zhang and B. Han, *Acc. Chem. Res.*, 2012, **46**, 425–433.

[40] Y.C. Pei, Y.J. Huang, L. Li, and J.J. Wang, *J. Chem. Thermodyn.*, 2014, **74**, 231–237.

16

[41] J. Bibette, F.L. Calderon, and P. Poulin, *Rep. Prog. Phys.*, 1999, **62**, 969–1033.

[42] P. Taylor, *Adv. Colloid Interface Sci.*, 1998, **75**, 107–163.

[43] J. Weiss, *Langmuir*, 2000, **16**, 6833–6838.

[44] S.L.I. Toh, J. McFarlana, C. Tsouris, D.W. DePaoli, H. Luo, and S. Dai, *Solvent Extr. Ion Exch.*, 2006, **24**, 33–56.

[45] W.I. Higuchi and J. Misra, *J. Pharm. Sci.*, 1962, **51**, 459.

[46] P. Walstra, Marcel Dekker, 2002, p. 541.

[47] S. Tcholakova, Z. Mitrinova, K. Golemanov, N.D. Denkov, M. Vethamuthu, and K.P. Ananthapadmanabhan, *Langmuir*, 2011, **27**, 14807–14819.

[48] D. Li, *J. Colloid Interface Sci.*, 1996, **181**, 34–44.

[49] T. Krebs, K. Schroën, and R. Boom, *Soft Matter*, 2012, **8**, 10650–10657.

[50] H. Feng, N.A.L. Verstappen, A.J.C. Kuehne, and J. Sprakel, *Polym. Chem.*, 2013, **4**, 1842–1847.

[51] J. Bibette, D.C. Morse, T.A. Witten, and DA. Weitz, *Phys. Rev. Lett.*, 1992, **69**, 2439–2442.

[52] R. Pons, P. Taylor, and T.F. Tadros, *Colloid Polym. Sci.*, 1997, **275**, 769–776.

[53] A. Acevedo, X. Gutierrez, and H. Rivas, *J. Colloid Interface Sci.*, 2001, **242**, 230–238.

[54] S. Tcholakova, N.D. Denkov, I.B. Ivanov, and B. Campbell, *Adv. Colloid Interface Sci.*, 2006, **123-126**, 259–293.

[55] W. Ramsden, *Proc. R. Soc. London*, 1903, 156–164.

[56] S.U. Pickering, *J. Chem. Soc.*, 1907, 2001–2021.

[57] J.W.J. de Folter, M.W.M. van Ruijven, and K.P. Velikov, *Soft Matter*, 2012, **8**, 6807–6815.

[58] S. Guillot, de Azevedo C. Bergaya, F., F. Warmont, and J.F. Tranchant, *J. Colloid Interface Sci.*, 2009, **333**, 563–569.

[59] J.I. Amalvy, S.P. Armes, B.P. Binks, J.A. Rodrigues, and G.F. Unali, *Chem. Commun.*, 2003, 1826–1827.

[60] B.P. Binks and S.O. Lumsdon, *Phys. Chem. Chem. Phys.*, 1999, **1**, 3007–3016.

[61] T. Young, *Philos. Trans. R. Soc. London*, 1805, **95**, 65–87.

[62] P.-G. de Gennes, F. Brochart-Wyart, and D. Quere, *Capillarity and wetting phenomena*, 2002.

[63] F. Neumann, *Vorlesungen ber die Theorie der Capillaritt*, 1894.

[64] D.M. Kaz, R. McGorty, M. Mani, M.P. Brenner, and V.N. Manoharan, *Nat. Mater.*, 2012, **11**, 138–142.

[65] R.G.J. Lopetinsky, J.H. Masliyah, and Z. Xu, *Solids-stabilized emulsions: a review*, Cambridge University Press, 2006, pp. 186–224.

[66] X. Zhai and S. Efrima, *J. Phys. Chem.*, 1996, **100**, 11019–11028.

[67] H.G. Bungenberg de Jong and H.R. Kruyt, *Proc. K. Ned. Akad. Wet.*, 1929, **32**, 849–856.

[68] J. van der Gucht, E. Spruijt, M. Lemmers, and M.A. Cohen Stuart, *J. Colloid Interface Sci.*, 2011, **361**, 407–422.

[69] E. Spruijt, A.H. Westphal, J.W. Borst, M.A. Cohen Stuart, and J. van der Gucht, *Macromolecules*, 2010, **43**, 6476–6484.

17

[70] N. Pawar and H.B. Bohidar, *Adv. Colloid Interface Sci.*, 2011, **167**, 12–23.

[71] L.S. Jourdain, C. Schmitt, M.E. Leser, B.S. Murray, and E. Dickinson, *Langmuir*, 2009, **25**, 10026–10037.

[72] I.M. Tucker, J.T. Petkov, C. Jones, J. Penfold, R.K. Thomas, S.E. Rogers, A.E. Terry, R.K. Heenan, and I. Grillo, *Langmuir*, 2012, **28**, 14974–14982.

[73] L. Jourdain, M.E. Leser, C. Schmitt, M. Michel, and E. Dickinson, *Food Hydrocolloids*, 2008, **22**, 647–649.

[74] C. Schmitt, E. Kolodziejczyk, and M.E. Leser, *Food colloids: interactions, microstructure and processing*, Royal Society of Chemistry, 2001, pp. 284–300.

[75] G. Decher, *Science*, 1997, **277**, 1232–1237.

[76] E. Dickinson and K. Pawlowsky, *J. Agric. Food Chem.*, 1997, **45**, 3799–3806.

[77] E. Dickinson, *Food Hydrocolloids*, 2003, **17**, 25–39.

[78] T.B.J. Blijdenstein, A.J.M. van Winden, T. van Vliet, E. van der Linden, and van Aken G.A., *Colloids Surf., A*, 2004, **245**, 41–48.

[79] D.J. McClements, *Langmuir*, 2005, **21**, 9777–9785.

[80] Ph. Lavalle, C. Gergely, F.J.G. Cuisinier, G. Decher, P. Schaaf, J.C. Voegel, and C. Picart, *Macromolecules*, 2002, **35**, 4458–4465.

[81] V. Pardo-Yissar, E. Katz, and O. Lioubashevski, *Langmuir*, 2001, **17**, 1110–1118.

[82] C. Picart, J. Mutterer, and L. Richert, *Proc. Natl. Acad. Sci.*, 2002, **99**, 12531.

[83] W.O. Baker, *Ind. Eng. Chem.*, 1949, **41**, 511–520.

[84] H. Ni, H. Kawaguchi, and T. Endo, *Colloid Polym. Sci.*, 2007, **285**, 819–826.

[85] K. Tauer, D. Gau, S. Schultze, A. Volkel, and R. Dimova, *Colloid Polym. Sci.*, 2009, **287**, 299–312.

[86] H.G. Schild, *Prog. Polym. Sci.*, 1992, **17**, 163–249.

[87] J.D. Debord and L.A. Lyon, *Langmuir*, 2003, **19**, 7662–7664.

[88] K. Landfester, M. Willert, and M. Antonietti, *Macromolecules*, 2000, **33**, 2370–2376.

[89] S.Y. Teh, R. Lin, L.H. Hung, and A.P. Lee, *Lab on a Chip*, 2008, **8**, 198–220.

[90] W. McPhee, K.C. Tam, and R. Pelton, *J. Colloid Interface Sci.*, 1993, **156**, 24–30.

[91] T. Ngai, S.H. Behrens, and H. Auweter, *Chem. Commun.*, 2005, 331–333.

[92] T. Ngai, H. Auweter, and S.H. Behrens, *Macromolecules*, 2006, **39**, 8171–8177.

[93] S. Brugger and W. Richtering, *Langmuir*, 2008, **24**, 7769–7777.

[94] S. Brugger, B.A. Rosen, and W. Richtering, *Langmuir*, 2008, **24**, 12202–12208.

[95] S. Tsuji and H. Kawaguchi, *Langmuir*, 2008, **24**, 3300–3305.

[96] S. Berger, H.P. Zhang, and A. Pich, *Adv. Funct. Mater.*, 2009, **19**, 554–559.

[97] S. Brugger, S. Ruetten, K.-H. Phan, M. Moeller, and W. Richtering, *Angew. Chem. Int. Ed.*, 2009, **48**, 3978–3981.

[98] M. Destribats, V. Lapeyre, M. Wolfs, E. Sellier, F. Leal-Calderon, V. Ravaine, and V. Schmitt, *Soft Matter*, 2011, **7**, 7689–7698.

[99] S. Schmidt, T.T. Liu, S. Rutten, K.H. Phan, M. Moller, and W. Richtering, *Langmuir*, 2011, **27**, 9801–9806.

[100] K. Geisel, L. Isa, and W. Richtering, *Langmuir*, 2012, **28**, 15770–15776.

[101] M. Destribats, M. Wolfs, F. Pinaud, V. Lapeyre, E. Sellier, V. Schmitt, and V. Ravaine, *Langmuir*, 2013, **29**, 12367–12374.

[102] Z.F. Li, K. Geisel, and T. Richtering, W. Ngai, *Soft Matter*, 2013, **9**, 9939–9946.

[103] K. I. Geisel, L. Isa, and W. Richtering, *Angew. Chem. Int. Ed.*, 2014, **53**, 4905–4909.

[104] T. Liu, S. Seiffert, J. Thiele, A.R. Abate, D.A. Weitz, and W. Richtering, *Proc. Natl. Acad. Sci.*, 2012, **109**, 384.

[105] H. Monteillet, M. Workamp, J.M. Kleijn, F.A.M. Leermakers, and J. Sprakel, *Adv. Mater. Interfaces*, 2014, **1**, 1300121.

[106] H. Karbstein and H. Schubert, *Chem. Eng. Process.*, 1995, **34**, 205–211.

[107] L.R. Arriaga, S.S. Datta, S.-H. Kim, E. Amstad, T.E. Kodger, F. Monroy, and D.A. Weitz, *Small*, 2014, **10**, 950–956.

[108] W.J. Duncanson, L.R. Arriaga, W.L. Ung, J.A. Kopechek, T.M. Porter, and D.A. Weitz, *Langmuir*, 2014, **30**, 13765–13770.

[109] K. van Dijke, G. Veldhuis, K. Schroën, and R. Boom, *Lab on a Chip*, 2009, **9**, 2824–2830.

[110] A.A. Maan, K. Schroën, and R. Boom, *J. Food Eng.*, 2011, **107**, 334–346.

[111] H. Feng, J. Sprakel, D. Ershov, T. Krebs, M.A. Cohen Stuart, and J. van der Gucht, *Soft Matter*, 2013, **9**, 2810–2815.

[112] H. Feng, D. Ershov, T. Krebs, K. Schroën, M.A. Cohen Stuart, J. van der Gucht, and J. Sprakel, *Lab on a Chip*, 2015, **15**, 188–194.

[113] A.A. Hafiz, H.M. El-Din, and A.M. Badawi, *J. Colloid Interface Sci.*, 2005, **284**, 167–175.

[114] *World Commission on Environment and Development*, 1987.

[115] S.M. Jafari, E. Assadpoor, Y. He, and B. Bhandari, *Food Hydrocolloids*, 2008, **22**, 1191–1202.

[116] K. Schroën, O. Bliznyuk, K. Muijlwijk, S. Sahin, and C.C. Berton-Carabin, *Current Opinion in Food Science*, 2015, **3**, 33–40.

[117] V. Misuk, A. Mai, K. Giannopoulos, F. Alobaid, B. Epple, and H. Loewe, *Lab on a Chip*, 2013, **13**, 4542–4548.

[118] J. Fan, Y. Fan, Y. Pei, K. Wu, J. Wang, and M. Fan, *Sep. Purif. Technol.*, 2008, **61**, 324–331.

Part I

CHARGE-DRIVEN
COMPLEXATION AT INTERFACES

Chapter 2

Polyelectrolyte complexation across oil-water interfaces

In this chapter, we present a simple strategy to co-assemble oppositely charged polyelectrolytes across oil-water interfaces. We use an oil-soluble anionic polyelectrolyte, poly(fluorene-*co*-benzothiadiazole-*co*-benzoic acid), in combination with a cationic polyelectrolyte that is dissolved in the aqueous phase. When only one of the charged components is present, no positive adsorption is observed in interfacial tension measurements. By contrast, when both polyelectrolytes are present, in the oil and water phases, a rapid decrease of the interfacial tension is observed indicating co-adsorption of the anionic and cationic polyelectrolytes. Confocal microscopy and colocalization analysis further verify the presence of both polyelectrolytes at the interface. The complexation strength can be tuned through changes in ionic strength or pH. With this approach, emulsions can be stabilized for several weeks; moreover, using the sensitivity of the complex to changes in pH, we are able to reversibly break and make the emulsions on-demand.

2.1 Introduction

Colloidal systems such as dispersions, emulsions and foams are often stabilized against aggregation through electrostatic repulsions between the primary particles or droplets. The solvated surface charges, either chemically bound or physically adsorbed, and the diffuse cloud of ions surrounding the surface, commonly known as the double layer, prevent close approach of a second colloid of like charge. The electrostatic repulsion that arises due to overlap of these diffuse double layers prevents colloids from approaching each other close enough to enter the regime where attractive van der Waals forces reign. [1]

By contrast, if the double layers of two macro-ions of opposite charge overlap, an electrostatic attraction results. The ultimate strength of this attractive force depends on both enthalpic contributions, from the ion–ion pairs, and entropic contributions, from the release of counterions from the overlapping double layers into the bulk solution. Typically, electrostatic attractions lead to rapid destabilization of colloidal systems, giving rise to aggregation. [2–4] However, in some cases electrostatic attractions can be used to create co-assembled materials with well-defined microstructures, such as functional nanoparticles, [5] binary colloidal super-lattices [6,7] or hierarchical structures of emulsion droplets. [8] Even nature employs the strategy of electrostatic co-assembly to control materials at microscopic length scales; examples include the structure of nucleosomes that are governed by the electrostatic histone–DNA complex [9] and the sandcastle worm that builds its protective shelter using electrostatic complexes of proteins as a cement to bond sand grains together. [10]

These examples suggest that, when well controlled, electrostatic attractions between macro-ions, such as charged colloidal particles or (bio)polymers, can be efficiently used to create cohesive soft materials. Moreover, the strength and range of the interactions can be easily tuned through chemical parameters such as charge densities and ion species, and through environmental triggers such as pH and ionic strength. This flexibility makes electrostatic co-assembly a promising route for creating new materials with controlled microstructure and novel macroscopic functionality.

Polyelectrolytes are polymers that carry ionizable groups; hence they can interact through electrostatic interactions. Under most conditions, mixing oppositely charged polyelectrolytes in bulk solutions leads to macroscopic phase separation between the electrostatic complex and excess solvent plus small ions, a process known as complex coacervation. [11] Often the new coacervate phase that is formed in the aqueous solution is surface active and can be used to stabilize emulsion droplets by adsorption at the oil-water interface. [12,13] However, this stabilization

is kinetically limited as the complex needs to adsorb quickly during the formation of a new interface. A more controlled approach to create an interfacial electrostatic complex is through layer-by-layer assembly, in which the colloidal particles or droplets are first stabilized by one polyelectrolyte layer and then an oppositely charged polyelectrolyte is adsorbed to form a second layer on top. This process can be repeated as many times as necessary. [14,15] Although this method enhances the stability of the colloids and allows a good control of the interfacial properties, it requires a lengthy iterative procedure and a good control of the composition and preparation conditions to avoid aggregation of the droplets. General strategies to create complexes directly at interfaces are largely absent in the literature.

In this chapter, we present a strategy to create polyelectrolyte films through direct electrostatic co-assembly using oil-water interfaces as a scaffold. Each of the, oppositely charged and non-surface active, macroions is present in only one of the two immiscible phases; hence, electrostatic attractions between these polyelectrolytes occur exclusively across the interface. We use a new oil-soluble anionic polyelectrolyte, poly-(fluorene-*co*-benzothiadiazole-*co*-benzoic acid), in combination with a water-soluble cationic polyelectrolyte, either poly(diallyldimethylammonium chloride) or poly(L-lysine). We show how these complexes form at oil-water interfaces using tensiometry and confocal microscopy. Owing to the purely electrostatic nature of the complex formation we find that the complexes, and hence the stability of the interfaces, are ultimately sensitive to ionic strength and pH. We also illustrate that emulsion droplets can be stabilized with this approach for several weeks but simultaneously can be broken and reformed on-demand through environmental triggers.

2.2   Experimental details

2.2.1   Materials

We use poly(fluorene-*co*-benzothiadiazole-*co*-benzoic acid), an anionic oil-soluble polyelectrolyte with pH-dependent charges, poly(diallyldimethylammonium chloride), a cationic water-soluble polyelectrolyte with permanent charges and poly(L-lysine), a cationic water-soluble polyelectrolyte with pH-dependent charges. We choose poly(fluorene-*co*-benzothiadiazole-*co*-benzoic acid) as it is oil-soluble, charged and fluorescent; this unique combination allows us to directly observe the localization of the polymer at the interface using confocal microscopy.

Poly(fluorene-*co*-benzothiadiazole-*co*-benzoic acid), abbreviated F8BTBA, is synthesized through Suzuki-Miyaura polycondensation. [16] First, 1.25 mmol 2,5-dibromobenzoic acid, 0.5 mmol 2,1,3-benzothiadiazole-4,7-bis(boronic acid pina-
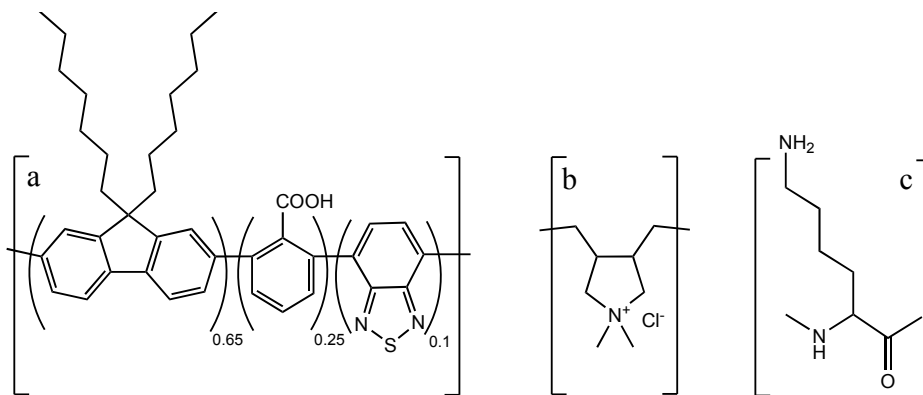
Figure 2.1: Chemical structure of (a) poly-(fluorene-*co*-benzothiadiazole-*co*-benzoic acid) abbreviated F8BTBA, (b) poly(diallyldimethylammonium chloride) abbreviated PDADMAC, (c) poly(L-lysine) abbreviated PLL.

col ester), 2 mmol 9,9-dioctylfluorene-2,7-diboronic acid bis(1,3-propanediol) ester and 1.25 mmol 9,9-dioctyl-2,7-dibromofluorene are dissolved in 25 mL tetrahydrofuran. After addition of 10 mL of a 2 M potassium carbonate solution, the biphasic reaction mixture is thoroughly degassed by purging with N_2. The reaction mixture is then heated to $60\,^{\circ}$C, after which the reaction is initiated by addition of 1 mol% of the catalyst tetrakis(triphenylphosphine) palladium(0) to the difunctional monomers. The reaction is allowed to proceed for 48 hours under a nitrogen blanket. After cooling the reaction mixture to room temperature, the organic and aqueous phases are separated. The product, contained in the organic phase, is obtained by precipitation in methanol and drying under vacuum. Residual catalyst and impurities are removed by Soxhlet extraction. The average molecular weight, determined by gel permeation chromatography against an a-methylpolystyrene standard, is found to be 17.5 kg/mol with a polydispersity $M_w/M_n = 1.8$. F8BTBA is dissolved in the oil phase, which consists of a 1:1 (w:w) mixture of decalin and tetrachloroethylene.

Poly(diallyldimethylammonium chloride) (20 wt% in water, $M_w = 400 - 500$ kg/mol), below abbreviated PDADMAC, is replaced by a fluorescently labeled cationic poly(L-lysine) (PLL) for the confocal microscopy experiments. For the labeling of PLL, first 10 mL poly(L-lysine) ($M_w = 150 - 300$ kg/mol) is mixed with 0.1 mg tetramethylrhodamine-isothiocyanate. The mixture is stored at $7\,^{\circ}$C for 2 hours and subsequently dialyzed against Milli-Q water for a week. The cut-off of the dialysis tube is 50 kg/mol.

The chemical structures of the polymers are shown in Figure 2.1. Unless stated otherwise, the reagents are purchased from Sigma-Aldrich and used without purifi-

cation. The polymer concentration in both aqueous and oil phases is 1 g/L.

2.2.2   Interfacial tension measurements

Dynamic interfacial tensions between macroscopic water droplets and a continuous oil phase are measured through pendant drop tensiometry (Sinterface Pat-1) using a reverse needle. The droplet formed at the tip of the needle is illuminated to capture and analyze the droplet profile using a CCD camera. The droplet shape is given by the Gauss-Laplace equation, which describes the balance between gravitational and surface energy forces acting on the droplet:

$$\gamma(\frac{1}{R_1} + \frac{1}{R_2}) = \Delta P_0 + gz\Delta\rho \qquad (2.1)$$

where γ is the interfacial tension, R_1 and R_2 are the principal radii of curvature, ΔP_0 is the pressure difference across the fluid interface, g is the gravitational acceleration, z is the height and $\Delta\rho$ is the density difference between the two fluids.

After formation of the droplet, the interfacial tension is recorded as a function of time for about 3 hours. For all measurements, the droplet volume is 7.5 mm^3 and the temperature is 22 °C. The pH of the water phase is varied by titrating 0.1 M HCl or 0.1 M NaOH and the ionic strength of the water phase is varied by adding NaCl to the cationic polyelectrolyte solution.

2.2.3   Emulsion preparation

Emulsions in a 9:1, 5:5 and 1:9 (water:oil) ratio by volume are prepared by shaking a cationic polyelectrolyte water phase with a F8BTBA oil phase.

2.2.4   Confocal microscopy

The localization of the oppositely charged polyelectrolytes is studied using a Zeiss Axiovert 200M confocal microscope fitted with a 100× oil immersion objective. F8BTBA, which is fluorescent due to its conjugated structure, is excited at 458 nm and PLL modified with tetramethylrhodamine-isothiocyanate is excited at 543 nm. The emission of both species are recorded on two separate channels to allow for a colocalization analysis. This analysis is typically used to demonstrate the spatial overlap in the distribution patterns of fluorescent probes.

2.2.5   Emulsion stability

The stability of the emulsion against coalescence and Ostwald ripening is analyzed by measuring the droplet size distribution over time by laser light scattering

(Malvern Mastersizer 2000). Prior to analysis, the emulsion is diluted with a solution of the same pH and salt concentration as the original emulsion to avoid contribution of multiple scattering and particle-particle interactions. The size distribution is characterized in terms of mean diameter, which can be defined in several ways. Here, the Sauter diameter $D_{3,2}$ is used:

$$D_{3,2} = \frac{\sum\limits_i N_i D_i^3}{\sum\limits_i N_i D_i^2} \tag{2.2}$$

where D_i is the diameter of droplets in the class i and N_i is the number of droplets in that class.

The stability of the droplets against coalescence is further investigated by measuring the critical disjoining pressure. A glass tube with an inner diameter of 15 mm is filled with 6 mL of emulsion, which contains 3 mL of the droplet phase. Subsequently, the emulsion is centrifuged at a speed of 200 g for 2 minutes to reach mechanical equilibrium. The critical disjoining pressure is then determined from the height of the remaining emulsion, the density difference between the oil phase and the water phase and the acceleration. [17]

The stability of the emulsion droplets is increased by cross-linking the polymer layer at the interface through an amidation reaction. To this end, we add 12 mg of N-(3-dimethylaminopropyl)-N'-ethylcarbodiimide hydrochloride (EDC) and 12 mg of a N-hydroxysulfoccinimide (NHS) to a 1-week-old emulsion and subsequently carefully mix the sample, which is then left to react at room temperature for 3 days.

2.3   Results and discussion

2.3.1   Complex formation

As a reference, the interfacial tension between the water phase and the oil phase, which consists of a mixture of decalin and tetrachloroethylene, is measured; we find $\gamma = 31$ mN/m, close to that found for pure decalin–water interfaces. [18] The addition of only F8BTBA, at 1 g/L, to the oil phase increases the interfacial tension to 44 mN/m, close to that found for pure tetrachloroethylene–water interfaces. [18] The surprising rise of the interfacial tension suggests negative adsorption, i.e. depletion, of F8BTBA at the oil–water interface. We see the same effect for the cationic and water soluble polymer, PDADMAC; the interfacial tension between oil and aqueous polyelectrolyte solution increases from 31 to 37 mN/m. Clearly, both polyelectrolytes are not surface active by themselves. By contrast, when both
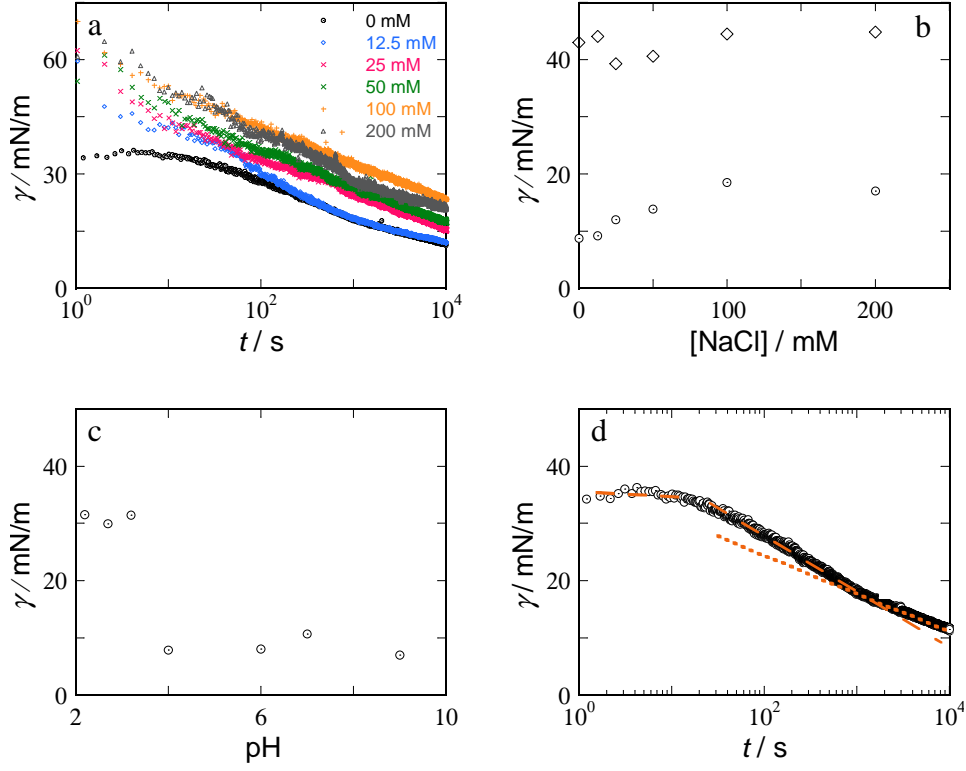
Figure 2.2: Interfacial tension as a function of (a) time at pH 7 upon complexation at different salt concentrations, (b) NaCl concentration in the aqueous phase at pH 7 for the interfacial complex (circles) and for F8BTBA alone (diamonds), (c) pH for the interfacial complex at 0 mM NaCl, (d) time after creating a bare interface: diffusion limited regime at shorter times and ageing regime at longer times. Fitting lines are added to guide the eye.

polyelectrolytes are present at the same time, F8BTBA in the oil phase and PDAD-MAC in the water phase, a decrease of the interfacial tension results; after 10^4 s, $\gamma = 7$ mN/m, indicating a strong co-adsorption.

These results suggest that electrostatic attractions between the two oppositely charged polymers cause their accumulation and complexation at the interface. If this behavior originates from electrostatic interactions alone, it should be sensitive to the ionic strength due to screening of attraction between oppositely charged ions or ionic groups. Indeed, increasing the ionic strength in the aqueous phase results in a decrease in the interactions, as shown by the significant increase of the interfacial tension, from 7 mN/m at 0 mM NaCl to approximately 20 mN/m at 100 mM NaCl (circles in Figure 2.2b); as a control we verify that the addition of salt to the

water phase does not change the behavior of F8BTBA alone (diamonds in Figure 2.2b). While the sensitivity to ionic strength suggests an electrostatic origin of the adsorption, we cannot completely suppress the complexation but only increase the timescale to reach equilibrium through the addition of salt up to 100 mM (Figure 2.2a). It is established that the critical salt concentration at which bulk coacervation vanishes depends on the charge density of the polyelectrolytes, the chain length of the polyelectrolytes, the type of salt and the specific chemistry.[19] It might therefore be possible that a higher salt concentration or another type of salt would prevent the complexation.

Our anionic polymer, F8BTBA, carries pH-sensitive benzoic acid groups, with a pK_a between 2.4 (pK_a of a benzoic acid in a π-conjugated system[20]) and 4.2 (pK_a of benzoic acid alone[20]); this should, in principle, make it possible to completely suppress electrostatic complexation by full protonation of the anionic polymer. Indeed, this is what we observe: for pH values below 3.5, the interfacial tension adopts its value for the bare oil–water interface and the complexation is entirely suppressed, as shown in Figure 2.2c. Upon increasing pH, the interfacial tension decreases to adopt a steady value around 7 mN/m. This result suggests that the driving force for complexation is an entropy gain through the counterion release.

The formation of the complex appears to occur in two distinct stages, as illustrated by time-dependent interfacial tension measurements after creating a bare interface (Figure 2.2d). Initially, we observe a fast diffusion-limited adsorption process, characterized by an exponential decay of the interfacial tension (dashed line), followed by a much slower logarithmic process (dotted line). During the first, rapid stage, the polymers diffuse from the dilute bulk solutions and co-adsorb at the interface. During the second stage, more and more material from the oil and the water phases is recruited. This stage, characterized by slow "glassy" dynamics, results from the increasingly hindered interpenetration of the two oppositely charged polymers and has also been observed for complex coacervation in bulk.[21] These data indicate the formation of a thick complex skin at our oil-water interface.

This is further supported by brightfield images of macroscopic droplets during complexation, as shown in Figure 2.3. Over time, the droplet, in transmission illumination, becomes less and less transparent, which indicates the slow formation of the skin. Surprisingly, the hindered light transmission across the droplet suggests that this layer is inhomogeneous on optical length scales, which might be due to the slow relaxation of the complexes.[21] The changes in the droplet shape with time also suggest that even after 48 hours equilibrium is not yet reached.
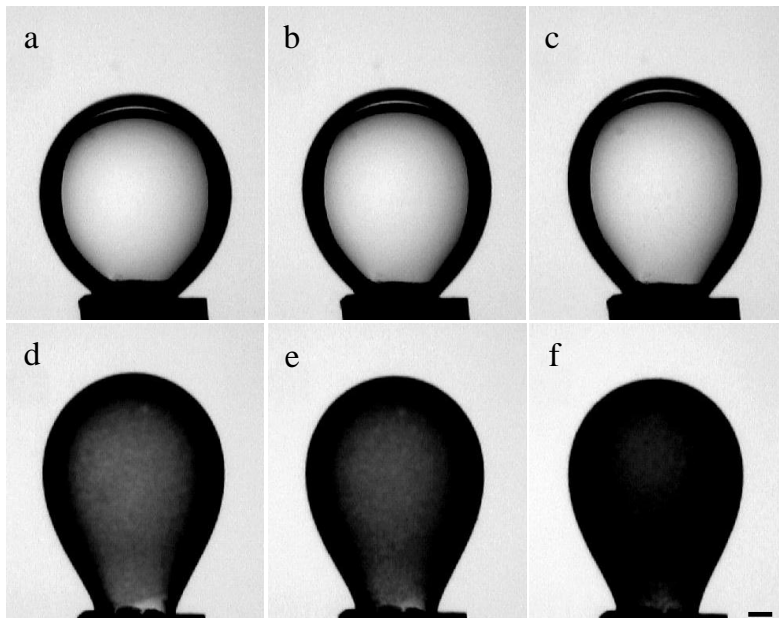
Figure 2.3: Brightfield images of a PDADMAC water droplet in a F8BTBA oil phase during complexation: (a) 0 h, (b) 0.5 h, (c) 1 h, (d) 18 h, (e) 24 h, (f) 48 h. Scale bar indicates 500 μm.

2.3.2   Complex localization

To visualize the interfacial complexation, we use emulsion droplets as microscopic interfacial templates. We use fluorescently labeled cationic poly(L-lysine) (PLL), which displays the same behavior as PDADMAC as confirmed by interfacial tension measurements, and a water:oil ratio of 1:9 by volume. Confocal microscopy images of these droplets clearly show the positive accumulation of both polyelectrolytes, F8BTBA and PLL, at the interface (Figures 2.4a–c). The high intensity of the fluorescence at the interface, as compared to that in the bulk oil and water phases, provides a strong indication for the formation of a thick complex layer at the interface. A co-localization analysis gives further evidence, within optical resolution (200 nm), that both polymers are interpenetrated within this surface layer (Figure 2.4d). In these images no large inhomogeneities are observed.

In many applications, oil-in-water emulsions are used, yet certain applications require inverted emulsions. The empirical Bancroft rule suggests that water-in-oil emulsions are produced by emulsifying agents that are more soluble in the oil phase than in the water phase.[22] In our case, the interfacial complex forms a new phase at the interface and does not seem to have a strong preference for any of the oil
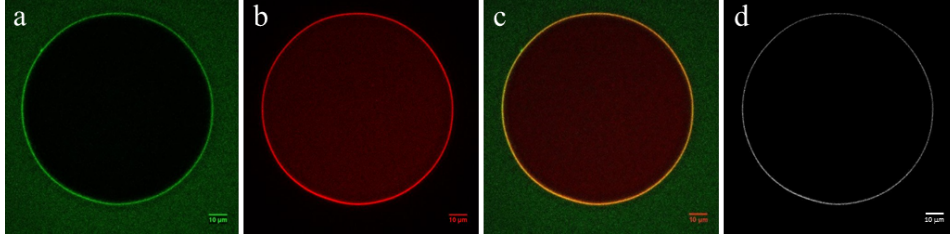
Figure 2.4: Confocal microscopy images of a water droplet in a continuous decalin/tetrachloroethylene phase, stabilized by a polyelectrolyte complex formed at the oil-water interface; (a) the anionic oil-soluble polymer F8BTBA is given in green, (b) the cationic water-soluble polymer PLL in red, (c) combined channels, (d) co-localization analysis showing high intensity where both green and red channels are co-localized and low intensity where there is no co-localization. Scale bars indicate 10 μm.
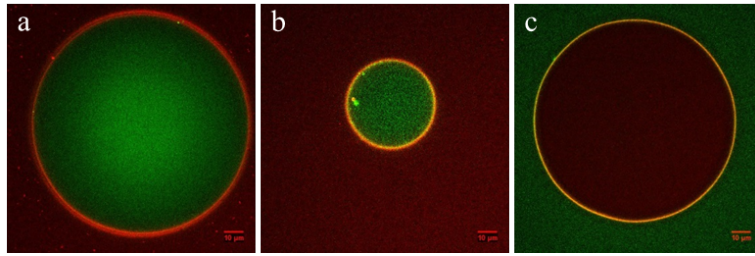

Figure 2.5: Confocal microscopy images of emulsion droplets at different water:oil volume ratios with (a) 9:1, oil-in-water emulsion; (b) 5:5, oil-in-water emulsion; (c) 1:9, water-in-oil emulsion. Scale bars indicate 10 μm.

and the water phases. To confirm this, we vary the water:oil ratio. It appears that the type of emulsion that is formed depends only on the ratio of water and oil. The phase present in the highest quantity is the continuous phase, as shown in Figure 2.5. Therefore, inverted emulsions can also be stabilized by the same electrostatic complex.

2.3.3 Emulsion stabilization and breaking on-demand

The electrostatic co-assembly of two oppositely charged polyelectrolytes at the interface of an emulsion droplet can be used to stabilize these emulsions against coalescence. With this approach we can prepare oil-in-water and water-in-oil emulsions that are stable for at least several weeks: the mean droplet diameter $D_{3,2}$ is constant at 100 +/- 10 μm for at least 30 days. To quantify the stability of these complex-stabilized droplets against coalescence, we measure the critical disjoining
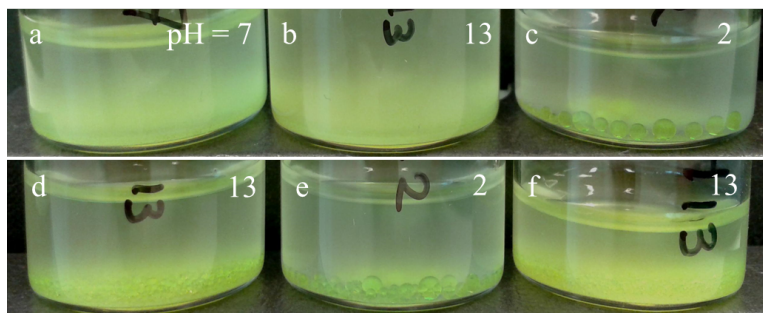
Figure 2.6: Oil-in-water emulsion stabilized by a PDADMAC-F8BTBA complex at various successive pH values showing reversible breaking and re-emulsification (a-f).

pressure.[17] Upon pressing two emulsion droplets together, a restoring force, called the disjoining pressure, acts on the thin film separating the two interfaces. Once the applied pressure exceeds the critical value of this disjoining pressure, coalescence may occur. For the complex-stabilized droplets, we find a critical disjoining pressure of 580 Pa. While this indicates that dilute emulsions are stable, this is not sufficient to create emulsions that are stable at high concentrations. We can significantly improve the emulsion stability against coalescence through crosslinking of the complex after it has formed. Using a standard amidation reaction between the carboxylic groups on F8BTBA and the primary amines on PLL we crosslink the interface and find at least an order of magnitude increase in the critical disjoining pressure, to 6780 Pa.

Although this enhanced stability may be beneficial in some cases, in other applications, for example when using emulsions for liquid phase extraction, on-demand breaking of the emulsion is a requirement. From the interfacial tension measurements, we concluded that the complexation is suppressed at pH < 3.5 (Figure 2.2c); this effect can also be used to our advantage. When the pH of a complex-stabilized emulsion, prepared at neutral pH, is rapidly decreased below 3.5, we observe an almost instantaneous demixing of the emulsion into two macroscopic phases. Moreover, this process is fully reversible (Figure 2.6): increasing the pH again, by addition of NaOH and mild shaking, leads to instant restoration of a stable emulsion. This process can be repeated several times.

2.4   Conclusion

Electrostatic attractions across an interface provide a convenient method to induce interfacial adsorption of surface-inactive polyelectrolytes. The presence of only one

of the polyelectrolytes causes depletion at the interface whereas the presence of an anionic polyelectrolyte in the oil phase and a cationic polyelectrolyte in the water phase leads to a significant surface accumulation. In principle, this strategy could be used for any combination of oil-soluble and water-soluble oppositely charged polyelectrolytes.

Due to the electrostatic nature of the complex that is formed across the oil-water interface, it can be manipulated both by pH and ionic strength. In this way, emulsions can be stabilized for several weeks, yet can be broken and reformed on-demand using environmental triggers. Using this approach, tuning of the strength of the interfacial complex is possible, either through pH-triggered emulsion breaking and formation or through a chemically cross-linked complex skin.

Electrostatic co-assembly is a promising route to impart functionalities to emulsions, such as biological functionality, by interfacial complexation of any charged water-soluble biopolymer, e.g. DNA or enzymes, or catalytic activity through the use of colloidal particles such as those formed from hematite or titania.

References

[1] E.J.W. Verwey, *J. Phys. Chem.*, 1947, **51**, 631–636.

[2] P. Luckham, B. Vincent, C.A. Hart, and T.F. Tadros, *Colloids Surf.*, 1980, **1**, 281–293.

[3] P. Luckham, B. Vincent, J. MacMahon, and T.F. Tadros, *Colloids Surf.*, 1983, **6**, 83–95.

[4] E. Spruijt, H.E. Bakker, T.E. Kodger, J. Sprakel, M.A. Cohen Stuart, and J. van der Gucht, *Soft Matter*, 2011, **7**, 8281–8290.

[5] J. Wang, A.H. Velders, E. Gianolio, S. Aime, F.J. Vergeldt, H. Van As, Y. Yan, M. Drechsler, A. de Keiser, and M.A. Cohen Stuart, *Chem. Commun.*, 2013, **49**, 3736–3738.

[6] P. Bartlett and A.I. Campbell, *Phys. Rev. Lett.*, 2005, **95**, 128302.

[7] M.E. Leunissen, C.G. Christova, A.P. Hynninen, C.P. Royall, A.I. Campbell, A. Imhof, M. Dijkstra, R. van Roij, and A. van Blaaderen, *Nature*, 2005, **437**, 235–240.

[8] J.V.M. Weaver, S.P. Rannard, and A.I. Cooper, *Angew. Chem. Int. Ed.*, 2009, **48**, 2131–2134.

[9] D.J. Clark and T. Kimura, *J. Mol. Biol.*, 1990, **211**, 883–896.

[10] R.J. Stewart, C.S. Wang, and H. Shao, *Adv. Colloid Interface Sci.*, 2011, **167**, 85–93.

[11] H.G. Bungenberg de Jong and H.R. Kruyt, *Proc. K. Ned. Akad. Wet.*, 1929, **32**, 849–856.

[12] L.S. Jourdain, C. Schmitt, M.E. Leser, B.S. Murray, and E. Dickinson, *Langmuir*, 2009, **25**, 10026–10037.

[13] I.M. Tucker, J.T. Petkov, C. Jones, J. Penfold, R.K. Thomas, S.E. Rogers, A.E. Terry, R.K. Heenan, and I. Grillo, *Langmuir*, 2012, **28**, 14974–14982.

[14] S. Ogawa, E.A. Decker, and D.J. McClements, *J. Agric. Food. Chem.*, 2003, **51**, 2806–2812.

[15] Y.S. Gu, A.E. Decker, and D.J. McClements, *Langmuir*, 2005, **21**, 5752–5760.

[16] B. Bao, L. Yuwen, X. Zheng, L. Weng, X. Zhu, X. Zhan, and L. Wang, *J. Mater. Chem.*, 2010, **20**, 9628–9634.

[17] G. Narsimhan, *Colloids Surf.*, 1992, **62**, 41–55.

[18] A.H. Demond and A.S. Lindner, *Environ. Sci. Technol.*, 1993, **27**, 2318–2331.

[19] J. van der Gucht, E. Spruijt, M. Lemmers, and M.A. Cohen Stuart, *J. Colloid Interface Sci.*, 2011, **361**, 407–422.

[20] R. Wegscheider, *Monatsh. Chem.*, 1916, **37**, 219–250.

[21] E. Spruijt, J. Sprakel, M. Lemmers, M.A. Cohen Stuart, and J. van der Gucht, *Phys. Rev. Lett.*, 2010, **105**, 208301.

[22] W.D. Bancroft, *J. Phys. Chem.*, 1913, **17**, 501–519.

Chapter 3

Complex coacervates at liquid interfaces: a Self-Consistent Field analysis

In this chapter, we use the Scheutjens-Fleer self-consistent field theory to study polyelectrolyte complexation across an oil-water interface. We focus on the formation and the stability of such interfacial coacervate phase as well as its lateral homogeneity. The stability of the coacervate increases with decreasing ionic strength and increasing specific affinity between the oppositely charged polymer segments. Remarkably, the coacervate exists also in the absence of such specific affinity. The complex formation is driven by the polyelectrolyte selectivity for the oil or the water phase. An unusual wetting scenario presents itself in these systems due to two distinct length scales of interactions. On the segmental length scale the oil-water interface wants to be wetted by the complex coacervate and a jump-like transition takes place from a microscopically thin to a mesoscopically thin film. However, the mesoscopically thin film is subject to long-ranged attractive electrostatic interactions and cannot grow to macroscopic dimensions. As a result, a pseudo-partial wetting scenario unfolds. The bulk correlation length controls the thickness of the mesoscopically thin film and therefore the wetting transition takes place extremely close to the bulk critical point. These results explain experimental observations for the formation of the coacervate phase across the oil-water interface.

3.1 Introduction

Polyelectrolytes are polymers that contain ionizable groups, which in water dissociate into charged polymer chains and small counterions. They are named polycations when they carry positive charges and polyanions when they have negative charges. Mixing two solutions of oppositely charged polyelectrolytes leads to a macroscopic phase separation, a process known as complex coacervation.[1] If one of the polyelectrolytes contains a neutral water-soluble block, the macroscopic phase separation becomes restricted to the colloid domain with the formation of micelles.[2,3] Fundamentally, the formation of these polyelectrolyte complexes is an ion-exchange process; the polymer-counterion pairs are replaced by polymer-polymer ion pairs. The main driving force is the entropy gain through the counterion release often augmented with an enthalpy gain through the shorter distances between the oppositely charged groups of the polyelectrolytes compared to the distances between the polyelectrolytes and their counterions.[4] Non-ideal solvency effects, i.e. when the polyelectrolytes in the absence of charges have only a limited solubility in the water, often give an additional enthalpic driving force.

Recently, we reported a new strategy of polyelectrolyte complex formation across the oil-water interface.[5] We used oppositely charged polyelectrolytes, each of the polyelectrolytes being selective for only one of the two phases; the polyanion is selective for the oil phase whereas the polycation is selectively dissolved in the water phase. When only one of the polyelectrolytes is present in the system, the polyelectrolyte is depleted from the oil-water interface. However, when both polyelectrolytes are present, they become surface active. A polyelectrolyte complex film then develops at the oil-water interface and stabilizes oil droplets in water for several weeks. As the oil and the water phases are reservoirs of the polyelectrolytes and as there appears no obvious stopping forces for the growth of the complex, a thick complex layer can develop at the oil-water interface over time. We used a pendant drop tensiometer to follow the kinetics of adsorption of these polyelectrolytes at the oil-water interface; this technique also allowed us to do macroscopic observations of a water droplet in oil over time. We observed, in transmission illumination, a dramatic loss of transparency of the water droplet in time. This scattering of the light suggests spatial inhomogeneities in the coacervate film.[6] This chapter tries to shed light on this darkening issue by evaluating the formation and the stability of a coacervate film that forms across the liquid-liquid interface.

Molecular scale observations of the formation of a complex coacervate phase at an oil-water interface are not trivial. Many complications arise from the number of components, such as two solvents, two polyelectrolytes, etc. and the multitude of control parameters, such as pH, salt concentration, etc. Any experimental ob-

servation of the formation of the coacervate phase at the liquid-liquid interface is therefore influenced by a large number of parameters and this may hamper a true molecular level interpretation of the observed phenomena. In such situations, molecular modeling is of more than average interest. Molecular dynamics or Monte Carlo simulations are from first principle the best options to do so. However, to date there are no such simulations available. This is not too surprising because interfaces are challenging for simulations due to the huge time and length scales involved. The computation complications increase when in addition to the simple liquid-liquid interface there are polyelectrolytes with corresponding long-range interactions in the system.[7] In such a situation it is natural to consider approximate models. These models invariable rely on a mean-field approximation of some sort. Here we will turn our attention to self-consistent field (SCF) models. In doing so one can formulate a (mean field) free energy in terms of potentials and densities. The optimization of this free energy results in the SCF machinery. On the mean-field level we obtain structural as well as thermodynamic information for the system of interest.

Below we will present a SCF model in which a coacervate phase of oppositely charged polymers can be studied. Similar to our experiment, this model features a two-phase system; the two solvents are referred to as oil and water. One of the polyelectrolytes is preferentially dissolved in the oil phase and the other one in the water phase. As each solvent should remain electroneutral, the polyelectrolytes are accompanied by their counterions. Upon complexation, the counterions are allowed to distribute in both phases; this release can give an entropic driving force to the complexation. Additionally to entropic contributions, enthalpic ones such as hydrogen bonding, solvency effects, etc. may also play a role.

The Scheutjens−Fleer SCF method uses a mean-field approximation, the method therefore does not account for all the contributions to the free energy. More specifically it is commonly believed that the lack of correlations prevents one to study the complexation of oppositely charged polyelectrolytes.[8] One way to see the issue is to realize that with this method all polymers are Gaussian chains in the reference phase. Hence also the polyelectrolytes remain ideal in the reference state and such chains do not need to accumulate any counterions in their vicinity: in the reference phase, both the polymers and the ions are homogeneously distributed. As a consequence, upon polyelectrolyte complexation from just one solvent (e.g. complexation from the water phase) the counterion release effect does not occur in the calculations. Moreover, the close to electroneutrality keeps the electrostatic potentials low throughout the coacervate phase and hence the segments have a negligible electrostatic contribution to the driving force for co-assembly. In the absence of electrostatic driving forces the chains refuse to accumulate in a dense

polymer phase. One way to correct for the missing correlations or equivalently the missing ion-release effect is to impose an attractive interaction parameter for the interaction of oppositely charged segments. In such case it makes sense to completely disregard the electrostatics. This approach has been used to model the formation of complex coacervate core micelles. [9] It appears that for coacervate formation across an interface we have to reconsider our standpoint regarding the applicability of the SCF theory to analyze the coacervate formation.

When there is an interest in the composition of the three phases, oil-rich, water-rich and coacervate, it is not necessary to account for the interfaces. Indeed, it is possible to simplify the calculations and develop a Flory-Huggins model with the additional requirement that each phase is electroneutral. [10,11] At equilibrium, the chemical potential is the same for each molecular species in all phases. In addition to the molecular composition of each phase, we also obtain the so-called Donnan potential. In this paper we do not follow this route; instead, we incorporate the Poisson equation in a one-gradient approximation. The local electroneutrality in each bulk phase is guaranteed and our procedure gives the same phase diagram of the mathematically simpler Flory-Huggins model sketched above. However, compared to this method, we obtain segment density and electrostatic potential profiles throughout the system and across the interfacial regions. The SCF equations also allow an evaluation of the interfacial tensions of all interfaces and hence we can predict the wetting scenario for the system. According to the classical wetting theory, which accounts for short-range interactions only, when a new phase develops between two other phases there are two possible scenarios. The new phase appears either as a drop, partial wetting case, or as a film, complete wetting case, at the liquid-liquid interface. By tuning some control parameter, one can induce a wetting transition from partial to complete wetting or *vice versa*. However, our system is more complex as besides the interactions on the segment-level we also have electrostatic interactions in the film, which operate on the mesoscale and therefore we should anticipate wetting phenomena beyond the ones covered by the classical theory. We will show that the coacervate film has a complex wetting pattern and corresponding intricate issues regarding the lateral homogeneity.

The remainder of this chapter is the following. To anticipate the discussion about non-classical wetting scenarios, we start by outlining both the classical wetting theory [12–15] with interactions on short length scales and the pseudo-partial wetting scenario [16] applicable for systems with interactions on competing length scales. We then present the premises of the self-consistent field theory while discussing the molecular models that are used; we refer to the appendix for more details. We divide the result section into three subsections. In the first subsection we show that the adsorption of a single polyelectrolyte at a liquid-liquid interface

has an unusual dependence on the polymer concentration. In the second part we consider two polyelectrolytes oppositely charged and dissolved in the complementary solvent. This system is used to analyze the formation and stability of the coacervate phase. In the third and final subsection we deal with systems that are asymmetric with respect to the concentrations. For these systems we consider adsorption isotherms, which reveal an unusual wetting scenario, known as pseudo-partial wetting in the literature. Finally, in the discussion we return to the experimental observation that triggered this self-consistent field analysis.

3.2   Wetting

Wetting usually refers to a system containing three phases with typically a substrate S and a binary liquid A and B with a solubility gap. When the two liquids coexist there is a phase α, rich in component A, and a phase β, rich in component B. The bulk binodal specifies exactly how much of B is dissolved in A and *vice versa*. Using dimensionless concentrations we refer to the binodals as volume fractions $\Phi_B^{\#}$ and $\Phi_A^{\#}$. The interfacial tension of the interface between the phases α and β is given by $\sigma_{\alpha\beta}$. In this case the wetting theory focuses on how the two phases interact with this substrate. Basically there are three cases: (i) Phase α prefers to sit next to S and there are two interfaces $S - \alpha$ and $\alpha - \beta$, (ii) Phase β sits next to S and we have again two interfaces $S - \beta$ and $\beta - \alpha$ and (iii) There is a drop of either phase α or β at the interface and we now have three interfaces $S - \alpha$, $S - \beta$ and $\alpha - \beta$. In wetting language (i) and (ii) refer to complete wetting of α and β, which is equivalent to complete drying of β and α respectively, and (iii) refers to partial wetting.

In the current system we have three liquids and we will adopt a slightly different nomenclature. The two bulk phases are rich in A and B (loosely referred to oil and water) and will be referred to as phases α and β respectively. The complex coacervate phase is referred to as γ. We consider the wetting problem how the three phases are organized. In the complete wetting case we have two interfaces namely $\alpha - \gamma$ and $\gamma - \beta$ whereas in the partial wet state we have three interfaces $\alpha - \gamma$, $\beta - \gamma$ and $\alpha - \beta$ (see Figure 3.1). The interfacial free energies can be such that $\sigma_{\alpha\beta} < \sigma_{\alpha\gamma} + \sigma_{\beta\gamma}$ and then we have partial wetting; complete wetting obeys to $\sigma_{\alpha\beta} > \sigma_{\alpha\gamma} + \sigma_{\beta\gamma}$. It is common to define a spreading parameter:[17]

$$S = \sigma_{\alpha\beta} - \sigma_{\alpha\gamma} - \sigma_{\beta\gamma} \tag{3.1}$$

A positive S corresponds to a complete wet state whereas a negative S represents a partial wet state; the wetting transition occurs for $S = 0$. There exists a
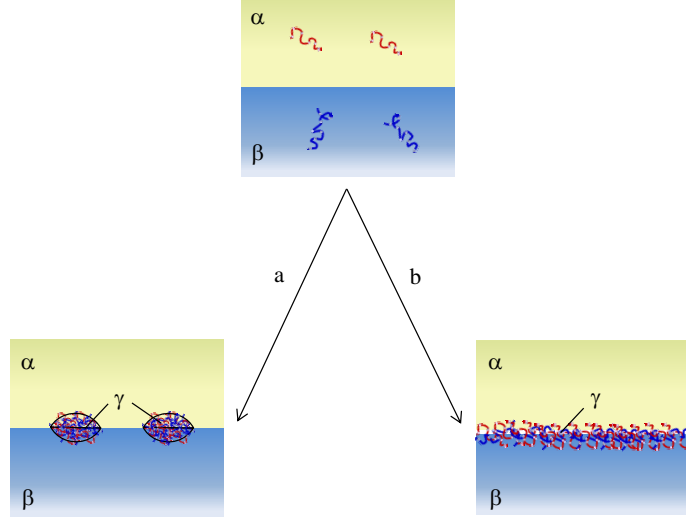
Figure 3.1: Schematic representation of: (a) Partial wetting, three interfaces $\alpha - \gamma$, $\beta - \gamma$ and $\alpha - \beta$ co-exist; (b) Complete wetting, two interfaces $\alpha - \gamma$ and $\beta - \gamma$ co-exist.

strong correlation between the spreading parameter and the contact angle as specified by Young for the solid substrate case and by Neumann for the droplet case. Here we will not go into these details. It must be clear that we consider macroscopic interfaces and we disregard curvature effects and therefore the evaluation of S strictly takes place at the specified binodal concentrations in all coexisting phases. In the three-phase systems we have in each phase three such concentrations.

The transition from complete wetting to partial wetting is a phase transition as the number of interfaces in the system changes by one.[13,18] Only in the complete wetting case the lateral homogeneity of the coacervate film is guaranteed and this explains why our interest is drawn to these transitions. Classical wetting theory makes a distinction between first and second order wetting transitions. The model for classical wetting theory is the regular solution model wherein monomeric molecular species experience short-range, nearest-neighbor (Flory-Huggins) type interactions only. Hence longer ranged van der Waals forces nor longer ranged electrostatic interactions are considered. We allow concentration gradients of all components in the z-direction. In this regular solution model the start is an $\alpha - \beta$ interface; we have a phase α in equilibrium with a phase β and we have $\varphi_A(z)$ and $\varphi_B(z)$ profiles. Without loss of generality we have phase α at low z-coordinates. For the sake of our arguments we consider here the case that the wetting phase is composed of one type of molecule, referred to by C, where it is clear that in

our results the component C is in fact replaced by a pair of oppositely charged polymers. The idea is to add to this system the component C, which will eventually form the γ phase. Hence, we go from a two-phase to a three-phase system. The idea is to study so-called adsorption isotherms of the C component onto the $\alpha - \beta$ interface and focus on the formation of the new phase γ. From a family of isotherms, obtained by varying some wetting control parameter, we can deduce the order of the wetting transition.

Adsorption of component C at the $\alpha - \beta$ interface requires a strategy to quantify the adsorbed amount. Here we use the Gibbs excess Γ_C, which is computed with respect to a Gibbs plane z^{Gibbs}.

$$\Gamma_C = \sum_{z=0}^{z^{\mathrm{Gibbs}}} \varphi_C(z) - \varphi_C^{\alpha} + \sum_{z=z^{\mathrm{Gibbs}}}^{M} \varphi_C(z) - \varphi_C^{\beta} \qquad (3.2)$$

In the SCF part our z-coordinate has discrete values $z = 0, 1, 2, \cdots, M$ and that is why we assume here the lattice model as well. The layer $z = 0$ is a coordinate deep in the α phase while the layer $z = M$ is a coordinate deep in the β phase. Similar equations can be used to find the excess quantities for the other two components in the system. It is clear that the resulting Gibbs excess depends on the value of the Gibbs plane. We choose the Gibbs plane such that the Gibbs excess is zero for the B component. In an incompressible system we then have $\Gamma_C = -\Gamma_A$. In general when we add an amount of C to the system we will obtain a Gibbs excess Γ_C and two bulk concentrations φ_C^{α} and φ_C^{β}. As the two bulk concentrations are coupled (they correspond to the same chemical potential) we can again without loss of generality take the β-phase as our 'bulk'. Upon gradual increase of the amount of C in the system we record so-called adsorption isotherms i.e. we record the dependence $\Gamma_C \varphi_C^{\beta}$.

In reality Γ_C is an increasing function of φ_C^{β}. In the (mean-field) regular solution model one can have multiple values of Γ_C for a given bulk concentration. This occurs for example when the isotherm exhibits a van der Waals loop or when the isotherm enters the super-saturated region and we should know how to interpret these loops. To cut a long story short, we can read from the isotherms the wetting scenario. Indeed, upon increasing the bulk concentration φ_C^{β}, the adsorbed amount increases smoothly and diverges when the bulk concentration tends to the binodal value Φ_C^{β}. The system is in the complete wetting state: all possible film thicknesses are stable and when the saturation value is reached the film is macroscopically thick. Alternatively, when the isotherm crosses the binodal at a finite adsorbed amount, the system may be in the partial wet state and not all film thicknesses are stable. The isotherm then typically continues with a loop and only returns to the binodal at sufficiently large adsorbed amounts i.e. in the limit $\Gamma_C \to \infty$. This limiting

value can be approached from the direction of the super-saturated solution (that is from the 'right') or from the under-saturated solution (that is from the 'left').

Let us denote the adsorbed amount at the first crossing of the adsorption isotherm with the binodal as $\Gamma_C^{\#}$ and assume that we have a control parameter by which we can influence the wetting state. Our interest is in how $\Gamma_C^{\#}$ goes from a finite value to the infinite value upon a change of the control parameter. If the isotherm comes from the 'right' we typically find that $\Gamma_C^{\#}$ grows gradually towards infinite upon the approach of the wetting point. This transition is known as second order or critical wetting. By contrast, when the isotherms come from the 'left', we see that $\Gamma_C^{\#}$ remains finite below the wetting transition and then suddenly jumps to infinite at the wetting transition. The reason for this behavior is the van der Waals loop in the isotherm. When the transition point (as found by a Maxwell construction[19]) that corresponds to the adsorption loop occurs at the binodal condition, we witness a jump in the isotherm from a microscopic thick to a macroscopic thick film. This wetting transition is thus of first-order type. Upon a further increase of the control parameter to even better wetting states, the loop in the isotherm occurs at a bulk concentration below the binodal value. Then at a given bulk volume fraction of C the adsorbed amount jumps from a microscopic to a mesoscopic value. This jump is called a prewetting step and always takes place off-coexistence. Prewetting steps are the hallmark of a first-order wetting transition. After the prewetting step the isotherm diverges upon the approach towards the binodal value, indicating complete wetting.

We may construct a so-called wetting phase diagram with on the x-axis the control parameter value and on the y-axis the chemical potential at which the prewetting step is found. In this phase diagram the prewetting points are collected in a prewetting line, which starts at the wetting transition (when the transition occurs at the binodal value) and ends at the prewetting critical point. Below we will construct such wetting phase diagram. Going to even better wetting conditions leads to isotherms that do no longer have a van der Waals loop and the isotherm becomes monotonic increasing as a function of φ_C^{β}; the adsorbed amount smoothly diverges upon increasing the concentration of the wetting component up to the binodal value.

There exists only few guidelines on how to change the control parameter to go from a partial wet state towards a complete wet state. Cahn argued that such a wetting transition should occur when the system is closer and closer to the bulk critical point for the wetting component.[18] In our system the argument is easily illustrated by looking at the spreading parameter S. So our starting point is sufficiently far from such a critical point for which it happens that $S < 0$, that is the interfacial tension $\sigma_{\alpha\beta}$ is larger than the sum $\sigma_{\alpha\gamma} + \sigma_{\beta\gamma}$. When the system goes

towards the situation that the γ phase no longer exists, the γ phase becomes closer and closer to either α or β or closer to both of them. As a result, the interfacial tensions with the γ phase become smaller and smaller and the value of S quite naturally increases and becomes zero; the interface between α and β will not become critical during this change of the control parameter.

So far, we have discussed the classical wetting theory valid for short-ranged interactions only. However, we anticipate a more complex wetting scenario due to the presence of polyelectrolytes in our system. Additionally to the nearest-neighbor contact energies, we also have electrostatic interactions that operate on the length scale of the Debye length, which easily exceeds the monomer length scale. In such competing length scale system, it may happen that interactions on the micro-scale signal complete wetting and the film is allowed to thicken but then on the longer length scale, other interactions take over and the system remains partially wet. Indeed, the trend on the longest length scale will ultimately control the macroscopic behavior. In the literature such interactions with competing length scales resulting in the frustrated wetting state is referred to as pseudo-partial wetting.[16,20] A key challenge is to understand why (apparently) a mesoscopically thick film can be stable, or in other words why the layer does not thicken spontaneously to macroscopic values. Below we will argue that there is an electrostatic attraction across the coacervate phase: the interfaces on both sides of the coacervate have opposite charges and therefore the interfaces are electrostatically attracted to each other.

To the best of our knowledge we do not know a report in the literature wherein the Cahn argument is tested in the context of the pseudo-partial wetting scenario. In such scenario there is a mesoscopically thin coacervate film at the oil-water interface in combination with drops of the same material. Upon approaching the critical point both the mesoscopic thin film and the droplets have comparable interfaces. However, the mesoscopic film is thin and close to the critical point, the width of one (or both) interfaces increases; the electrostatic attraction, which keeps the coacervate film thin, is counteracted by the increase of width of the interface. In other words, the bulk correlation length takes control over the thickness of the mesoscopically thin film and it is unclear if the wetting transition proceeds the bulk critical point.

3.3   Self-Consistent Field Theory

It is often believed that the mean-field approximation renders the self-consistent field theory ineffective to study polyelectrolyte complexation. The argument is that in this approach one cannot recover the entropy gain due to the release of counterions. This argument is accurate when complexation takes place from a single

solvent and when the driving force is purely entropic in nature. However, when we consider a pair of solvents (oil/water), which have a solubility gap and when a pair of polyions with opposite selectivity is used, there are several scenarios for which the ion release effect is in reasonable approximation accounted. Apart from this entropic contribution, SCF will account for (sometimes sneakingly hidden) enthalpic contributions, which can contribute to the co-assembly. Hence the SCF theory is effective to study the coacervate formation at the interface between two immiscible liquids.

In this study, we use the self-consistent field theory developed by Scheutjens and Fleer[21,22] and later elaborated by Leermakers and Scheutjens.[23] Complete details about the method can be found in the Appendix. In the following we summarize the main approximations while giving the details about the model implemented in this work.

Lattice sites are used to discretise the space. The use of a lattice prevents us to consider structural details that are smaller than the discretisation length. For larger scale features, there are few adverse effects of using a lattice. Molecules, such as the solvents, the ions and the polymers are considered to be composed of segments. The size of the segments is taken identical to the characteristic length of a lattice unit i.e. a segment exactly fits on a lattice site. To evaluate the mean-field free energy one needs to evaluate the single-chain partition functions. We use the freely-jointed chain model to evaluate these. We further account for the excluded volume interactions using the short-range Flory-Huggins interaction parameters. The number of segment-segment contacts are approximated using the well-known Bragg-Williams approximation, that is the number of contacts is based on the volume fraction of segments in a given lattice layer. Hence segment-segment correlations are ignored. From these volume fraction profiles it is trivial to find the charge density profiles. These charge density profiles enter in the Poisson equation to obtain the electrostatic potentials profile, which feature, as in the Poisson-Boltzmann theory, in the segment potentials. An incompressibility condition is implemented: the sum over all volume fractions add up to unity (at each coordinate). Such compressibility relation is necessary to select a relevant SCF solution of the system of interest.

We consider a system with a water-rich phase, an oil-rich phase and in between a planar interface. The adsorption of polyelectrolytes at this interface is assumed to take place in a laterally homogeneous way. Main density gradients are therefore expected to be perpendicular to the interface and less important density fluctuations occur parallel to the interface. This motivates the implementation of a mean-field approximation parallel to the interface, which renders the density gradients to be one dimensional, perpendicular to the interface. Hence lattice layers are numbered $z = 1, 2, \cdots, M$. Typically the lattice contains $M = 150$ layers and the interface

46

is roughly positioned near $z = M/2$. The oil-rich phase is positioned to the left side of the interface, by default the water phase is then located at the right side of the interface. The lattice site length is set to $b = 0.2$ nm. The interfacial tensions (see Appendix for information on how these are computed) are presented in units $k_B T/b^2$. At room temperature we have a conversion by 0.1 to find the interfacial tension in N/m^2. The conversion of volume fractions ϕ_i to molar concentrations c_i is done with the relation: $c_i = k\phi_i$ and k depends on the chain volume $N_i b^3$ and Avogadro's number N_a: $k = 1/(N_i N_a b^3 1000) \approx 2 \times 10^2/N_i$.

The system encompasses of several types of molecules. Here we stick to a model that is as symmetric as possible. In the system we have two types of solvents, which we refer to as 'oil' and 'water'. We represent the oil as a linear decamer i.e. having 10 monomers with segment type O. Water is also represented by a chain that occupies 10 sites with segment type W. In part we can motivate this by recalling that water is able to form clusters through hydrogen bonding. In the SCF theory it is possible to consider the oil to have a low dielectric constant and water to have a high one however, we choose here not to implement this. Hence the dielectric constant for both solvents is, in accordance to our goal to have a symmetric system, taken identical, namely $\varepsilon = 80$.

In most of our calculations we have two types of polyelectrolytes accompanied by their counterions. We model these polyelectrolytes as linear homopolymers with a fixed length of $N = 100$ monomers. Both types of chains have the same charge density, namely 1 charge for 5 segments (more accurately, each segment has a valence of 0.2). The water-soluble polyelectrolyte has positive segments named PW and the oil-soluble polyelectrolyte has negatively charged segments named NO. We model a 1:1 electrolyte and refer to it by the monomer names Na and Cl, which have a valence of 1 and -1, respectively.

Below we will consider an oil-water interface with just one polymer i.e. the PW one with its counterion in a salt solution. After that we will add the complementary polymer with its counterion. In this complex system we will first consider systems that are fully symmetric composition wise. Hence in these cases there are equal amounts of oil and water in the system. Also the concentration of the two polyelectrolytes in the system is the same, where it is understood that the two polymers have complementary concentrations in the solvents i.e. $\varphi_{PW}^{\alpha} = \varphi_{NO}^{\beta}$. Finally, in the default case also the amount of the two ions is identical. Their concentration in the bulk phases, in such symmetric situation, obeys to $\varphi_{Na}^{\alpha} = \varphi_{Cl}^{\beta}$ and $\varphi_{Na}^{\beta} = \varphi_{Cl}^{\alpha}$. In the end of the chapter we will consider cases wherein we fix the concentration of one of the polymers and record adsorption isotherms of the other polymer. Such systems deviate strongly from the default system with respect to the concentrations but remain symmetric with respect to the other parameters.

Table 3.1: Flory-Huggins interaction parameters (χ) between various pairs of segments (W: water, O: oil, PW: cationic water-soluble polyelectrolyte, NO: anionic oil-soluble polyelectrolyte, Na: positive electrolyte and Cl: negative electrolyte).

χ	W	O	PW	NO	Na	Cl
W	0	0.6	0	0.5	0	0
O	0.6	0	0.5	0	0	0
PW	0	0.5	0	0	0	0
NO	0.5	0	0	0	0	0
Na	0	0	0	0	0	0
Cl	0	0	0	0	0	0

The short-range interactions between segments are estimated by the Bragg-Williams mean-field approximation (see Appendix). This means that the number of contacts between segments are estimated using the volume fractions. The interactions are weighted using the Flory-Huggins (FH) interaction parameters. Our strategy is to take an idealized set of Flory-Huggins χ parameters, with as few different values as possible, implementing the segregation of the two solvents and selective solvation of the polymers in their respective solvent. Again, our primary interest is in setting up a model that is also with respect to the interactions as symmetric as possible. Positive χ-values correspond to repulsive interactions and negative χ-values to attractive interactions and interactions between like segments are taken as the reference and therefore have the value zero.

Table 3.1 collects the default interaction parameters used in the symmetric situation. Referring to this table we notice $\chi_{O-W} = 0.6$, which is three times higher than the critical value for the demixing of two decamer solvents. This choice gives a relatively sharp interface between oil and water. The critical value for demixing of a polymer with length $N = 100$ and a solvent with $N = 10$ is 0.08. We do not want the positively charged polymer to dissolve in the oil nor the negatively charged polymer in the water phase. Hence poor-solvent conditions $\chi_{PW-O} = \chi_{NO-W} = 0.5$ are used. Athermal solvent conditions are used for their 'own' solvent, that is $\chi_{PW-W} = \chi_{NO-O} = 0$. Unless mentioned otherwise, we take all other interaction parameters equal to zero. For the ions this means that by default they are not selective with respect to the solvents. We will follow the same strategy for the ion solubilities. The default values are zero, but when non-zero values are used we will change the parameters such that $\chi_{Na-O} = \chi_{Cl-W}$ and $\chi_{Na-W} = \chi_{Cl-O}$; $\chi_{Na-Cl} = 0$ in all cases.

The FH parameter between the two types of polyelectrolyte segments needs a bit more attention. The default value is $\chi_{PW-NO} = 0$, which means that there

are no specific interactions between oppositely charged polyelectrolyte segments (in addition to the electrostatic interactions). It is expected that the stability of the coacervate phase is promoted with negative values of χ_{PW-NO}, the oppositely charged units are driven towards each other and suppressed by positive ones. As SCF is lacking some 'correlations' one may argue that (small) negative values of this parameter may compensate for this SCF 'error'. We show below that such *ad hoc* correction is not necessary for the formation of a stable coacervate phase across the oil-water interface. Nevertheless, we will use this parameter to modify the cohesiveness of the complex coacervate phase.

It is clear that our default system is fully symmetric. The interface is positioned exactly in the middle of the system and all properties of the system are mirrored with respect to the position of the interface. When a system parameter differs from the default case we will clearly state the deviation.

3.4   Results

Three systems will be discussed. (i) We start with a system containing only one polyelectrolyte and given salt concentrations. (ii) We then move on to the default system with oppositely charged polyelectrolytes and non-selective ions and further explore this system by imposing various solvation parameters for the ions. (iii) Finally, we study systems that are asymmetrical with respect to the polymer concentrations while keeping the ions athermal.

3.4.1   One polyelectrolyte chain at an oil-water interface

Negative adsorption results in an increase of the interfacial tension of the liquid-liquid (L-L) interface. We observed such effect experimentally and therefore concluded that when only one of the polyelectrolytes is present in the system, it is depleted from the oil-water interface whereas when both polyelectrolytes are present, they adsorb.[5] Other groups have studied the polyelectrolyte adsorption at the oil-water interface and have shown that this adsorption occurs under specific conditions. For example, poly(acrylic acid) densely packs at the oil-water interface at low pH whereas at high pH no adsorption takes place.[24] Therefore, before studying more complex systems, we need to understand which parameters influence the polyelectrolyte adsorption at the L-L interface. In this section we start off by briefly discussing what happens when only one polyelectrolyte is in the system.

The classical theory for the adsorption of uncharged polymers is well known.[25] When a polymer adsorbs at an interface, it looses some conformational entropy due to its reduced degree of freedom compared to the bulk. In the absence of energy

gain (adsorption energy), the polymer avoids the interface and a polymer depletion layer develops near the interface. By contrast, if there is an enthalpic compensation for the conformational entropy loss a polymer chain will adsorb. This adsorption energy is estimated to be around 0.2 $k_B T$ per segment. Above this value we find strong adsorption because of the cooperative nature of polymers. This adsorption transition from depletion to adsorption is known to be of the second order type, which means that the transition is smooth without coexistences or jumps.

The situation is more complex for polyelectrolytes. One complicating issue is that in polyelectrolyte systems there are in addition to the solvent always counterions and often coions in the system. When the ions are seen as ideal point charges, they are spectators i.e. they do not actively adsorb at the L-L interface because volumeless segments cannot screen the unfavorable interactions between the two solvents. However, when the ions have volume, as it is the case in our study, they are not simple spectators; they can indeed insert themselves at the interface to prevent unfavorable solvent-solvent interactions. Interestingly, in contrast to polyelectrolytes, ions do not loose any conformational entropy. The ions may therefore compete with the polyelectrolytes for the interface.

In this section we choose to study the adsorption of the hydrophilic polycation at the oil-water interface in the presence of salt. When this polycation lacks affinity for the interface, a depletion zone appears on the water-side of the oil-water interface. The counterion may enter the depletion zone. Hence a weak electric double layer develops, which fully resides in the water phase, where an excess negative charge is in the depletion zone followed by an excess positive charge. The positive charge is in part formed by the polycation (secondary adsorption) and the coions in the system. In the presence of salt the secondary adsorption of polycations is less than the depletion and thus the overall excess of the polymer should be negative for all polycation concentrations.

Our SCF predictions are condensed in Figure 3.2. Figure 3.2a shows adsorption isotherms for the polycation for different salt concentrations in the bulk phase with the default parameter settings. Clearly, we observe two different regimes. When $\varphi_{PW}^{\beta} < \varphi_S^{\beta}$ the Gibbs adsorbed amount with respect to the water component is negative: the polyelectrolyte depletes from the interface for reasons explained above. By contrast, when $\varphi_{PW}^{\beta} > \varphi_S^{\beta}$ the adsorbed amount is positive, the polyelectrolyte adsorbs at the interface. This unusual concentration dependent adsorption transition is influenced by salt, which suggests that electrostatic interactions govern the polyelectrolyte adsorption. To interpret these results, one needs to look more specifically at the ion distribution. At low polyelectrolyte concentrations, the conformational entropy loss prevents the adsorption of the polyelectrolyte. As only few ions are needed to maintain the electroneutrality in the bulk phase, the ma-
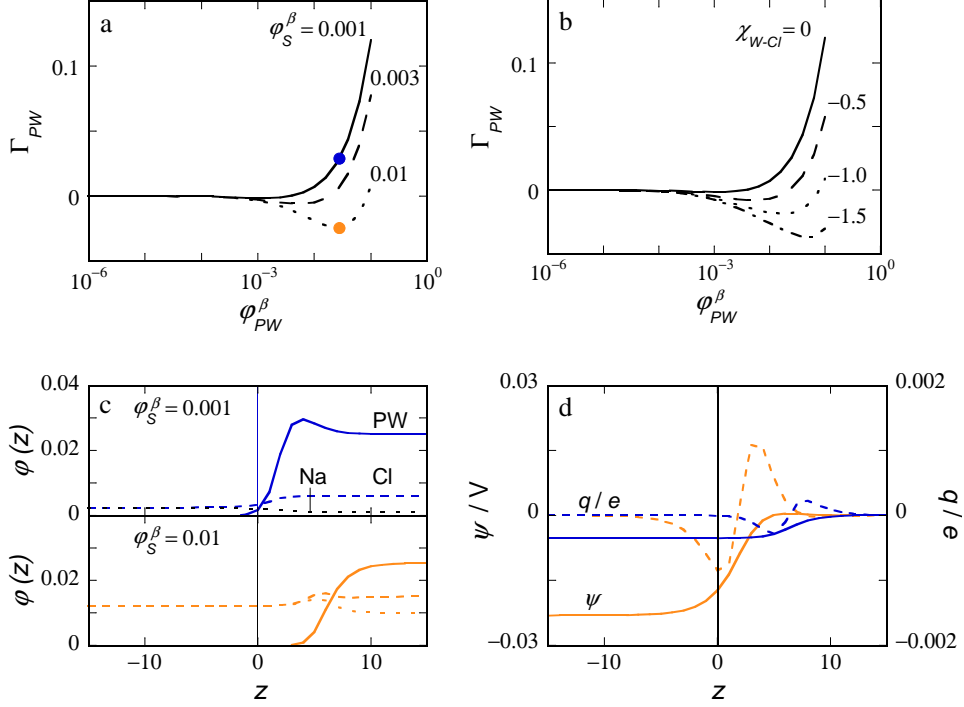
Figure 3.2: Gibbs adsorbed amount of the cationic water-soluble polymer as a function of the volume fraction of this polymer in phase β for: (a) different values of the salt concentration as indicated and fixed $\chi_{W-Cl} = 0$ (the blue and orange spots indicate the points for which in panel (c) the profiles are shown) (b) different values of $\chi_{W-Cl} = \chi_{O-Na}$ as indicated and fixed added salt concentration $\varphi_S^\beta = 0.001$. (c) Volume fraction profiles $\varphi(z)$ of the cationic water-soluble polyelectrolyte, the Cl and Na ions. (d) Electrostatic potential ψ and charge density q/e profiles. Panels (c) and (d) are the profiles for the blue and orange spots in panel (a); the vertical line represents the Gibbs plane.

jority of the ions can distribute over the whole system and both Na and Cl ions preferentially adsorb at the oil-water interface to reduce the number of unfavorable contacts between the oil and the water phases. However, this tendum adsorption does not generate a significant excess charge. The counterions (Cl) accumulate in the depletion zone and set up a weak electric double layer in the water phase. Upon increasing the polyelectrolyte concentration, the Cl ion concentration in the bulk phase increases to maintain the electroneutrality condition. At the same time the Na ions (coions) have a fixed concentration. So gradually a concentration difference of the two small ions builds up, and as both ions have the same affinity for the L-L interface, the counterion starts dominating at the interface. This surface enrichment subsequently generates a more negative electrostatic potential and the

polycation gains electrostatic energy to adsorb directly onto this layer of adsorbed counterions. Hence, the electric double layer shifts closer to the Gibbs plane but more importantly the adsorption of polycation becomes positive.

The shift of this electric double layer can be seen in Figure 3.2d. The charge distribution is zero far away from the Gibbs plane and has a characteristic double layer structure. The sum over the charge distribution equals zero as the overall system is electroneutral. The positive excess in the case of depletion is due to the excess of positive ions, which are overpopulated in the depletion region of the polymer. In the case of adsorption the excess is due to the adsorption of the polycation. Recall that the two cases are for fixed polycation concentration in the bulk. For low salt concentration the relative difference between coion and counterion concentrations is large and the L-L interface is preferentially populated by counterions and adsorption of the polycation is significant. By contrast, when the salt concentration is high, the coion and counterion concentrations are similar and the electric double layer is to the right of the Gibbs plane; the Gibbs excess of the polycation is then negative.

As can be seen from Figure 3.2d the electrostatic potential is taken to be zero far from the interface in the phase β and is negative in the phase α. With increasing salt concentration the electrostatic potential difference across the interface decreases, a phenomenon known as screening by salt.

For two points on the adsorption isotherms (blue/orange circles in Figure 3.2a), we plot the volume fraction profiles of the polyelectrolyte and the ions (one case with a negative and another case for positive excess polycation adsorption) in Figure 3.2c. Profiles for the polycation and both ions are presented and most of the features of these profiles have already been mentioned above. In the high ionic strength case the polymer is clearly depleted from the interface while in the low ionic case the polymer has a significant positive excess.

As the ions play an important role in polyelectrolyte adsorption we show also a few results for which the solvent quality of the ions deviates from athermal. Figure 3.2b reports adsorption isotherms of the polyelectrolyte for $\chi_{W-Cl} = \chi_{O-Na}$ varied from 0 to -1.5 i.e. we render the counterion more selective for the same phase as the polycation. We observe that the lower the χ_{W-Cl} is, the less the polyelectrolyte adsorbs for this range of concentrations. This is in agreement with our interpretation presented above. The affinity of the anion for the water increases and mirror-image wise the affinity for the coion for the oil phase, fewer ions adsorb at the L-L interface and therefore the adsorption transition is shifted to higher polycation concentrations.

From the above it is clear that at sufficiently high concentration the polycation is expected to accumulate at the interface. We could repeat the same calculations

with the polyanion and the result would be the same (mirror-wise): the polyanion would also adsorb at the interface at sufficiently high polymer concentration. Hence in the case that both polyelectrolytes are present in the system we should expect to find interpolyelectrolyte complexes at the interface. When only one polymer is present the adsorption layer at the L-L interface remains monomolecular in size. When both polymers are present this should not be necessarily the case instead, we anticipate the formation of a complex coacervate phase.

3.4.2   Oppositely charged polyelectrolytes at an oil-water interface

We have seen in the previous section that the presence of an oppositely charge excess at the interface drives the adsorption of the polyelectrolyte. Hence, the hydrophilic polycation is attracted by the negatively charged interface on the oil side while the hydrophobic polyanion is attracted by the positively charged interface on the water side. Both polyelectrolytes therefore adsorb at the interface and form interpolyelectrolyte complexes. In the default system both polyelectrolytes are present in the system with equal amounts. The respective counterions with athermal interactions accompany the polyelectrolytes and there is a fixed added salt concentration in the system. Let us first present a typical result for the segment density profiles and the corresponding potential and normalized charge distributions for a completely symmetric system. In Figure 3.3 we show such distributions for the case that a sufficient amount of polyelectrolytes is added so that a reasonably large complex coacervate has formed across the oil-water interface. We will later analyze its stability in more detail. Here we first focus on the structure of this coacervate film.

Figure 3.3a shows the volume fraction profiles of various molecular species for a salt volume fraction $\varphi_S^\beta = 0.001$. Clearly, we observe the co-existence of three phases with from left to right, the oil-rich phase α, the coacervate phase γ and the water-rich phase β. As in the default system $\chi_{PW-NO} = 0$, this result implies that also in the absence of specific interactions (correlation attraction) between the polyelectrolyte segments, co-assembly across the $\alpha - \beta$ interface occurs. It is tempting to argue that the driving force for this co-assembly is the counterion release. Indeed, when the two polyelectrolytes are in the bulk the corresponding counterions are 'constrained' to their respective half-spaces to neutralize the charges. Upon formation of the interpolyelectrolyte complexes, the counterions are not needed any more and hence can distribute throughout the system; the resulting entropy increase may help the formation of the coacervate phase. We will prove below that this ion release effect does not provide the main driving force in our case.
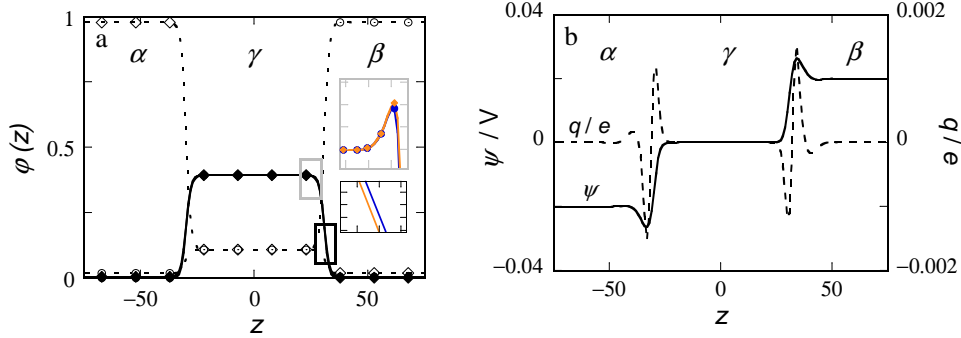
Figure 3.3: An example for a fully symmetric three-phase system with default parameter setting. (a) Volume fraction profiles φ of $\diamond$ oil, $\odot$ water, $\blacklozenge$ anionic oil-soluble polyelectrolyte, $\bullet$ cationic water-soluble polyelectrolyte for a salt concentration $\varphi_S^\beta = 0.001$. The insets give the density profiles zoomed-in on the edge of the coacervate layer; in this inset, the water-soluble polyelectrolyte is represented in blue and the oil-soluble polyelectrolyte in orange. (b) Corresponding electrostatic potential ψ in volt and dimensionless charge density q/e profiles in the system. The $z = 0$ point is chosen to be at the center of the γ phase. The amounts of polyelectrolytes are taken equal (symmetric system) and (arbitrarily) large so that the γ has a significant width. The binodal values are: $\varphi_{PW}^\alpha = \varphi_{NO}^\beta = 2.0 \times 10^{-10}$, $\varphi_W^\alpha = \varphi_O^\beta = 1.7 \times 10^{-2}$.

As the default system is fully symmetric, the γ phase contains exactly the same amounts of the two polyelectrolytes: the γ phase is at stoichiometry. Close inspection of the profiles reveals the presence of horns at the periphery of the γ phase (grey inset in Figure 3.3a), which implies that subtle adsorption processes take place at the $\alpha - \gamma$ and $\beta - \gamma$ interfaces. The two polymer distributions deviate slightly in these interfacial regions: the polycation is slightly higher in concentration near the water-coacervate interface whereas the polyanion accumulates slightly preferentially at the oil-coacervate interface (black inset in Figure 3.3a).

As can be seen from Figure 3.3a the two solvents have a finite concentration in the coacervate phase; their presence is limited to a volume fraction of about 0.1. Apparently, high amounts of solvent are rejected by the coacervate. The polycation pushes out the oil whereas the polyanion does not like the water phase. As a result, the coacervate is effectively submerged in a poor solvent and separates from the water as well as from the oil phase. We believe that these enthalpic (poor solvent) effects are a consequence of the main driving force, electrostatic interactions, for complex formation. The two ions have a very low concentration in the bulk phases ($\varphi_S = 0.001$) and their concentration is suppressed for excluded volume reasons in the coacervate phase (see below), that is why we do not present these distributions in Figure 3.3a. The ions do follow the electrostatic potential profile as in the

Poisson-Boltzmann theory and the variations of the ion profiles can be inferred from the distribution of the electrostatic potential across the system.

As our system contains oppositely charged polyelectrolytes and their respective counterions, it is of interest to look at the electrostatic potential and the charge density profiles. Let us start with the charge distributions shown in Figure 3.3b. The charge density is zero at very high z-values (phase β), at very low z-values (phase α) and also near $z = 0$ i.e. at the center of the γ phase. This means that all bulk phases are electroneutral. As mentioned already the polycation adsorbs preferentially on the coacervate-water interface and the polyanion does the same on the coacervate-oil interface; we indeed notice a local maximum/minimum in the charge density profiles at these two interfaces. To maintain electroneutrality these adsorptions are flanked by excesses of the opposite charge. That is, near the coacervate-water interface there are negative charges in excess both in the coacervate phase as well as in the water phase. These electric double layers have a decay length given by the local Debye length, which differs in the coacervate film from those in the two solvents. Most of the 'surface' charge that is generated by the polyelectrolytes is compensated in the coacervate phase and only a small part of the compensation takes place in the solvent phases.

By choice, in this graph we have set the electrostatic potential (Figure 3.3b) to be 0 at the center of the γ phase. Therefore the potential is negative in the α phase and positive in the β phase and roughly zero throughout the γ phase. The electrostatic potential has a local extremum at the two interfaces and a set of double layers develops at each boundary. We note that through the Poisson equation (see Appendix), the second derivative of the electrostatic potential is related to the charge distribution and therefore the electrostatic potential contains similar information as the charge distribution. The electrostatic potential of the coacervate-water interface is close to 25 mV and the other interface has the opposite value of -25 mV. When the film is very thick, as in the current example, the two interfaces do not feel each other because the electric double layers in the coacervate phase have relaxed completely. However, when the film is significantly thinner, we should anticipate that the two interfaces interact electrostatically with each other. Indeed, the opposite value of the potential indicates that thin coacervate films will experience electrostatic attraction, which will work against the thickening of the coacervate film. We will return to this point below when we consider the spontaneous formation of the coacervate phase across the oil-water interface.

There is a number of parameters by which we can tune the structure of the coacervate phase. A selection of our results is presented in Figure 3.4. Let us introduce the overall polymer density ϕ in the center of the coacervate phase (that
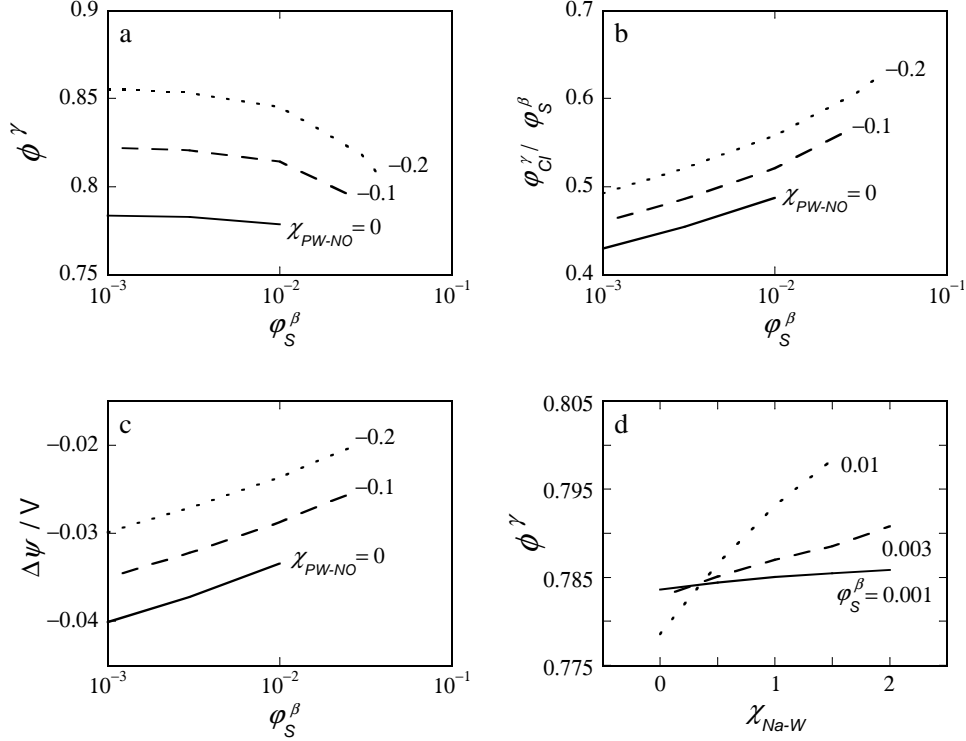
Figure 3.4: (a) Volume fractions of polyelectrolytes ϕ^γ, (b) Ratio of volume fractions of salt in phases γ and β, $\varphi_S^\gamma/\varphi_S^\beta$, (c) Electrostatic potential differences across the coacervate film (in V), as a function of the salt concentration in bulk $\varphi_S^\beta = \varphi_S^\alpha$ in lin-log coordinates for three different values of the correlation attraction, χ_{PW-NO}, as indicated. The curves cover only a limited range of salt concentrations and terminate because the systems approach the critical region wherefore computations become challenging. (d) Volume fraction of polyelectrolytes ϕ^γ in the coacervate phase as a function of $\chi_{Na-W} = \chi_{Cl-O}$ for different salt concentrations φ_S^β as indicated.

is at $z = 0$) as the sum over the two polyelectrolytes:

$$\phi^\gamma \equiv \varphi_{PW}(0) + \varphi_{NO}(0) \tag{3.3}$$

This overall volume fraction is given in Figure 3.4a as a function of the salt concentration in the solvent phases for three values of the 'correlation' attraction χ_{PW-NO}. The polymer density in the coacervate decreases with increasing salt concentration and with decreasing affinity between the segments. Indeed, both trends correspond to weakening the cohesive forces in the coacervate film. The coacervate phase tends to go to a fixed density at very low volume fractions of salt but this density can increase when the attraction between the segments is increased. For salt concentrations larger than approximately 0.01 the density of the

coacervate tends to drop. This polymer density drop results in solvent taking up and we move towards an instability. Eventually when the density is below a critical value the coacervate falls apart. We expect the stronger the correlation is, the higher the salt concentration needed to break the coacervate is. We were not able to find coacervate phases with an overall density lower than 0.75. This is the reason why the curves in Figure 3.4a cover only a limited range of salt concentrations.

In Figure 3.4b we present results for the corresponding amounts of salt in the coacervate phase. In all cases the concentration of salt in the coacervate is lower than the concentration in the bulk: the ratio between the concentrations in the γ and $\beta=\alpha$ phases is invariable smaller than unity. The suppression of the salt concentration can be traced to the excluded volume effect. When the polymer concentration is high, the ions are more suppressed. Hence the salt concentration ratio increases towards unity when the density of polymer in the coacervate drops, that is with increasing salt concentration and with lower value of the correlation attraction. Only when we give the ions an affinity to the polymer segments we may anticipate that the segments will accumulate in the coacervate phase. Such an effect may in fact destabilize the coacervate phase.

Let us define the difference of electrostatic potential across the interface as:

$$\Delta\psi \equiv \psi(-\infty) - \psi(\infty) \tag{3.4}$$

where in practice we substitute for $-\infty$ the largest negative value of z (far in phase α) used in the system and ∞ the highest positive value of z (far in phase β) in the system. The potential difference is expected to increase with decreasing ionic strength. In the lin-log coordinates an approximately linear dependence is found. The slope does not depend on the value of the correlation attraction and amounts to about about 7 mV per decade in salt concentration. At high salt concentrations, the density of the coacervate decreases and a small deviation to a higher slope is noticed. The interpretation of this dependence is complicated by the fact that the polyelectrolyte concentrations in the bulk phases are not constant, but also increase with the salt concentrations (not shown). Hence we can not expect a simple Nernstian behavior. The absolute value of the electrostatic potential difference increases with 5 mV for a change of $\Delta\chi_{PW-NO} = 0.1$. Such 50 mV for one unit difference in χ_{PW-NO} may be a subject of experimental observations.

We have discussed the importance of the ion properties in the case of adsorption of polyelectrolytes at the L-L interface. Let us therefore also touch upon the effect of the solvation of the ions. As we try to keep the system symmetric with respect to the interactions we choose corresponding but opposite interactions for the two ions in the system, hence we keep $\chi_{Na-W} = \chi_{Cl-O}$. A positive value of χ_{Na-W} implies that Na prefers to sit in the oil phase. Similarly, the positive value of

χ_{Cl-O} implies that Cl likes the water phase better than the oil phase. Hence, with increasing $\chi_{Na-W} = \chi_{Cl-O}$ we consider the case that the polycation and its counterion both prefer the water phase over the oil and the polyanion with its counterion both prefer the oil phase. In Figure 3.4d we present the polymer density in the complex coacervate phase as a function of χ_{Na-W} for different values of the salt concentrations. From this figure we see that the polymer density in the coacervate phase increases with increasing selectivity of solvation of the ions. This result suggests that the coacervate phase becomes increasingly stabilized. From an ion-release perspective we could not have anticipated this result; upon complexation of the polymers, the respective counterions now remain in their own half-space. There is less entropic gain compared to the case that the ions could choose for both solvents. We therefore conclude that ion release is not important for the coacervate formation in our calculations.

In Figure 3.4d we notice that there is approximately a common intersection point. Below a value of $\chi_{Na-W} \approx 0.3$ the polymer density in the complex coacervate phase decreases with increasing salt concentration. Above this value the polymer density of the coacervate phase increases with salt concentration. The explanation of this effect is rather straightforward. When both the polyelectrolyte and its counterion prefer the same solvent, the chemical potential of the polyelectrolyte chains decreases compared to the default case. Indeed, in such situation the counterion is less frustrated to remain near its polyion. As the chemical potentials of the polyions are lower in the case of selective solvation of the ions, the coacervate phase must also be more stable. Hence, the polymer density can increase. It would be of significant interest to test experimentally this prediction.

In the system we study, three phases are present with the oil, the water and the coacervate phase. It is of considerable interest to know whether the coacervate sits at the interface as drops or whether we have a homogeneous film in between the oil and water phases. Cahn's argument explains that a system close to the critical point is more likely to be in a complete wet state while systems that are further away from the critical point are more likely to be in a partial wet state. Indeed, the stronger is the cohesive force inside the coacervate phase the more likely the interfacial free energy for a thick film in between the oil-water interface, $\sigma_{\text{thick}} = \sigma_{\alpha\gamma} + \sigma_{\beta\gamma}$, is higher than the interfacial free energy for a thin film in between the oil-water interface, $\sigma_{\text{thin}} = \sigma_{\alpha\beta}$. In the latter we may have adsorption of ions or polyions on the oil-water interface but this layer remains microscopically thin (Figure 3.2). Obviously, we need to compare these two situations at exactly the same chemical potentials of all components in the system. The parameter of interest is the spreading parameter S, which corresponds to the difference between σ_{thick} and σ_{thin}. When this value is negative we have the case of partial wetting.
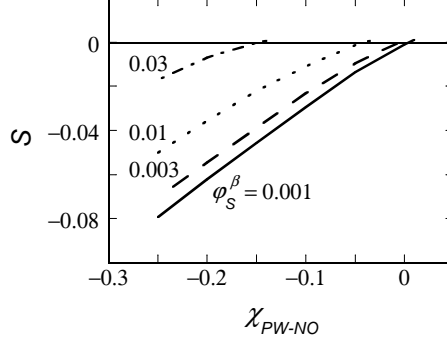
Figure 3.5: Spreading parameter S as a function of the Flory-Huggins interaction parameter between the polymer segments χ_{PW-NO} for different salt concentrations φ_S^α as indicated. Parameters are the same as for Figures 3.4a-c.

We first construct a symmetric system with a thick coacervate phase. From this result, we take the grand potential of the system which amounts to σ_{thick} (as done above) and we record all relevant chemical potentials (these are the chemical potentials for the binodal in the system). We then consider a bare L-L interface, we add the two polyelectrolytes and the ions and we fix the chemical potentials to the binodal values. Two scenarios are then possible. In the first scenario we find the thick film once again; we conclude that there is only one solution for the specified chemical potentials and the coacervate wets the L-L interface. In the second scenario there is a very thin film of interpolyelectrolytes present at the L-L interface. Hence, the thick film can coexist with a microscopically thin film. We now can easily evaluate the value of the spreading parameter. We note that with this protocol we explicitly assume that the isotherm crosses the binodal once when the film is microscopically thin, and touches the binodal when the film is macroscopically thick. Later we prove that this assumption can be violated when there is a second crossing of the binodal.

Figure 3.5 shows the spreading parameter S as a function of the correlation attraction χ_{PW-NO} for different salt concentrations as indicated. The tendency to find drops increases with increasing cohesiveness of the complex coacervate phase i.e. the more negative values of the spreading parameters are found with increasing strength of attraction between the polymer segments and with decreasing salt concentration. Inversely, decreasing the stability of the complex coacervate phase will push the spreading parameter towards zero. For low salt concentrations the system needs less correlation attraction to reach the complete wet case than for high salt concentrations. In other words when there is a strong correlation attraction we need a lot of salt to deteriorate the cohesive interactions in the complex

59

coacervate.

Interestingly, Figure 3.5 also shows that the spreading parameter crosses zero and can take small positive values. However, this is only possible when a loop is present in the adsorption isotherm (see below). As soon as the prewetting step occurs in the isotherm we have the situation that there is a first crossing of the binodal for microscopically thin films (which may be metastable and thus has a relatively low tension) and a macroscopically thick film such that the spreading parameter is positive. As a positive value of the spreading parameter is possible we should conclude that the wetting transition is first order. In the next paragraph, wherein we will consider compositionally asymmetric systems, we will prove that this interpretation is wrong.

In general there can be two critical points in the system by which the complex coacervate vanishes: either the difference between the α and γ or the difference between the β and γ phases vanishes. In a fully symmetric system, as we considered so far, it is necessary that the system approaches both critical conditions at the same time. Calculations near the critical point are challenging because the corresponding interfaces become wider and wider while more solvent penetrates into the coacervate. Indeed, it is found that just beyond the χ_{PW-NO} for which the spreading parameter becomes positive, the system is close to such bi-critical point. The χ_{PW-NO} for the bi-critical point is thus expected to be lower for higher salt concentrations. These results are fully in line with the Cahn argument: based on the spreading parameter we find a wetting transition not far from the critical points in the system.

3.4.3   Pseudo-partial wetting

To get full insights in the wetting characteristics of a system one needs to consider adsorption isotherms. In multi-component systems, one should fix as many chemical potentials as possible and record the Gibbs excess adsorbed amount of one of the components as a function of the bulk concentration of this compound. Without loosing generality we will fix both the bulk volume fraction of the hydrophilic polycation φ_{PW}^{β} in the water phase as well as the added salt concentration to $\varphi_S^{\beta} = 0.001$. We focus on the adsorption isotherm of the polyanion, that is, we record the Gibbs excess adsorbed amount at the L-L interface of the hydrophobic polyanion as a function of the bulk volume fraction φ_{NO}^{β}. There exists only one specific value for φ_{PW}^{β} for which at the binodal $\varphi_{NO}^{\beta} = \varphi_{PW}^{\beta}$. Such result has been reported above for the symmetric case. We will refer to this bulk volume fraction of the anionic polymer at the binodal by φ_{NO}^{*}.

In general we will have the situation that $\varphi_{NO}^{*} \neq \varphi_{PW}^{\beta}$. Here we focus on the
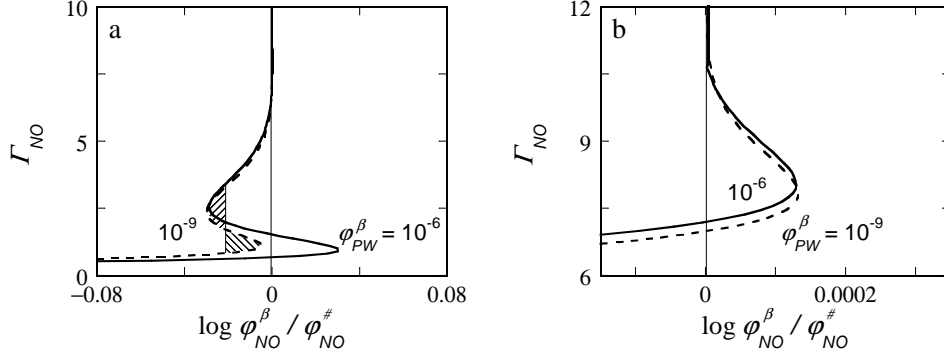
Figure 3.6: (a) Gibbs excess of the oil-soluble polyelectrolyte at the oil-water interface as a function of $\log(\varphi_{NO}^{\beta}/\varphi_{NO}^{\#}$ for $\varphi_{PW}^{\beta} = 1.0 \times 10^{-6}$ and 1.0×10^{-9}. $\varphi_{NO}^{\#}$ is the volume fraction of NO at the binodal (in phase β). (b) Zoom of (a). The volume fraction of salt is fixed to $\varphi_{S}^{\beta} = 0.001$. All interaction parameters have the default value. For the isotherm with $\varphi_{PW}^{\beta} = 1.0 \times 10^{-9}$ a thin line shows where the step in the isotherm takes place and the two shaded regions have the same area (equal area argument).

situation that at the binodal $\varphi_{NO}^{*} > \varphi_{PW}^{\beta}$. Indeed, the lower the value of φ_{PW}^{β} the more difficult it becomes to form the complex coacervate and thus the higher the binodal value of $\varphi_{NO}^{\#}$ in the β phase. It is natural to expect a limiting value $\varphi_{PW}^{\mathrm{cr}}$ in the β phase below which there is no longer a complex coacervate phase possible. At this critical point the phases α and γ become identical and we return to a two-phase system $\alpha\beta$, where the α phase is supercritical and contains much more polymers than the β phase. Going towards this critical point the width of the $\alpha\gamma$ interface widens while the width of the $\beta\gamma$ interface remains sharp. We trust that it is understood that by zooming in on $\varphi_{NO}^{*} < \varphi_{PW}^{\beta}$ we can approach the other critical point in the system. Here we will not do the latter and restrict our analysis to the regime for which $\varphi_{NO}^{*} > \varphi_{PW}^{\beta}$.

In Figure 3.6a we present two examples of adsorption isotherms of the polyanion recorded at fixed polycation concentrations of $\varphi_{PW}^{\beta} = 1.0 \times 10^{-6}$ and 1.0×10^{-9}, respectively. The salt concentration (added salt) was fixed in both cases to $\varphi_{S}^{\beta} = 0.001$. In line with the result presented in Figure 3.5 we see that both isotherms have a prewetting-like step in the isotherm. It is seen that for both isotherms the step in the isotherm, which may be found by an equal area argument, takes place below the bulk binodal value $\varphi_{NO}^{\#}$ and that the lower φ_{PW}^{β} the step occurs further away from the binodal value. At the prewetting step the adsorbed amount of polymers at the L-L interface jump-like increases from a microscopically thin value to a mesoscopically thin one. The closer the prewetting step occurs to the bulk binodal the larger is the thickness of the mesoscopically thick film. Clearly,
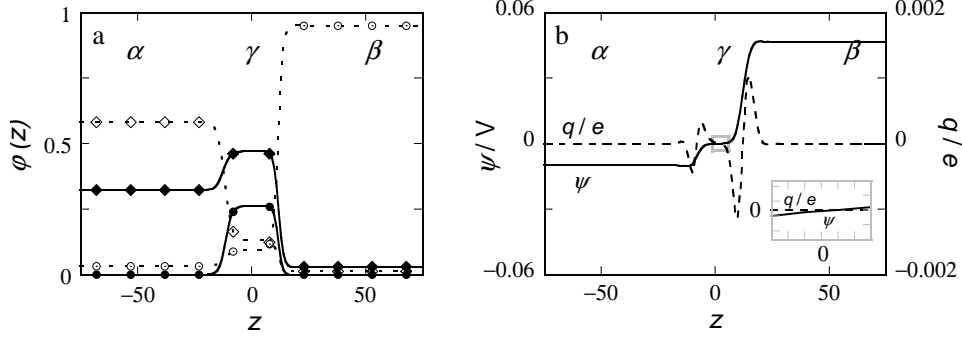
61

Figure 3.7: (a) Volume fraction profiles φ of $\diamond$ oil, $\odot$ water, $\blacklozenge$ anionic oil-soluble polyelectrolyte, $\bullet$ cationic water-soluble polyelectrolyte for $\chi_{PW-NO} = 0$, $\varphi_S^\beta = 0.001$ and $\varphi_{PW}^\beta = 1.0 \times 10^{-12}$, (b) Potential ψ in volts and dimensionless charge density q/e profiles at the same conditions. The system is exactly at coexistence: the adsorbed amount equals $\Gamma_{NO}^\#$. The value of $z = 0$ is taken at the point where the charge $q(z) = 0$ (approximately in the middle of the coacervate phase). The potential is set to zero at $z = 0$.

the step in the isotherm at $\varphi_{PW}^\beta = 1.0 \times 10^{-6}$ is larger than for $\varphi_{PW}^\beta = 1.0 \times 10^{-9}$, and thus the wetting transition is expected slightly above $\varphi_{PW}^\beta = 1.0 \times 10^{-6}$.

A close inspection of the isotherms reveals a surprise. Indeed, the isotherms do not, as expected, smoothly diverge after the prewetting step upon approaching the bulk binodal. As can be seen from the zoomed-in version of the isotherm in Figure 3.6b, the isotherms cross the bulk binodal once again at some mesoscopic value of the adsorbed amount, and in the super-saturated region of the adsorption isotherm there is a 'belly'. Both isotherms reach the bulk binodal at large adsorbed amounts coming from the right, that is from the super-saturated side. The latter trend is the signature of a second order wetting transition. This means that both isotherms presented in Figure 3.6 correspond to the partial wet state. In the literature this situation combining a pre-wetting step with a partial wet condition is named pseudo-partial wetting. In the previous section, we used the spreading parameter (based on the first crossing of the binodal value) to get insight into the wetting state of this system. We now understand that the isotherm crosses multiple times the saturation axis and that the conclusions about wetting were premature.

Let us denote the adsorbed amount at coexistence by $\Gamma_{NO}^\#$. A close inspection of the Figure 3.6b proves that $\Gamma_{NO}^\#$ for $\varphi_{PW}^\beta = 1.0 \times 10^{-6}$ is slightly higher than for $\varphi_{PW}^\beta = 1.0 \times 10^{-9}$. Follow Cahn again we should anticipate that the latter is closer to the wetting transition and apparently $\Gamma_{NO}^\#$ decreases upon the approach towards the critical point. Again we need structural information of the system to rationalize what happens.

In Figure 3.7 we present structural information for the case that $\varphi_{PW}^{\beta} = 1.0 \times 10^{-12}$. Compared to the conditions for which the two isotherms were presented in Figure 3.6, the conditions for Figure 3.7 are even closer to the wetting transition. This system obviously is also closer to the critical point than the ones reported in Figure 3.6. In Figure 3.7a we give the density profiles of the molecular species and in Figure 3.7b the corresponding electrostatic potential and dimensionless charge density profiles are shown. We have selected the point in the isotherm for which the adsorbed amount is $\Gamma_{NO}^{\#}$, i.e. the system is exactly at the bulk binodal and the coacervate film in between the oil and water phases is the relevant mesoscopic one that may be found in an experimental situation.

There are many noteworthy features in Figure 3.7a. First of all we notice that the volume fraction of the polyanion in the oil phase is very high. In the coacervate the polyanion concentration is only slightly higher, and it is relatively low in the water phase. In all phases the polycation has a lower density than the polyanion. In the water phase it is very low ($\varphi_{PW}^{\beta} = 1.0 \times 10^{-12}$), the density is about a factor two lower than the polyanion in the coacervate phase and again it is very low in the oil ($\varphi_{PW}^{\alpha} = 9.0 \times 10^{-6}$). As the polyanion concentration in the oil is large, the volume fraction of oil is relatively low. In the water phase the water density remains relatively high because in the water the polymer concentration was kept low. The ion distribution can, as before, be deduced from the electrostatic potential profile, and is not shown. Considering the polyanion volume fraction profile $\varphi_{NO}(z)$ it is clear why the Gibbs excess is not particularly high: the polymer density in phase α does not differ so much from that in the γ phase, and as the Gibbs excess is the adsorbed amount with respect to the β and α phases, the Gibbs adsorption is modest even when the thickness of the mesoscopically thick film is significant.

As anticipated above, the example of Figure 3.7a is close to the critical point for which the α and γ phases become the same. In line with this we notice that the width of the oil-coacervate interface is already relatively wide. This must be contrasted to the water-coacervate interface, which remains sharp. Indeed, upon approaching the critical point the interface $\alpha\gamma$ progressively becomes wider and wider when the difference between the α and γ phases becomes less and less.

The difference in polyanion and polycation concentrations in the coacervate phase is about a factor of two in the current example. Indeed, upon approaching to the critical point this difference increases and this is exactly the reason why the stability of the coacervate phase deteriorates. At the same time φ_{PW}^{β} must increase as the α and γ phases must become equal in all respects at the critical point.

We have set $z = 0$ at the point wherein the charge density $q(z)$ inside the coacervate phase changes sign (Figure 3.7b). Unlike in the results of Figure 3.4 where the gradients inside the coacervate phase vanished, we have significant changes of

the charge q and thus also of the electrostatic potential ψ across the mesoscopically thin coacervate film. We have set $\psi(0) = 0$ but notice that the field strength at $z = 0$ is positive, that is, $E(0) = (\partial\psi/\partial z)_{z=0} > 0$. This implies that the two interfaces in the mesoscopically thin film are not independent from each other and that they 'see' each other electrostatically. Even though the mesoscopically thin film is far from its stochiometric composition, the rough features of the charge density and potential profiles near the edges are similar to the ones described in Figure 3.4b and we will not repeat the description here. The oil-coacervate interface has a negative electrostatic potential whereas the coacervate water interface has a positive one. Hence there is an electrostatic attraction operating in this system. This electrostatic attraction stabilizes the mesoscopically thin film and it is the origin of the pseudo-partial wetting phenomena. Indeed, the film can not grow to arbitrary thick values due to this electrostatic attractive force.

We also notice that the coacervate-water interface has much more defined peaks in the charge distribution than the oil-coacervate interface. Upon approaching towards the critical point we foresee that these local peaks in the charge distribution gradually vanish around the $\alpha\gamma$ interface due to the widening of the interface. As a result, the electrostatic attraction, which keeps the mesoscopic film thin, will diminish and eventually vanish and the coacervate will eventually wet the L-L interface. However, this disappearance is strictly coupled to the disappearance of the coacervate phase.

Using a large set of adsorption isotherms similar to the ones given in Figure 3.6 we can build a so-called wetting phase diagram of the system. There are three types of isotherms. (i) Starting at rather high values of φ^{β}_{PW} we have isotherms for which the loop occurs in the supersaturated regime. In this case the system is in a strongly partial wet state. We recorded the adsorbed amount $\Gamma^{\#}_{NO}$ at the first crossing of the binodal value. This adsorbed amount corresponds to a microscopically thin film. (ii) At somewhat lower values of φ^{β}_{PW} we have isotherms as in Figure 3.6; there is a pre-wetting step that occurs below saturation. We recorded the φ^{β}_{NO} at which the prewetting step occurs, as well as the adsorbed amount $\Gamma^{\#}_{NO}$ for the mesoscopically thin film. (iii) At even lower values of φ^{β}_{PW} we no longer have a prewetting step but the isotherm still crosses the binodal and we record $\Gamma^{\#}_{NO}$ of the mesoscopically thin film.

In Figure 3.8a we present the wetting phase diagram, which features a prewetting line. Indeed, a line in a phase diagram signals a first-order phase transition: here this transition is the prewetting step in the isotherm. On the y-axis we give the log of the volume fraction of φ^{β}_{NO} at which the prewetting step is found (normalized to the binodal value) and on the x axis we have the value of the control parameter. The zero on the y axis means that the pre-wetting step occurs at the bulk binodal.
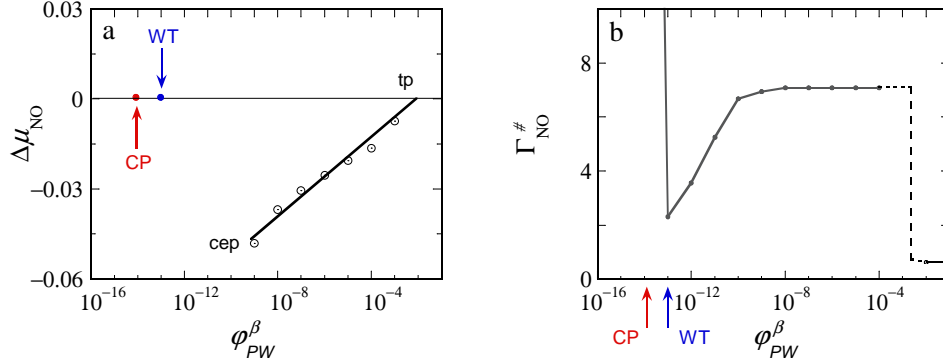
Figure 3.8: (a) Wetting phase diagram of a coacervate film at the oil-water interface where we plot the $\log \varphi_{NO}^{\beta}/\varphi_{NO}^{\#}$ as a function of the control parameter $\log \varphi_{PW}^{\beta}$. A line in this wetting phase diagram represents a first-order transition, corresponding to the prewetting step in the isotherm. Here 'cep' refers to the critical end point of the prewetting line (estimated), 'tp' the triple point, that is the point for which three layer thicknesses can coexist, 'WT' is the point where the wetting transition takes place and 'CP' the bulk critical point (estimated). The volume fraction of salt is $\varphi_{S}^{\beta} = 0.001$. A fitting line is added to guide the eye. (b) Gibbs excess at the binodal $\Gamma_{NO}^{\#}$ as a function of the volume fraction of the polycation concentration in the water phase φ_{PW}^{β} for $\varphi_{S}^{\beta} = 0.001$. The jump in the Gibbs excess corresponds to the spot where the prewetting step occurs at the binodal condition.

Indeed, the prewetting line terminates at the prewetting critical end point 'cep' around $\varphi_{PW}^{\beta} \approx 10^{-10}$ and it starts around $\varphi_{PW}^{\beta} \approx 10^{-3}$. At this starting point we have three possible layer thicknesses that coexist: there is the microscopically thin film, the mesoscopically thin film as well as the macroscopically thick film; this explains why we label this point as a triple point 'tp'.

In Figure 3.8b we have collected the adsorbed amount at coexistence $\Gamma_{NO}^{\#}$ as a function of the control parameter φ_{PW}^{β}, for $\varphi_{S}^{\beta} = 0.001$. Going from a high value of φ_{PW}^{β} to values closer to the critical point we first find a microscopic amount of polymer at the L-L interface. At the 'tp' the adsorbed amount jumps form a microscopic to a mesoscopic value. Upon a further decrease of φ_{PW}^{β} the Gibbs excess $\Gamma_{NO}^{\#}$ decreases and near the critical point, which is around $\varphi_{PW}^{\beta} = 10^{-14}$, the value levels off to low but finite value.

The location of a second order wetting transition is very delicate. The 'belly' in the isotherm becomes smaller and smaller and it is hard to estimate at which point it vanishes. We found that extremely close to the critical point we may have an isotherm for which the 'belly' was no longer found, but there are troubleling issues. In the classical case of wetting the adsorbed amount at coexistence (here

$\Gamma_{NO}^{\#}$) gradually increases and diverges at the wetting transition. In our calculations we found a continuous decrease of $\Gamma_{NO}^{\#}$, explained by the gradual loss in density difference between the β and γ phases, and a divergence of $\Gamma_{NO}^{\#}$, when the interface is wetted by the NO polymer. Therefore a wetting transition takes place before the critical point. This result is in line with Cahn's argument and suggests that this argument remains valid for pseudo-partial wetting scenario.

Our first isotherm for which up to numerical noise there was no 'belly' occured near $\varphi_{PW}^{\beta} = 10^{-13}$ and our estimate of the critical point was near $\varphi_{PW}^{\beta} = 10^{-14}$. Both the wetting transition as well as the critical point are a function of the salt concentration. Both increase to larger values of φ_{PW}^{β} with increasing salt concentration. We also found that $\Gamma_{NO}^{\#}$ for the mesoscopically thin films decreases with increasing salt concentration. The reason for this trend is traced to the observation that with increasing salt concentration the volume fraction of NO in the oil increases and therefore the difference with respect to the complex coacervate phase is less.

3.5   Discussion

The strategy of oppositely charged polyelectrolyte co-assembly across an interface is an interesting and potentially generic approach to stabilize emulsions. In our experiments we noticed a long term stability of such emulsion droplets. We believe that a significantly thick coacervate phase develops at this interface by spontaneous co-assembly of the polycation and polyanion. In a drop tensiometer the droplets lost transparency over time in transmission illumination, and we anticipated that this is due to the lateral inhomogeneity of the coacervate film.

The current SCF analysis focused on a highly idealized system wherein gradients in the dielectric permittivity were ignored and the molecular species, that is the oil, the water, both polyelectrolytes and the ions were assumed fully symmetric/complementary. In our experimental counter parts there are many details that are different. The macromolecules that were used, differ dramatically with respect to the molecular architecture, chain flexibility, molecular weight, etcetera. Moreover, the oil and water phases have a significant asymmetry and on top of this, the ions typically have an extreme preference for the water phase, albeit that one may use ionic liquids, which may have a higher affinity for the oil phase. Nevertheless, it is tempting to extrapolate our results to the real systems. We found that there is a large parameter space by which we expect that the coacervate film spontaneously forms across the interface, but that this film remains mesoscopically thin. The pseudo-partial wetting scenario may in fact be present also in experimentally more complex systems. As the interfacial tension between oil and water

is relatively high, the interactions on the segmental level may signal complete wetting for a wide range of salt concentrations and polymer concentrations. However, the mesoscopically thin film may generically have oppositely charged interfaces and the electrostatic attraction may be rather generically operational. Hence we believe that in many of our experiments a mesoscopically thin film readily forms across the oil-water interface. Such a film explains why the oil-in-water emulsions were stable in time. However, due to thermal fluctuations, an excess of polyelectrolytes in the systems may have caused coacervate droplets to form in this film over time. This results in films that are no longer laterally homogeneous and this explains the darkening of the droplets observed in our tensiometry experiment.

Contrary to the common belief that SCF theory is ineffective to study complex coacervate systems, we have shown that it is reasonable to use a self-consistent field theory to analyze complex coacervation across the oil-water interface. We argued that in our system the counterion release effect is of minor importance and that the major driving force that stabilizes the coacervate phase is the fact that one of the polymers rejects the oil and the other one the water. The complex therefore rejects both the oil and the water and these effects are well represented by our SCF theory. We have seen that when the ion solvation is taken such that counterion release was basically turned off in our system, the chemical potential of the polyelectrolytes became lower and this stabilized the coacervate phase. We hesitate to extrapolate this result to the true counterion release mechanism. In real life each polymer chain has 'arrested' its counterions and invariably these ions are released upon polyelectrolyte complexation. This effect is not included in the present SCF theory. However, we assume that in first order such effect is represented by a negative value of χ_{NO-PW}. Hence, we may qualitatively predict what happens when true counterion release effect is included in a more complete theory: the coacervate phase should become more stable.

There is a long list of predictions, which await experimental verification. We may recall the most important ones. (i) We have reported on an unusual transition going from depletion to adsorption upon an increase in the polyelectrolyte concentration in the case of a liquid-liquid interface. Again our model system was highly idealized but we believe that the mechanism by which the adsorption transition takes place is generic and justifies future systematic investigations. (ii) We report on the electrostatic potential difference between the oil and water phase in the presence of a coacervate film that develops across the interface. Such potential differences can be measured relatively easy experimentally and our model can be used to predict e.g the dependence on pH, ionic strength and polyelectrolyte concentrations. (iii) In wetting experiments it is not easy to use the polycation concentration to tune the wetting in a system. It is much more easy to vary the temperature

or some other external parameter to do so. Possibly, it is feasible to use the ionic strength in a setup wherein the system is in contact with a semi-permeable barrier that allows the transport of ions but not the polyelectrolytes. In such a case we may investigate the pseudo-partial wetting scenario systematically.

We should finally mention that from a modeling point of view there are also many possible extensions. We can easily implement models in which the oil and water phases are more realistically represented, the polymers have different molecular weights and different charge densities, and the ions have their own interactions with the oil, water, and polyelectrolytes. Hence we can tune the model to a specific experimental situation and such an exercise becomes relevant when detailed experimental data for such a system become available.

3.6 Conclusion

Based on the self-consistent field theory, we develop a model to investigate the formation and the stability of a coacervate film at the oil-water interface. We show that, despite the common belief, the theory can account reasonably accurately for the ion-release effect due to the presence of two solvents, especially when the polymer concentrations are in the semi-dilute regime. We find that the coacervate becomes less stable with decreasing correlation attraction, modeled by an attractive FH parameter for the polymer segments χ_{PW-NO}, and increasing ionic strength. By tuning the solvent quality of the co- and counterions we can further stabilize or destabilize the complex coacervate. Finally, by taking a large difference between the concentrations of the oppositely charged polymers, we can destabilize the complex coacervate. In compositionally asymmetric systems, complex coacervate films have a compositional imbalance of a factor of two, before the phase falls apart at the critical point. Interestingly, our system features a pseudo-partial wetting scenario, attributed to the presence of interactions on two length scales. A high interfacial tension between the oil and the water allows for the co-assembly of a significant amount of the oppositely charged polyions. However, the mesoscopically thin coacervate film is stabilized by attractive electrostatic interactions, and hence the film can not grow spontaneously to macroscopic sizes. Close to the bulk critical point the electrostatic attraction vanishes and the wetting transition occurs in line with Cahn's argument.

We touched briefly on how polyelectrolyte adsorption occurs at a liquid-liquid interface. We find an unusual adsorption transition by increasing the polyelectrolyte concentration. At low concentrations, the polyelectrolyte is depleted from the interface whereas adsorption occurs at higher concentrations. The adsorption of the small co- and counterions at the L-L interface plays an important role in

this adsorption transition.

Experimental observation of interpolyelectrolyte complexation across the oil-water interface motivated us to undertake this SCF study. Although our experimental parameters are very far from the idealized model, we believe that the pseudo-partial wetting scenario that is found in the modeling can explain why droplets in the drop tensiometer scattered more and more light in the coarse of time. The lateral inhomogeneity of the coacervate film (drops coexisting with a microscopically thin film) may occur due to thermal fluctuations.

References

[1] H.G. Bungenberg de Jong and H.R. Kruyt, *Proc. K. Ned. Akad. Wet.*, 1929, **32**, 849–856.

[2] A. Harada and K. Kataoka, *Macromolecules*, 1995, **28**, 5294–5299.

[3] M.A. Cohen Stuart, N.A.M. Besseling, and R.G. Fokkink, *Langmuir*, 1998, **14**, 6846–6849.

[4] J. van der Gucht, E. Spruijt, M. Lemmers, and M.A. Cohen Stuart, *J. Colloid Interface Sci.*, 2011, **361**, 407–422.

[5] H. Monteillet, F. Hagemans, and J. Sprakel, *Soft Matter*, 2013, **9**, 1127011275.

[6] E. Spruijt, F.A.M. Leermakers, R. Fokkink, R. Schweins, A.A. van Well, M.A. Cohen Stuart, and J. van der Gucht, *Macromolecules*, 2013, **46**, 4596–4605.

[7] J.J. Cerd, B. Qiao, and C. Holm, *Soft Matter*, 2009, **5**, 4412–4425.

[8] Y.O. Popov, J. Lee, and G.H. Frederickson, *J. Polym. Sci., Part B: Polym. Phys.*, 2007, **45**, 3223–3230.

[9] I.K. Voets and F.A.M. Leermakers, *Phys. Rev. E*, 2008, **78**, 061801.

[10] P.B. Warren, *J. Phys. II*, 1997, **7**, 343–361.

[11] M. Gottschalk, P. Linse, and L. Piculell, *Macromolecules*, 1998, **31**, 8407–8416.

[12] P. de Gennes, *Rev. Mod. Phys.*, 1985, **57**, 827–863.

[13] M. Schick, *An introduction to wetting phenomena*, Elsevier Science, 1990, pp. 415–497.

[14] J.O. Indekeu, *Acta Physica Polonica B*, 1995, **26**, 1065–1100.

[15] D. Bonn and D. Ross, *Rep. Prog. Phys.*, 2001, **64**, 1085–1163.

[16] D. Bonn, E. Bertrand, N. Shahidzadeh, K. Ragil, H.T. Dobbs, A.I. Posazhennikova, D. Broseta, J. Meunier, and J.O. Indekeu, *J. Phys. Condens. Matter*, 2001, **13**, 4903–4914.

[17] W.D. Harkins and A. Feldman, *J. Am. Chem. Soc.*, 1922, **44**, 2665–2685.

[18] J.W. Cahn, *J. Chem. Phys.*, 1977, **66**, 3667–3772.

[19] J. Clerk-Maxwell, *J. Chem. Soc.*, 1875, **28**, 493–508.

[20] F.A.M. Leermakers, J.H. Maas, and M.A. Cohen Stuart, *Phys. Rev. E*, 2002, **66**, 051801.

[21] J.M.H.M. Scheutjens and G.J. Fleer, *J. Phys. Chem.*, 1979, **83**, 1619–1635.

[22] J.M.H.M. Scheutjens and G.J. Fleer, *J. Phys. Chem.*, 1980, **84**, 178–190.

[23] F.A.M. Leermakers and J.M.H.M. Scheutjens, *J. Chem. Phys.*, 1988, **89**, 3264.

[24] D.K. Beaman, E.J. Robertson, and G.L. Richmond, *Langmuir*, 2011, **27**, 2104–2106.

[25] G.J. Fleer, M.A. Cohen Stuart, J.M.H.M. Scheutjens, T. Cosgrove, and B. Vincent, *Polymers at interfaces*, Chapman and Hall, 1993.

Appendix

Following the Ansatz of Scheutjens and Fleer we consider a one-gradient lattice model with planar layers of lattice sites numbered $z = 0, 1, \cdots, M$. In each layer there are L lattice sites. We distribute molecules of type $i = 1, 2, \cdots$, which are composed of segments $s = 1, 2 \cdots, N_i$ on this lattice. We consider homopolymer, that is, all segments within a given molecule are the same. For the monomeric components (ions) we have $N_i = 1$, the solvents and particularly the polyions are composed of a few or of many segments. The size of the segments matches the size of a lattice site, given by the length b. Let the number of segments of molecule type i in layer z be given by $n_i(z)$ then the volume fraction $\varphi_i(z) = n_i(z)/L$. The approximate nature of using volume fractions is perhaps best illustrated by considering the distribution of polymers on this lattice. When the concentration is in the dilute regime, the average density in layer z is much lower that the segment density within a particular coil. The mean field approximation is worst for dilute solutions, not too bad for semi-dilute solutions and close to exact for melts. In the lattice model, we do not allow empty sites. In other words we will insist on the incompressibility condition:

$$\sum_i \varphi_i(z) = 1 \qquad (3.5)$$

Complementary to the volume fractions, there are so-called segment potentials, $u_i(z)$. The segment potentials are used in a Boltzmann like equation similarly as external potentials. Unlike the gravitational potential, segment potentials are a function of the (local) volume fraction profiles. Physically, the segment potentials represent the potential energy contribution of bringing a segment from the bulk (where the potential is zero) to the coordinate z. We have three contributions in the (dimensionless -all our energies are normalized by the thermal energy $k_B T$) segment potential:

$$u_i(z) = \alpha(z) + \sum_j \chi_{ij} \left(\langle \varphi_j(z) \rangle - \varphi_j^b \right) + v_i \Psi(z) \qquad (3.6)$$

The first term gives the so-called Lagrange contribution, which value is adjusted until the system obeys the incompressibility constraint (see equation 3.5). The second term gives the (short-range) nearest neighbor contact interactions parameterized by the Flory Huggings parameters χ_{ij}. The number of contacts is evaluated using the Bragg-Williams approximation. The angular brackets are a short hand notation for a three layer average $\langle \phi(z) \rangle = (\phi(z-1) + 4\phi(z) + \phi(z+1))/6$ where a cubic lattice is assumed. The volume fraction of component j in the bulk, φ_j^b, is used in the second term in equation 3.6 to ensure that the potentials remain zero

in the reference bulk phase. In the third term of equation 3.6 the usual electrostatic potential contribution. Here $\Psi(z)$ is the dimensionless electrostatic potential $\Psi(z) = e\psi(z)/k_B T$, with e the elementary charge and $k_B T$ the thermal energy. v_i is the valence of a segment of molecule i.

As usual we need the Poisson equation to find the electrostatic potentials in the system. As long as the dielectric permittivity ϵ is constant throughout the system we can write:

$$\frac{\partial^2 \psi(z)}{\partial z^2} = -\frac{\sigma(z)}{\epsilon}$$
$$\langle \psi(z) \rangle - \psi(z) = -\frac{\sigma(z)}{\epsilon} \tag{3.7}$$

where in the first line the 'continuous' version of the Poisson and in the second line the lattice version is presented. In these equations the charge density is given in the lattice model by:

$$\sigma(z) = \sum_i \varphi_i(z) e v_i \tag{3.8}$$

For each molecule we need the single chain partition function q, which will collect the sum of statistical weights of all possible and allow conformations. We can compute this quantity when the segment potentials are known, that is, $q[u]$. The single chain partition functions are combined in a partition function for the system by $Q = \Pi_i q_i^{n_i}/n_i!$ and this quantity is needed to compute the Helmholtz energy of the system. For Gaussian chains the single molecule partition function is conveniently and exactly evaluated by using a diffusion equation. Edwards realized that by using the segment potentials one can (in first order) correct for the excluded volume interactions. The mapping of the Edwards equation on the lattice transforms the chain model to the freely jointed chain model:

$$\frac{\partial G_i(z, s|1)}{\partial z} = \frac{1}{6} \frac{\partial^2 G_i(z, s|1)}{\partial z^2} - u_i(z) G_i(z, s|1)$$
$$G_i(z, s+1|1) = G_i(z)\langle G_i(z, s|1) \rangle \tag{3.9}$$

where $G_i(z, s|1)$ is the Green function, which collects the statistical weight of all conformations of molecules i that started with segment $s = 1$ and ends in segment s at coordinate z and therefore these quantities are known as the end-point distribution functions. $G_i(z) = \exp{-u_i(z)}$ is the statistical weight of a free (unconstrained) segment, and hence is referred to as the free segment distribution function. The lattice variant of the Edwards equation is known as the propagator equation as it elongates the chain by one segment. The propagators can conveniently be used to find the complete set of end-point distribution functions when for the first segment (starting conditions) the free segment distribution functions

are used $G_i(z,1|1) = G(z)$. The single chain partition function is found by integrating or taking the sum over all end-point distributions of the N_i^{th} segment: $q_i = \sum_z G_i(z, N|1)$.

The evaluation of the volume fraction profiles is straightforward from the endpoint distribution functions. For homopolymers we can make use of the symmetry in the molecule and find for the freely jointed chain:

$$\varphi_i(z,s) = \frac{\varphi_i^b}{N_i} \frac{G_i(z,s|1)G_i(z,N_i-s+1|1)}{G_i(z,s)} \tag{3.10}$$

The summation over all segments gives the volume fraction per component, i.e., $\varphi_i(z) = \sum_{s=1}^{N_i} \varphi_i(z,s)$. Note that the evaluation of the volume fractions of equation 3.10 requires knowledge of the bulk volume fractions. It is easily shown that $\varphi_i^b = \frac{\theta_i}{q_i}$, wherein θ_i gives the sum of the volume fractions over all coordinates:

$$\theta_i = \sum_{z=0}^{M} \varphi_i(z) \tag{3.11}$$

In our system we have molecules for which the bulk volume fraction is given as an input (grand canonical). For other molecules in the system it is more convenient to specify the amount θ_i. Finally we have a solvent molecule (W). The normalization of this component is taken such that the bulk is incompressible:

$$\varphi_W^b = 1 - \sum_{i \neq W} \varphi_i^b \tag{3.12}$$

Note that the bulk volume fractions are also needed to find the reference potentials in equation 3.6.

The above equations are closed in the sense that the segment potentials can be computed when all volume fractions are known and vice versa the volume fractions can be computed when all potentials are known. This mutual dependence is formally expressed by:

$$\varphi[u] \longleftrightarrow u[\varphi] \tag{3.13}$$

The fixed point of these equations is found numerically by an iteration. We arrive routinely to seven significant digits.

In both sides of our system, that is on both $z = 0$ and $z = M$ we implement mirror-like, reflecting boundary conditions. In such a case there are multiple SCF solutions to the equations. An initial guess is needed to prevent the system to chose the homogeneous solution and we choose the guess for the potentials such that the phase α is on the lower values of z, the phase β at high values of z -this phase we will also assign to be the 'bulk' phase, and the phase γ is in between. Sometimes

we will shift the z-coordinate system to have $z = 0$ at the symmetry plane in the system but we trust that this will not confuse the reader.

Returning for a moment to the propagator, equation 3.9. It is clear that in the phase for which the free segment distribution has the values $G_i(z) = 1$, that subsequently end-point distributions $G_i(z, s|1) = 1$ for all z and s. Then from the composition law 3.10 it follows that the segment densities assume the value $\varphi_i(z, s) = \varphi_i^b$. Indeed, as already mentioned above, this is the problem of using the Edwards equation: for the chains in the reference phase (in fact in all homogeneous phases) the intra-molecular excluded volume effects are smeared out such that the chains do not feel their own segments. The chains are then Gaussian, they do not have an 'internal' potential and hence polyelectrolytes can not maintain their own cloud of counterions. This is why complex coacervation in bulk, i.e. wherein both chains and all ions are coming from the same phase, will not form polyelectrolyte complexes and no associative phase transition is observed. Below we do study such a phase behavior but we are limited to those cases that the polyelectrolytes and their coions do not have the same interaction parameters and therefore have different *a priori* distribution functions.

Essential for the study of wetting effects we need to evaluate the interfacial free energies of the system. In the SF-SCF approach there is a closed expression for the grand potential per unit area, $\Omega = F - \sum_i \mu_i n_i$, where F is the Helmholtz energy (per unit area) and μ_i the chemical potential of component i. The grand potential can be written as a summation over the grand potential density $\Omega = \sum_z \omega(z)$ where:

$$
\omega(z) = -\sum_i \frac{\varphi_i(z) - \varphi_i^b}{N_i} - \sum_i u_i(z)\varphi_i(z) -
$$
$$
\sum_i \sum_j \chi_{ij} \left(\varphi_i(z)\langle\varphi_j(z)\rangle - \varphi_i^b \varphi_j^b \right) - \sum_i \frac{1}{2} q(z)\psi(z)/k_B T
$$

(3.14)

Note that Ω is the overall grand potential of the system and that when there are multiple interfaces in the system, the grand potential gives the sum over all these interfacial free energies. By taking partial sums over the subset of coordinates such that the inhomogeneities from one specified interface are summed over, one will obtain the surface tension of this interface, $\sigma = \sum'_z \omega(z)$ where the prime indicates that the sum is only over those layers that 'belong' to one particular interface. Note that when the interfacial film of the coacervate phase is only mesoscopically thick, the interfaces usually interact with each other and there is no operational way to disentangle the grand potentials to contribute to one of the interfaces. Then only the total grand potential is operational.

Part II

SOFT COLLOIDS AT INTERFACES

Chapter 4

Microgels at oil-water interfaces

In this chapter we introduce composite microgel particles that contain a solid, fluorescently labeled, polystyrene core embedded into a microgel shell. This design allows direct and accurate visualization without the necessity of potential perturbing sample preparation techniques. By combining *in-situ* imaging and tensiometry, we determine that these composite microgels anchor strongly at a wide variety of oil-water interfaces, with adsorption energies of approximately 10^6 k_BT, typical for particle adsorption. Yet they accumulate spontaneously without any energy barrier at the interface, which is more typical for polymers. The high adsorption energies allow the particle to spontaneously form very dense crystalline packings at the liquid interface in which the microgels are significantly compressed with respect to their swollen state in bulk solutions. Finally, we demonstrate the unique nature of these particles by producing highly stable and monodisperse microgel-stabilized droplets using microfluidics.

4.1 Introduction

Microgel particles, typically consisting of a water-swollen crosslinked hydrogel network of colloidal dimensions, are soft and deformable. While often referred to as a colloidal suspension, technically, a microgel system is a solution as the composition within the microgel is thermodynamically balanced with the solvent in which it is dissolved. A balance between osmotic pressure within the particle, arising from hydrated monomers and possible ionic groups, and the entropic elasticity, arising from the crosslinked polymer chains, determines the equilibrium size of the microgel in dilute solution. Changing the external conditions, either affecting the osmotic conditions inside the particle, for example by changing the solvent quality with temperature, or adjusting the charge density with pH can thus give rise to changes in the particle size.[1] Similarly, increasing the particle concentration in bulk solutions can induce osmotic compression of the particles and lead to a size reduction.[2] By contrast, microgel particles display much of the same characteristic phase behavior that solid, dispersed, colloidal suspensions exhibit, such as crystallization,[3] glass formation[4,5] and gelation.[6] Microgels thus display a fascinating polymer-particle duality;[7,8] this is reflected in, for example, the particle-like scaling of rheological data at intermediate concentrations and the polymer-like behavior in dense systems.[9]

While recent work has established the versatility of microgels in stabilizing fluid interfaces,[10–22] the details of their adsorption, conformation and organization remain largely elusive. Moreover, how their compressibility and deformability interplay with the other forces that act on particles at a liquid interface is still largely unknown. Cryo-SEM imaging, upon freeze-fracturing of microgel-stabilized emulsions, has shown that significant deformation of the soft particles may occur.[16–18] This suggests a subtle interplay between the forces acting on the particles at the interface, such as capillary forces, and the internal elasticity of the microgels. However, due to the thermosensitivity and delicate nature of microgels this information would ideally be obtained from non-invasive methods that do not require extreme temperature changes or phase changes in the two immiscible liquids. Direct and accurate imaging of solvent-swollen microgels is difficult as their refractive index is inherently close to that of the aqueous solvent that swells them. Moreover, addition of a fluorescent dye, even in small amounts, can significantly alter their interfacial properties.

Composite microgels effectively stabilize oil-water interfaces.[23,24] In this chapter, we prepare composite microgel particles in which a highly fluorescent solid core is embedded into a pH and temperature responsive microgel shell; this design allows accurate and *in-situ* visualization of the structure of microgel-laden fluid

interfaces. Combining in-situ observation with tensiometry allows us to estimate the adsorption energy and the particle elasticity. We place our observations in the light of various possible scenarios for the adsorption mechanism of microgels in an attempt to unify our, and others', observations. Moreover, we show that the spontaneous adsorption of these microgels at a variety of oil-water interfaces, together with their ability to provide extended stability of emulsion droplets, allows the formation of highly monodisperse and well-defined emulsion droplets using flow-focused microfluidics.

4.2   Experimental details

4.2.1   Materials

N-isopropylacrylamide (NIPAm), N,N-methylbisacrylamide (BIS), methacrylic acid (MA), potassium persulfate (KPS), styrene, sodium dodecyl sulfate (SDS), divinylbenzene (DVB), decane, silicon oil (viscosity of 100 mPa.s), carbon tetrachloride (CCl_4), dimethylformamide (DMF) and toluene were purchased from Sigma-Aldrich. Potassium nitrate (KNO_3) was purchased from Merck. The fluorescent dyes Pyrromethene 546 and Pyrromethene 605 were purchased from Exciton. PolyFluorTM 570 was purchased from PolySciences, Inc.

All chemicals were used as received. Milli-Q water was used for the synthesis and characterization of the microgel particles and the preparation of the emulsions.

4.2.2   Composite microgel synthesis

Core-shell microgels are synthesized in a two-step procedure. First, fluorescent cores, with a diameter of 0.2 μm, are synthesized by emulsion polymerization. To this end, 3.75 g NIPAm, 48 g styrene, 100 mg SDS and 50 mg fluorescent dye Pyrromethene 546 are dissolved in 130 mL Milli-Q water. The mixture is stirred at 500 rpm, heated to 75 °C and purged with N_2 for 15 minutes. The reaction is initiated by the addition of 100 mg KPS dissolved in 5 mL Milli-Q water and the reaction is left to proceed overnight. The reaction mixture is filtered and the cores are cleaned by repeated centrifugation and resuspension in Milli-Q water.

Second, a microgel shell is grown around the cores by precipitation polymerization. 1.0 g NIPAm, 100 μL MA and 40 mg BIS are dissolved in 95 mL Milli-Q water. Then, 0.3 g cores are added and the mixture is sonicated for 2 minutes. The mixture is stirred at 500 rpm, heated to 75 °C and purged with N_2 for 15 minutes. The reaction is initiated by the addition of 100 mg KPS dissolved in 5 mL Milli-Q water and the reaction is left to proceed for 2 hours. The reaction mixture

is filtered and the composite microgels are cleaned by repeated centrifugation and resuspension in Milli-Q water.

4.2.3 Emulsion preparation

We prepare a stock solution of microgels ($c = 27$ g/L). For the emulsion preparation, we first dilute the microgel dispersion to the desired concentrations of particles and salt using Milli-Q water and a solution of 15 mM of KNO_3, we then mix the microgel dispersion with oil weight ratio 9:1. Mixing is done by vortexing for 30 s or by using a high speed mixer Ultra Turrax for 1 min at 1200 rpm. Alternatively, a microfluidic flow focusing device is used to create monodisperse droplets. The chip is made of glass and the inlet and outlet sections are connected to Teflon tubing. The microgel dispersion and the oil phase are dosed using syringe pumps, respectively at flow rates of 100 μL/min and 8 μL/min.

4.2.4 Experimental methods

The hydrodynamic radius of the synthesized particles R_h is measured as a function of pH and temperature, using dynamic light scattering. The interfacial tension γ between a droplet of the microgel dispersion and a continuous oil phase is measured through pendant drop tensiometry (Pat-1, Sinterface Technologies). The interfacial tension is followed during adsorption upon creating a pristine interface at t = 0, with a sampling rate of 2 Hz and a droplet size of 10 mm^3, at room temperature. Confocal images are recorded using a Zeiss Axiovert 200M microscope equipped with a LSM 5 EXCITER and fitted with a 100$\times$ oil-immersion objective. Quantitative image analysis is done with a minimum of 8 unique images, in which particle centroids are located using standard 2D particle tracking algorithms, with 15-20 nm spatial resolution. Data analysis is done on the average of the ensemble images. All characterization experiments are done in 15 mM KNO_3 solutions, of which the pH is set with 0.1 M HCl or 0.1 M NaOH.

4.3 Results and discussion

4.3.1 Particle characterization

A plethora of recent work has demonstrated the versatility of soft microgel particles as stabilizers for liquid interfaces. [10–22] However, the exact mechanism of their adsorption at oil-water or air-water interfaces and their conformation at these liquid
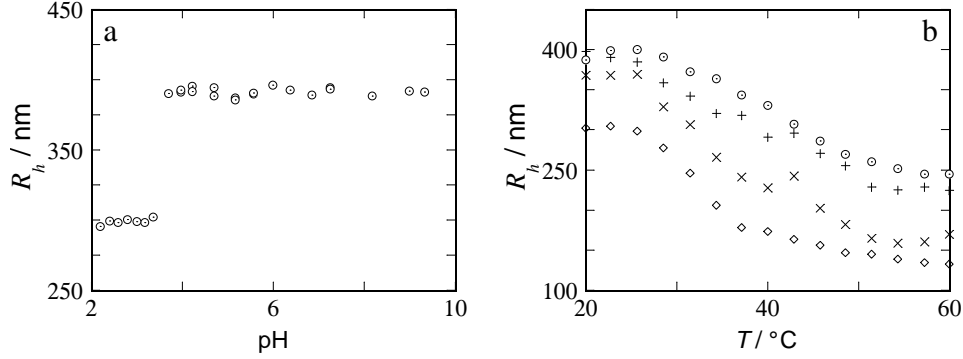
Figure 4.1: Hydrodynamic radius R_h of the composite microgel particles as a function of: (a) pH at 22 °C, (b) temperature for different pH values: $\diamond$ pH = 3.2, $\times$ pH = 5.3, + pH = 7.2, $\odot$ pH = 11.8. For both experiments, the salt concentration is fixed (15 mM KNO$_3$).

interfaces remains speculative at best. Answering these questions is in part hindered by the difficulty in real-space and real-time imaging of microgel particles at liquid interfaces. While micron sized poly(N-isopropylacrylamide-co-methacrylic acid) microgels, abbreviated p(NIPAm-co-MA), quickly accumulate at the interface of a decane droplet in water and form an ordered colloidal lattice, their inherently minimal refractive index contrast with the aqueous solution that swells the particles, limits their visualization and quantitative image processing.

Here, we introduce a solid, submicrometer sized, fluorescently-labeled polystyrene particle, inside a shell of p(NIPAm-co-MA). The hydrophobic fluorescent dye is trapped inside the glassy matrix of the polystyrene core; we observe no measurable leaching of this dye into the aqueous phase during the entirity of the experiments. The presence of a solid fluorescent core, with high fluorescent intensity, allows high resolution confocal imaging and accurate detection of the particle centre-of-mass, as compared to imaging with undyed or dyed microgels. [5,25] Moreover, the encapsulation of the fluorescent dye inside a inert solid core ensures that the addition of fluorescent label in no way influences the interfacial properties of the microgels.

To verify that with the introduction of a solid core the pH- and temperature-responsivity of these microgels, which are two of the features that make them of interest in emulsion stabilization, remains we determine by dynamic light scattering the hydrodynamic diameter of the core-shell particles as a function of both pH and temperature (Figure 4.1). Upon increasing the pH at room temperature, the composite microgels swell from a radius of 300 nm at pH < 3.5 to approximately 390 nm at pH > 3.5 (Figure 4.1a). The composite microgels have pH-dependent charges in their shell originating from the methacrylic acid monomers that are
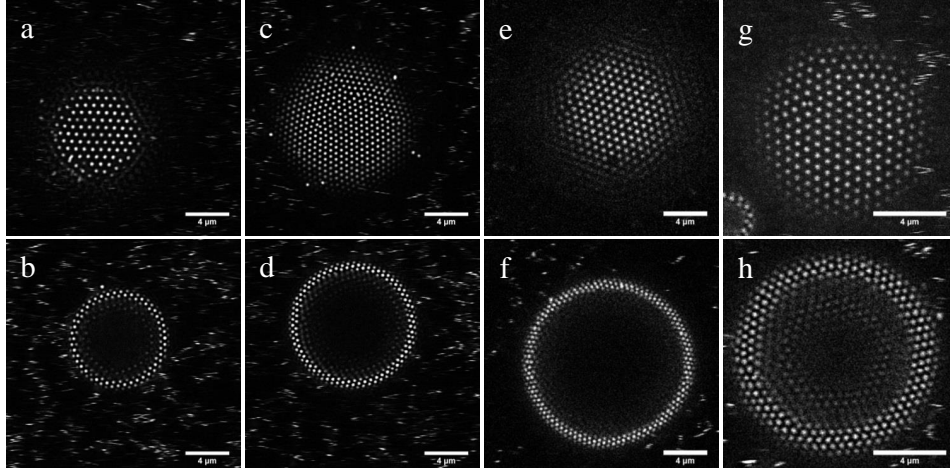
Figure 4.2: Confocal microscopy images of oil droplets stabilized by composite microgels at $\varphi_{oil} = 0.1$, $c = 2.7$ g/L, pH $= 5.9$ and $I = 15$ mM: (a-b) decane, (c-d) silicone oil, (e-f) toluene, (g-h) CCl$_4$. The top row shows a top view of the droplet, the bottom row is a single confocal slice through the droplet.

copolymerized. At pH values below 3.5, the composite microgels are mostly uncharged. Here, the equilibrium size of the particles is set by a balance between the internal osmotic pressure of the hydrated monomers and the elasticity of the crosslinked network. By contrast, at pH values above 3.5 the carboxylic groups become progressively deprotonated; this gives rise to an electrostatic contribution to the osmotic pressure within the microgel shell and a new and larger equilibrium size results. Interestingly, this seems to be an abrupt transition. Similar results are observed for homogeneous pH responsive microgels. [1] We also verify the thermosensitivity of these core-shell particles; as for homogeneous microgels, we find a collapse transition at approximately 32 °C for uncharged particles at low pH, and this transition shifts to higher temperature and broadens with increasing pH (Figure 4.1b). [1] These data show that the introduction of a solid core does not change the responsivity of the microgel shell to both pH and temperature.

4.3.2   Emulsion stabilization

To explore the universality of these composite microgels as emulsifiers, we prepare emulsions from a variety of apolar solvents like decane and silicone oil. These emulsions are made by gentle mixing of an aqueous suspension of composite microgels and the oil phase through 30 s of vortexing. We find that emulsions of decane-in-water and silicone oil-in-water are easily prepared in this way; in both cases, well

stabilized droplets with hexagonally-packed surfaces result (Figures 4.2a-d). To emulsify apolar liquids that are a good solvent for polystyrene, an uncrosslinked polystyrene core with a physically embedded dye would lead to dissolution of the core and leaking of the dye. To overcome this problem, we synthesize core particles that are crosslinked using divinylbenzene and co-polymerized with a fluorescent monomer. Using core-shell microgels prepared with these crosslinked cores, we are able to form stable emulsions, again with well-ordered and fully covered interfaces, of a large variety of apolar solvents that have a miscibility gap with water; this is demonstrated by preparing emulsions of toluene and carbon tetrachloride (Figures 4.2e-h). This is remarkable as true Pickering emulsions, formed from solid particles such as silica[26,27] or polystyrene[28–30] often require fine-tuning of the surface chemistry to ensure good anchoring of the particles at the interface.

This raises questions regarding the mechanism of adsorption of microgel particles and their conformation at the oil-water interface, topics that have received significant interest recently.[16–21] We can envision a few possible scenarios. For classical Pickering emulsions, in which solid undeformable particles adsorb at the air-water interface, the appropriate thermodynamic description is given by Young, as illustrated in Figure 4.3a, in which a contact angle between an oil phase, an aqueous solution and a solid substrate with infinite rigidity, is defined as:

$$\cos \theta = \frac{\gamma_{s-aq} - \gamma_{s-oil}}{\gamma_{aq-oil}} \tag{4.1}$$

in which three interfacial energies γ_{a-b} are defined between the three immiscible phases.

By contrast, if the solid is replaced by a third liquid or a very soft solid, the contact line takes on the typical cusp-shape sketched on the right in Figure 4.3b. When the rigidity of the third phase, here still denoted as solid (s), vanishes, the situation is described by Neumanns triangle:

$$\frac{\gamma_{s-oil}}{\sin \theta_{aq}} = \frac{\gamma_{s-aq}}{\sin \theta_{oil}} = \frac{\gamma_{aq-oil}}{\sin \theta_s} \tag{4.2}$$

For soft solids with finite moduli, a balance between the capillary forces at the contact line, and the elasticity of the soft solid, create a situation intermediate to that described for the two limiting situations by Young and Neumann. In this elastocapillary regime, substantial deformations of the solid can occur due to forces acting at the contact line; this has been demonstrated both experimentally[31] and theoretically.[32] For cases of soft solids at a fluid interface, it is convenient to define an elastocapillary length as:

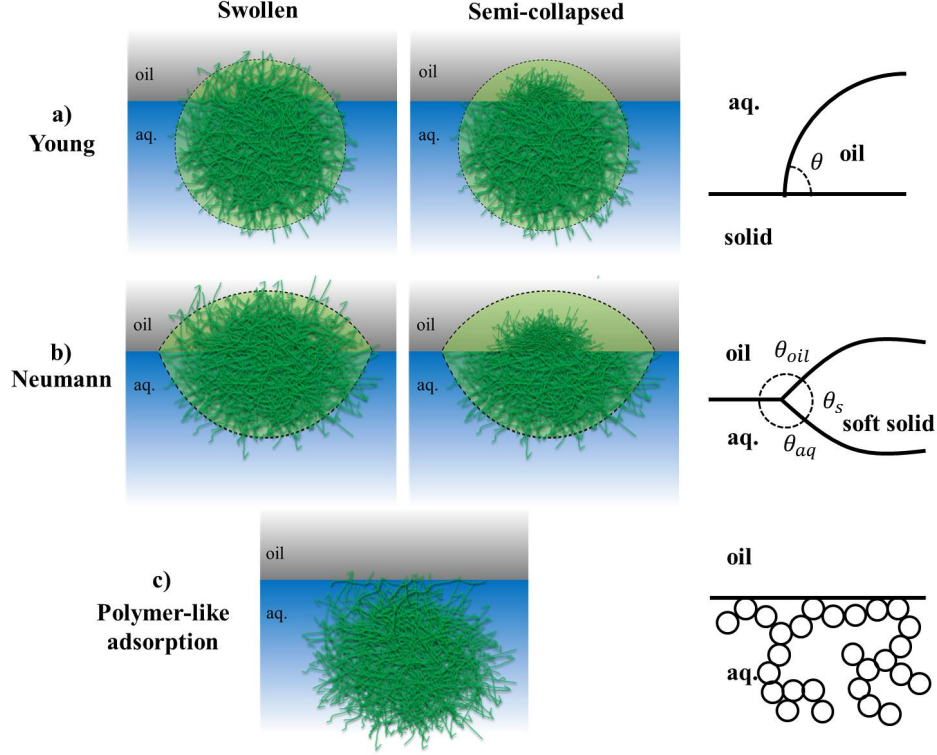$$l_{EC} = \frac{\gamma_{aq-oil}}{E} \tag{4.3}$$

Figure 4.3: Adsorption scenarios for an isolated microgel particle: (a) Young, (b) Neumann. The left schematic images correspond to a swollen microgel in both aqueous and oil phases whereas the right schematic images show a collapsed state in the oil phase and a swollen state in the water phase. The light green is the microgel size in the swollen state. An alternative to these scenarios is a polymer-like adsorption (c).

in which E is the elastic modulus of the soft solid; l_{EC} gives an estimate for the magnitude of the elastic deformation of the soft solid due to the capillary forces. This can be made into a dimensionless elasto-capillary number:

$$EC = \frac{\gamma_{aq-oil}}{Ea} \tag{4.4}$$

in which a is a characteristic length scale. When a is defined as a molecular scale, such as the typical mesh size of the soft solid, this dimensionless number predicts the transition from a Neumann-type cusp profile, $EC > 1$, to a classical Young contact line for $EC \ll 1$.[33] Here we can also define a as a macroscopic dimension, such as the radius of the microgel particle, to evaluate the significance of elastocapillary deformations.

For an order of magnitude estimate, we take $\gamma_{aq-oil} = $ 10-100 mN/m, which

encompasses typical values found for water-air and most water-oil combinations. For the elasticity of the microgel particles, which obviously varies with crosslinking density, we take a typical value of 100 kPa;[34] this gives an elastocapillary length of $l_{EC} = 0.1$-1 μm. Clearly, interfacially-induced deformations of microgel particles, as demonstrated in previous studies[16–20] could be explained within this approach, as can the variation of the relative deformation with crosslinking density through variations in E. By contrast, for hard particles such as polystyrene with Youngs moduli of order GPa, we find an elastocapillary length smaller than 0.1 nm, hence any interface-induced deformations can be safely ignored.

4.3.3   Interfacial structure analysis

The major advantage of the composite microgels with a fluorescently-labeled core, which we use here, is that imaging of the particles at the surface of the droplet can be done *in-situ* with non-invasive confocal microscopy, without the need for sample treatments such as freezing/vitrification and freeze-fracture as employed in previous studies. We determine the center-of-mass of our particles at the cap of a spherical droplet, prepared by vortexing the aqueous and the oil phases, with a lateral resolution of approximately 15 nm.[25] Visual inspection of the images shows an increase in the particle-particle separation distance with increasing pH (Figure 4.4). To quantify this, we compute the radial distribution functions of the particle positions *g(r)*. These show the characteristic pattern for a 2D hexagonal packing, with distinct peaks at 1, $\sqrt{3}$, 2, $\sqrt{8}$ and 3 × the nearest neighbor distance. Upon increasing the pH, the separation distance between nearest neighbors increases as evidenced from the corresponding peak shifting to larger values of r.

To evaluate if the particles spread at the interface, we normalize $g(r)$ with the hydrodynamic diameter D_h of the particles in dilute bulk solutions of the same pH and ionic strength, as measured by dynamic light scattering. This collapses the nearest-neighbor peaks of all pair correlation functions into a single peak at a normalized distance $r/D_h \approx 0.9$. This suggests that our composite microgels are slightly compressed when adsorbed at the interface. Previous work has shown that microgels can spread, remain undeformed, or are compressed, at a liquid interface depending on a variety of factors such as crosslinking density,[17] shear history,[20] charge density[22] and interfacial tension.[18] Note that previous observations for homogeneous microgels are made with potentially invasive techniques in which the sample, containing thermoresponsive particles, is first cooled and then freeze-fractured, while our observations are made in situ. It cannot be excluded that the sample preparation for the freeze-fracture SEM observations has changed the particle conformation and density at the oil-water interface. Others have in-
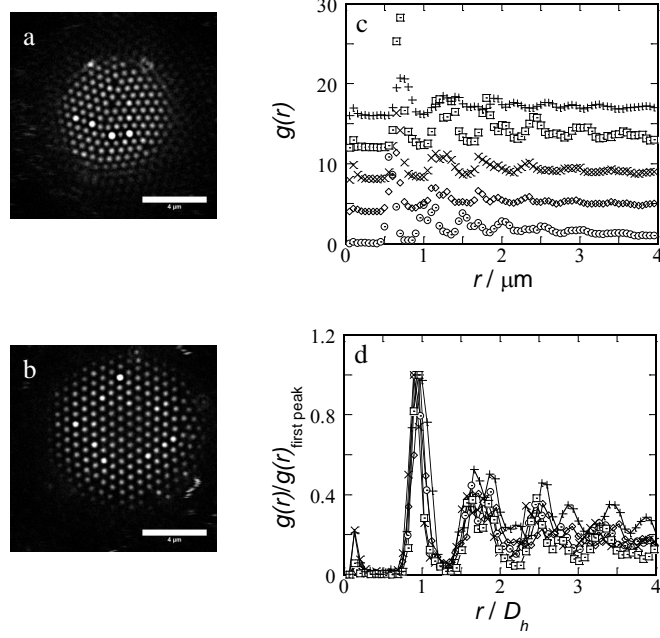
Figure 4.4: Influence of pH on the interfacial assembly of composite microgels: confocal microscopy images of decane droplets stabilized by composite microgels at $\varphi_{oil} = 0.1$, c = 2.7 g/L, I = 15 mM for (a) pH = 2.9 and (b) pH = 9.8; (c) pair correlation function $g(r)$ for different pH values: ∘ pH = 2.9, ⋄ pH = 4.1, × pH = 6.0, □ pH = 7.0 and + pH = 9.8, (d) normalized pair correlation function.

vestigated the packing of similar core-shell particles, with a silica core instead of a polystyrene core, using scanning force microscopy.[35] In this case, the imaging occurs under artificial conditions, requiring drying of the sample; also here, sample preparation-induced changes to the surface structure cannot strictly be excluded.

For the particles we use in this paper, the thickness of the soft shell that surrounds the undeformable core, R_{shell} = 300 nm is smaller than the elastocapillary length $l_{EC} \approx 500$ nm. This intuitively suggests that the core should diminish the deformation of the particles at a liquid interface. However, preliminary finite-element calculations indicate that the deformation generated by the contact line forces is highly localised, and with the shell thickness we use not significantly altered by the presence of a solid core. This remains speculative and a topic for future study.

If a microgel particle adsorbs in this Pickering, sometimes called Mickering, fashion, it raises the question what happens with the swollen part of the gel that protrudes into the apolar oil phase. In principle, it could expel its water and de-

swell to minimize the unfavorable contact between the aqueous microgel and the oil phase. The size of a microgel particle in its equilibrium state in an aqueous solution is governed by a balance between the internal osmotic pressure, due to hydrated segments and charges, and the restoring action of the entropic elasticity of the crosslinked polymer chains. Any additional perturbation to this balance necessarily must lead to a new equilibrium and hence a change in the size of the particle. Here, the unfavorable contacts between aqueous hydrogel and oil must therefore lead to shrinkage of that part of the particle that protrudes into the oil (Figure 4.3a,b middle column). The extent of this shrinkage depends strongly on the interfacial tension between the oil and swollen hydrogel. Recent work has suggested that microgels indeed adopt a pancake like conformation on the oil-side of the liquid interface.[19]

The argument of elasto-capillarity relies on the particles being anchored at the interface; thus, an important question to raise is the requirement of defining a three-phase contact line. However, for microgel particles, the solvent is continuous in the aqueous phase, hence it is troublesome to define a phase boundary between three immiscible phases. If we can define the microscopic hydrogels as a separate phase, it must be characterized by a very low surface energy γ_{s-aq} as the difference in chemical composition and water density may not vary significantly across this hypothetical water-microgel interface. Consequently, this should drive the system, in almost all cases, into full wetting for the microgel particles, suppressing the Pickering adsorption hypothesized in literature.

A characteristic hallmark of Pickering emulsification is the breaching of the air-water or water-oil interface, required for a solid particle to adopt its position at the liquid interface. In this process, the thin film that separates the solid surface of the particle and the liquid interface needs to break; this is an activated process, which for micronsized particles results in the requirement of significant energy input for adsorption to occur. As a result, Pickering adsorption of solid particles is non-spontaneous and irreversible, and is characterized by slow kinetically-limited dynamics.[36]

4.3.4   Adsorption kinetics and strength

To investigate the adsorption kinetics in our system, we measure the interfacial tension γ of a decane-water interface in presence of the core-shell particles as a function of time upon creating a pristine interface at $t = 0$. We plot the results as the surface pressure $\pi_s(t) = \gamma_0 - \gamma(t)$, in which γ_0 is the interfacial tension of the bare decane-water interface; here we find $\gamma_0 = 51$ mN/m, which is in agreement with the literature.[37] The cores alone, without the subsequently grown microgel
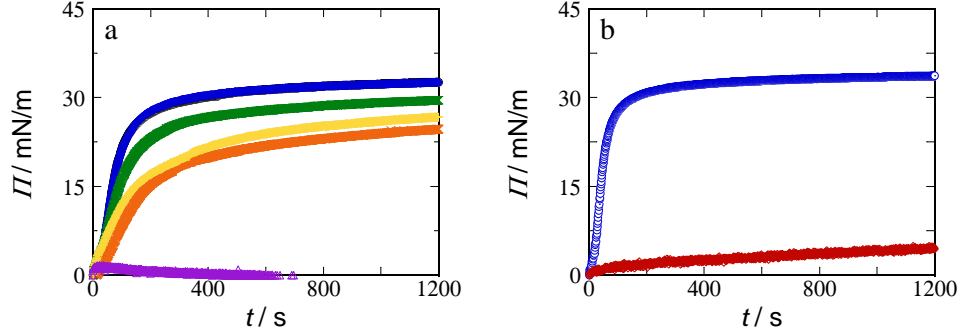
Figure 4.5: Surface pressure as a function of: (a) time for the cores (purple) and for the microgel solutions with $c = 2.7$ g/L and different pH values: blue pH = 4.1, green pH = 6.0, orange pH = 7.0 and yellow pH = 9.1, (b) microgel concentrations at pH = 4.0: blue $c = 2.7$ g/L, red $c = 0.27$ g/L.

shell, are not surface active, as shown in Figure 4.5a. However, the core-shell microgels display a rapid increase in surface pressure for all pH values investigated (Figure 4.5a). As reported previously, lowering the pH, i.e. decreasing the charge density in the microgels, gives rise to higher surface pressures.[13] However, we offer a different interpretation of these results.

Interestingly, despite their large size, the microgels adsorb spontaneously suggesting that the energy barrier is either very small or absent. This barrier-free adsorption, atypical for solid colloidal particles, is typical for adsorption of polymers and surfactants, in which no film between the adsorbing species and the interface needs to be breached. For molecular adsorption, such as adsorption of surfactants and polymers, the initial stages can be followed by the increase of surface pressure even in the limit where the adsorbed species do not yet interact. An estimate of the surface pressure in the ideal gas limit, only applicable for very low surface concentrations, can be made by analogy to the ideal gas: $\pi \approx \frac{n}{A} k_B T$, in which the area number density n/A is the inverse of the area per adsorbed species. For the large particles we study, with a radius of approximately 400 nm, this pressure is negligible up to a fully covered surface for which A/n becomes equal to the particle cross section, giving an entropic surface pressure $\pi_s = 10^{-8}$ N/m. This is well below the measurement limit of any tensiometric method.

Hence, any surface pressure that is measurable ($\pi_s > 1$ mN/m) must originate from particle interactions instead. Consequently, the use of diffusion-limited models to describe the initial stages of adsorption, in which Langmuir-type process are relevant, seems inappropriate. Rather, once during the interfacial tension measurements an increase in surface pressure is observed, this must be related to

the insertion of extra particles into an already relatively dense layer. In this limit the measured surface pressure cannot be easily related to the surface coverage as this requires knowledge of the two-dimensional equation of state. Although this is not known for these systems in detail, we can safely assume that for particles of this size, the pressure increases steeply once a critical (overlap) concentration is reached, as was demonstrated for bulk suspensions of microgel particles.[9]

Thus, we need to consider the interactions between the microgels, the thermodynamic balance between the internal osmotic pressure in the microgel, and the pressure at the surface. The surface pressure that acts on a particle must be balanced by the osmotic pressure within the microgel. In bulk solution, the balance between the osmotic pressure, due to hydrated monomers and charges, and the entropic elasticity of the polymer network sets the equilibrium size of the microgel. When the microgel particle is brought to an interface, its internal osmotic pressure, π_p, which is an energy per unit volume, is balanced against the external surface pressure supplied by the densely packed layer at the interface: $\pi_s/R = \pi_p$. We find typical values of the surface pressure around 30-40 mN/m once the surface has reached an equilibrium. This implies that the internal osmotic pressure within the microgel $\pi_p = 100$ kPa, suggesting that the internal pressure is raised significantly when the particles attach to the interface in a dense and ordered layer.

The generated internal pressure, which is energetically highly unfavorable, must ultimately be counterbalanced by the adsorption, or anchoring, energy E_{ad} of the particles. As an order of magnitude estimate we take $E_{ad} = \pi_s A_p$ with A_p the particle cross-sectional area at the interface. Assuming $A_p = \pi R^2$, this gives an estimated adsorption energy of approximately 10^6 $k_B T$. Surprisingly, despite the spontaneous adsorption, we find an ultrastrong anchoring of the microgels at the oil-water interface. This is a striking demonstration of the polymer-particle duality of microgel particles, even at liquid interfaces. While the adsorption process itself occurs spontaneously, as commonly observed for polymers, the anchoring strength is extraordinary large, typically associated with Pickering adsorption of solid particles.

From these order-of-magnitude estimates, we can also estimate the bulk modulus of the microgel particles at the interface, typically defined as: $K = -V dP/dV$. From our microscopy experiments we know that the particles are compressed at the interface, leading to an effective radius of 0.9 times the radius of the particles in bulk solution (Figure 4.4). This apparently gives rise to an external pressure of approximately 100 kPa. From this we estimate the bulk modulus to be in the order of 100 kPa. This is in direct agreement with the values found for the bulk modulus of microgel particles of similar composition measured using a capillary micromechanics technique.[38] Interestingly, it appears that order-of-magnitude estimates

for microgel elasticity can be made from simple adsorption experiments.

The small yet significant decrease in the equilibrium surface pressure we observe with increasing pH suggests that the anchoring energy decreases when the particles become charged. As we can expect, the affinity of the microgel particle for an interface between water and an apolar solvent becomes less when more charges, which prefer to remain hydrated in the aqueous phase, are present.

As mentioned above, any measurable surface pressure that develops at a liquid interface due to the adsorption of micron-sized particles must result from particle interactions, rather than from the entropic pressure generated during the initial stages of particle attachment. Therefore, we feel that the development of the surface pressure should not be interpreted as a diffusion-limited, Langmuir-type, adsorption process describing the attachment of individual, isolated, particles at an interface. Rather, we speculate that the increase of surface pressure in time results from the insertion of additional particles in an already relatively concentrated monolayer. The addition of each subsequently particle leads to a highly non-linear contribution to the surface pressure; hence, making a direct link between the observed increase in surface pressure and the surface coverage is difficult. If rearrangements within the monolayer, required for inserting an additional particle, would be time limiting, we would expect a zero-order dependence of this adsorption process on bulk concentration. Rather, we find a super-linear dependence; decreasing the bulk concentration of particles by a factor of 10 slows down the final stage of the adsorption process by approximately 100 times (Figure 4.5b). A quadratic dependence of the time scale of adsorption and bulk particle concentration was described previously, which is indicative of a diffusion process. [21] Note that it is not likely a diffusion limited process of a microgel particle toward the interface but a surface diffusion process which sets the time scale of the surface rearrangements. These surface rearrangements are expected to be a function of temperature and pH.

So far, we have found that the anchoring of composite microgel particles is simultaneously ultrastrong but barrier-free; this suggests an intermediate behavior between that of classical polymer and classical Pickering adsorption. This could be consistent with a scenario in which microgel particles do not actually penetrate the interface but adsorb at the oil-water interface from the aqueous side as an ultra-high molecular weight branched polymer, as illustrated in Figure 4.4c. As polymer adsorption does not require the crossing of an energetic barrier, it occurs spontaneously. In this scenario, the spreading of the microgel particle at the interface, to maximize the polymer-interface contact, is again balanced with the internal elasticity of the microgel particle. A characteristic deformation length scale can now be defined as $l = \pi_s/E$ in which π_s is the surface pressure at the liquid interface
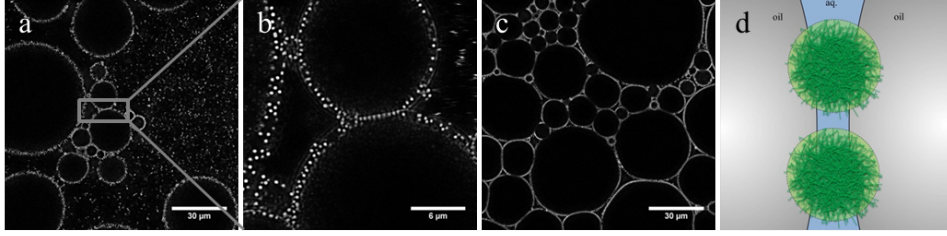
Figure 4.6: Confocal microscopy images of bridged droplets stabilized by composite microgels at $\varphi_{oil} = 0.1$, $c = 2.7$ g/L, pH $= 5.9$ and $I = 15$ mM for: (a-b) decane, (c) silicone oil; (d) is a schematic representation of two bridged droplets.

due to the adsorbed polymer segments. Typical surface pressures for adsorbed layers of poly(N-isopropylacrylamide) are on the order of 10-30 mN/m;[39] also here, deformation lengths of the order on 0.1-1 μm are feasible to achieve. Hence, this adsorption scenario could also account for the observed deformation of sufficiently soft microgels at oil-water interfaces, while being consistent with the scenario of spontaneous and reversible adsorption. However, in this case, no significant deformation of the liquid interface should be expected and capillary interactions, thought to be responsible for the ordered packing of the microgels at the interface of emulsion droplets, should be negligible.

4.3.5   Droplet bridging

One final observation that is in contradiction to a purely polymer-like adsorption scenario, is that when we prepare emulsions under conditions of high mechanical energy input, using a rotor-stator mixer, typically used to prepare Pickering emulsions, we observe severe particle bridging (Figure 4.6); two emulsion droplets are firmly anchored, evidenced by the significant faceting, by a single layer of particles. This can occur in Pickering systems, when the contact angle of the solid surface is significantly less than 90 degrees, such that a single particle can adsorb at the interface of two neighboring droplets at the same time. For polymer adsorption, bridging is only found under specific conditions where the amount of polymer is insufficient to cover all available surface area, while in our experiments the microgel particles are always present in excess. Moreover, for polymer bridging the expected adhesion forces are not sufficient to cause micron-sized faceted contacts between the droplets.

Destribats et al. showed that the shear forces during emulsion preparation can influence the packing of the particles at the interface.[20] Therefore we performed particle tracking analysis also on the bridged emulsion droplets. In this case, we

find no significant difference in the packing density, determined from the nearest-neigbor distance, between samples prepared with low or high shear.

We can speculate regarding a scenario in which these apparently conflicting observations are unified. This could consist of an intermediate scenario between polymer-like adsorption and true Pickering stabilization, in which, under low-mechanical energy conditions, the adsorption process begins with a spontaneous, polymer-like adsorption. Once bound to the interface the particles breach the interface and adopt a more Pickering like configuration. The kinetic surface tension measurements presented above, show a distinct two-step adsorption process, which could support this speculation. Under high-energy input conditions, it is possible that the energy barrier for breaching the interface, possibly responsible for the slow second stage in the adsorption, is lowered sufficiently that the Pickering state is reached immediately, resulting in the particle-bridged emulsion gels shown in Figure 4.6.

4.3.6 Microfluidics

Clearly, arriving at a conclusive answer to these questions will require significant effort in future research. The microgel particles we used here, allowing to separately control imaging possibilities and microgel chemistry, can be a valuable tool in this direction. To conduct well-controlled experiments on the behavior of soft particles at liquid interfaces, the preparation of particle-laden interfaces is another hurdle. As shown above, preparation of emulsion by simple mixing, renders the system highly sensitive to the shear history as samples easily transform from single stable droplets to a highly interconnected network of particle-bridged droplets. The use of microfluidic emulsification should in principle mitigate this problem as each droplet undergoes the exact same flow history. However, microfluidic preparation of solid particle stabilized Pickering emulsions is difficult as the laminar flow conditions typically do not provide the required forces to overcome the energy barrier for breaching the oil-water interface. Here, we may expect that the spontaneous adsorption of the microgels makes it possible to prepare well-defined and monodispersed emulsion droplets using standard microfluidic designs. We test this by preparing decane-in-water emulsions in a microfluidic flow focusing device, and find that at sufficiently high concentrations of core-shell microgels in the aqueous phase, we are able to prepare perfectly monodisperse droplets, stabilized by fully-covered hexagonally packed microgel layers at the interface, as shown in Figure 4.7. This opens up a wide variety of new possibilities to investigate the structure and stability of emulsions stabilized by soft and responsive particles.
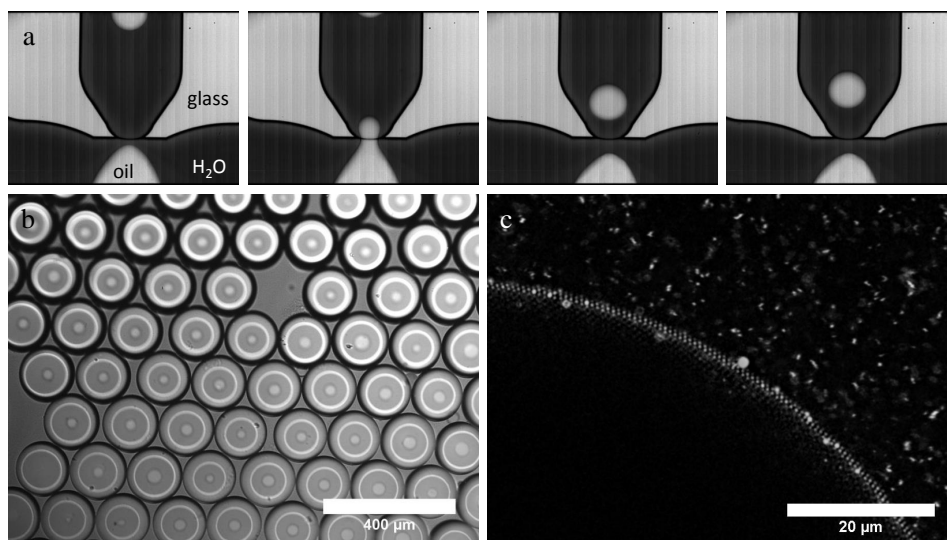
Figure 4.7: (a) Generation of monodisperse decane droplets using a focused flow droplet generator. (b) Brightfield image of decane droplets hexagonally packed. (c) Confocal microscopy image showing the hexagonal packing of the composite microgels at the decane surface droplet.

4.4   Conclusion

Composite microgels display a duality in their interfacial behavior: their spontaneous adsorption at the oil-water interface is typically for polymers while their high adsorption energy, which we determine to be 10^6 k_BT, points to a Pickering-like anchoring. Interestingly, these microgels appear to be a universal stabilizer of a wide variety of oils. Moreover, due to the spontaneous adsorption of these microgels at liquid-liquid interfaces, we are able to prepare monodisperse particle-stabilized emulsion droplets using a microfluidic device.

References

[1] M.J. Snowden, B.Z. Chowdhry, B. Vincent, and G.E. Morris, *J. Chem. Soc. Faraday. Trans.*, 1996, **92**, 5013–5016.

[2] M. Muluneh, J. Sprakel, H.M. Wyss, J. Mattsson, and D.A. Weitz, *J. Phys.: Condens. Matter*, 2011, **23**,.

[3] Z.R. Wang, A.M. Alsayed, A.G. Yodh, and Y.L. Lan, *J. Chem. Phys.*, 2010, **132**,.

[4] J. Mattsson, H.M. Wyss, A. Fernandes-Nieves, K. Miyazaki, Z.B. Hu, D.R. Reichman, and D.A. Weitz, *Nature*, 2009, **462**, 83–86.

[5] R. Higler, J. Appel, and J. Sprakel, *Soft Matter*, 2013, **9**, 5372–5379.

[6] W. Liao, Y.J. Zhang, Y. Guan, and X.X. Zhu, *Macromol. Chem. Phys.*, 2011, **212**, 2052–2060.

[7] M. Stieger, J.S. Pedersen, P. Lindner, and W. Richtering, *Langmuir*, 2004, **20**, 7283–7292.

[8] L.A. Lyon and A. Fernandez-Nieves, 2012, pp. 25–43.

[9] P. Menut, S. Seiffert, J. Sprakel, and D.A. Weitz, *Soft Matter*, 2012, **8**, 156–164.

[10] T. Ngai, S.H. Behrens, and H. Auweter, *Chem. Commun.*, 2005, 331–333.

[11] T. Ngai, H. Auweter, and S.H. Behrens, *Macromolecules*, 2006, **39**, 8171–8177.

[12] S. Brugger and W. Richtering, *Langmuir*, 2008, **24**, 7769–7777.

[13] S. Brugger, B.A. Rosen, and W. Richtering, *Langmuir*, 2008, **24**, 12202–12208.

[14] S. Tsuji and H. Kawaguchi, *Langmuir*, 2008, **24**, 3300–3305.

[15] S. Berger, H.P. Zhang, and A. Pich, *Adv. Funct. Mater.*, 2009, **19**, 554–559.

[16] S. Brugger, S. Ruetten, K.-H. Phan, M. Moeller, and W. Richtering, *Angew. Chem. Int. Ed.*, 2009, **48**, 3978–3981.

[17] M. Destribats, V. Lapeyre, M. Wolfs, E. Sellier, F. Leal-Calderon, V. Ravaine, and V. Schmitt, *Soft Matter*, 2011, **7**, 7689–7698.

[18] S. Schmidt, T.T. Liu, S. Rutten, K.H. Phan, M. Moller, and W. Richtering, *Langmuir*, 2011, **27**, 9801–9806.

[19] K. Geisel, L. Isa, and W. Richtering, *Langmuir*, 2012, **28**, 15770–15776.

[20] M. Destribats, M. Wolfs, F. Pinaud, V. Lapeyre, E. Sellier, V. Schmitt, and V. Ravaine, *Langmuir*, 2013, **29**, 12367–12374.

[21] Z.F. Li, K. Geisel, and T. Richtering, W. Ngai, *Soft Matter*, 2013, **9**, 9939–9946.

[22] K. I. Geisel, L. Isa, and W. Richtering, *Angew. Chem. Int. Ed.*, 2014, **53**, 4905–4909.

[23] S. Fujii, E.S. Read, B.P. Binks, and S.P. Armes, *Adv. Mater.*, 2005, **17**, 1014.

[24] S. Fujii, S.P. Armes, B.P. Binks, and R. Murakami, *Langmuir*, 2006, **22**, 6818–6825.

[25] Y.X. Gao and M.L. Kilfoil, *Optics Express*, 2009, **17**, 4685–4704.

[26] B.R. Midmore, *Colloid Surf. A*, 1998, **132**, 257–263.

[27] B.P. Binks and S.O. Lumsdon, *Langmuir*, 2000, **16**, 8622–8631.

[28] J.I. Amalvy, S.P. Armes, B.P. Binks, J.A. Rodrigues, and G.F. Unali, *Chem. Commun.*, 2003, 1826–1827.

[29] B.P. Binks, R. Murakami, S.P. Armes, and S. Fujii, *Angew. Chem. Int. Ed.*, 2005, **44**, 4795–4798.

[30] K. Golemanov, S. Tcholakova, P.A. Kralchevsky, K.P. Ananthapadmanabhan, and A. Lips, *Langmuir*, 2006, **22**, 4968–4977.

[31] R.W. Style, R. Boltyanskiy, Y.L. Che, J.S. Wettlaufer, L.A. Wilen, and E.R. Dufresne, *Phys. Rev. Lett.*, 2013, **110**,.

[32] B. Andreotti, A. Marchand, S. Das, and J.H. Snoeijer, *Phys. Rev. E*, 2011, **84**,.

[33] A. Marchand, S. Das, J.H. Snoeijer, and B. Andreotti, *Phys. Rev. Lett.*, 2012, **109**,.

[34] A. Burmistrova, M. Richter, C. Uzum, and R. von Klitzing, *Colloid Polym. Sci.*, 2011, **289**, 613–624.

[35] K.O Nazli, C.W. Pester, A. Konradi, A. Boker, and P. van Rijn, *Chem. Eur. J.*, 2013, **19**, 5586–5594.

[36] D.M. Kaz, R. McGorty, M. Mani, M.P. Brenner, and V.N. Manoharan, *Nat. Mater.*, 2012, **11**, 138–142.

[37] S. Zeppieri, J. Rodriguez, and A.L.L. de Ramos, *J. Chem. Eng. Data*, 2001, **46**, 1086–1088.

[38] H.M. Wyss, T. Franke, E. Mele, and D.A. Weitz, *Soft Matter*, 2010, **6**, 4550–4555.

[39] B. Jean, L.T. Lee, and B. Cabane, *Langmuir*, 1999, **15**, 7585–7590.

Chapter 5

Microgel-stabilized ionic liquid emulsions

In this chapter, we present a complete toolbox to use responsive ionic liquid emulsions for extraction purposes. We use temperature responsive microgels as stabilizers. This allows the formation of stable emulsions with permeable interfaces, which can be reversibly broken and re-emulsified on-demand. Moreover, by using a paramagnetic ionic liquid, droplets can be easily collected in low magnetic fields.

5.1 Introduction

The use of ionic liquids (ILs) as green extraction solvents in chemical and biotechnological industries shows great promise,[1] especially for the extraction of conformationally fragile and chemically sensitive compounds such as proteins,[2–8] lipids[9–11] or other biomolecules.[12–14] In liquid-liquid extractions hydrophilic ionic liquids are used in combination with salt solutions. However, this system has several drawbacks due to the potential ion exchange that can occur between the IL and the water and the mutual solubility of the IL with the water. An alternative to this consists of using hydrophobic ionic liquids, which contain long alkyl chains. These ionic liquids are usually quite viscous and therefore the mass transfer between the water phase and the ionic liquid phase is limited.

To enhance the efficiency of such extractions and minimize the time required to achieve good separation, the use of emulsions is highly favorable due to their inherently large surface area.[15] However, these emulsions must be stable against coarsening due to coalescence or Ostwald ripening, yet simultaneously must be easy to collect and break to obtain the product-loaded ionic liquid phase. Moreover, the stabilizer used to create these emulsions should ideally not interact in a detrimental way with the product to be extracted.

Creating IL/water emulsions is a challenge by itself. The inherently large miscibility of the two phases, and resulting low interfacial tension, combined with the fact that, contrary to oil–water interfaces, IL-water interfaces are highly structured due to charge hydration and correlations,[16] result in only partial relevance of the general rules of emulsion preparation and stability.[17] While IL (micro)emulsions[18–23] can be prepared using simple commercial surfactants, most of the desired requirements are not met. Due to the inherent water solubility of most ionic liquids,[24–28] Ostwald ripening leads to fast coarsening and emulsion destabilization. Additionally, surfactants interact strongly with a variety of biomolecules, often amphiphilic themselves, which can lead to irreversible changes in the desired product such as denaturation of proteins.[29,30] A universal strategy to prepare IL emulsions meeting these strict requirements is absent, precluding a more general application of IL-based green extraction processes.

In the previous chapter, we showed that microgel particles adsorb at a wide variety of oil–water interfaces.[31,32] In this chapter we demonstrate that microgel particles can also provide excellent stability to a wide variety of IL–water emulsions. The spontaneously formed and densely packed layer of microgels at the IL–water interface does not impart their use in extractions as the interface remains permeable to small biomolecules. Through ion exchange, the ionic liquid used for extraction can be rendered paramagnetic,[33,34] which allows facile collection of the droplets

from the extraction medium using a magnet. Utilizing the thermoresponsive na-
ture of the microgel particles, the emulsion, which is stable for at least several days
at room temperature, can almost instantaneously be de-emulsified using a small
temperature trigger. Once the ionic liquid phase has been collected, the microgel
particles, which remain in the aqueous phase, can be re-used for a new extrac-
tion. The combination of excellent stability and de-emulsification on-demand, the
magnetoresponsivity of the droplets and the reusability of the emulsifier offers a
complete and versatile toolbox for the sustainable application of IL emulsions in
extraction processes.

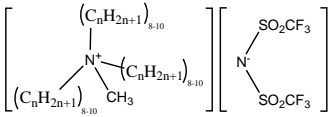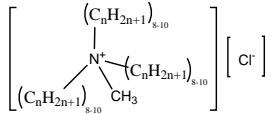## 5.2   Experimental details
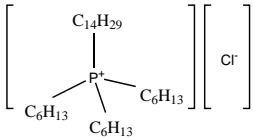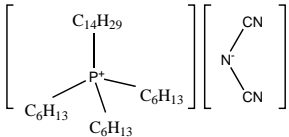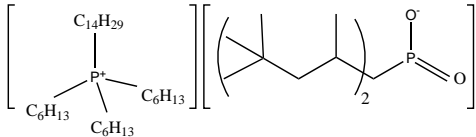
5.2.1   Materials
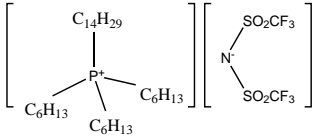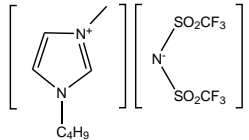
N-isopropylacrylamide (NIPAm), N,N-methylbisacrylamide (BIS), methacrylic acid
(MA), potassium persulfate (KPS), styrene, sodium dodecyl sulfate (SDS) and Brij-
98 were purchased from Sigma-Aldrich. Potassium nitrate (KNO_3) was purchased
from Merck. Phosphonium based ionic liquids, trihexyltetradecyl phosphonium
$[P_{6,6,6,14}]$ chloride [Cl], phosphinate [Phos], dicyanamide [DCA] and bistriflamide
$[NTf_2]$, were purchased from Cytec; the other ionic liquids, butylmethylimidazolium
bistriflamide [BMIM] $[NTf_2]$, methyltrioctylammonium bistriflamide $[N_{1,8,8,8}]$ $[NTf_2]$
and Adogen 464 $[N_{1,8-10,8-10,8-10}]$ [Cl] were purchased from Sigma-Aldrich. The
fluorescent dyes Pyrromethene 546 and Pyrromethene 605 were purchased from
Exciton. PolyFluorTM 570 was purchased from PolySciences, Inc.

The core-shell microgels used in this Chapter are the same than in Chapter
4. The room temperature paramagnetic ionic liquid $[P_{6,6,6,14}]$ $[FeCl_4]$ is prepared
by mixing 15.20 g of $[P_{6,6,6,14}]$[Cl] and 4,75 g of iron(III) chloride in a 250 mL
round-bottomed flask under a N_2 atmosphere at 50 °C for 48 h, yielding a dark
brown liquid. Analysis was limited to elemental analysis and moisture analyzer
for the water content. The elemental analysis, calculated for $C_{32}H_{68}PFeCl_4$, gives:
C 56.39 %, H 9.99 %, experimentally found: C 56.84 %, H 10.22 %. The water
content is 1.02 %.

All chemicals were used as received. Milli-Q water was used for synthesis and
characterization of the microgel particles and preparation of the emulsions. The
commercial names, abbreviations and chemical structures of the ionic liquids are
listed in Table 5.1.

Table 5.1: Ionic liquids used in this chapter

Commercial name	Abbreviation	Structure	Interfacial tension
Trihexyltetradecylphosphonium chloride	$[P_{6,6,6,14}][Cl]$		7.3
Trihexyltetradecylphosphonium dicyanamide	$[P_{6,6,6,14}][DCA]$		8.3
Trihexyltetradecylphosphonium phosphinate	$[P_{6,6,6,14}][Phos]$		10.2

Trihexyltetradecylphosphonium bistriflamide	$[P_{6,6,6,14}][NTf_2]$		12.4
Butylmethylimidazolium bistriflamide	$[BMIM][NTf_2]$		13.2
Methyltrioctylammonium bistriflamide	$[N_{1,8,8,8}][NTf_2]$		-
Adogen 464	$[N_{1,8-10,8-10,8-10}]\,[Cl]$		2.5

5.2.2 Interfacial tension measurements

Interfacial tension between IL and water is measured through pendant drop tensiometry (Sinterface Pat-1). For steady state values of the interfacial tensions, we equilibrate the droplet for at least 1h. For all measurements, the droplet size is 7.5 mm^3.

5.2.3 Preparation and characterization of the emulsions

The surfactant-stabilized emulsion was prepared by mixing for 2 min, using an Ultra Turrax, the Brij-98 solution with the IL (weight ratio 9:1). The microgel-stabilized emulsion was prepared by first diluting the microgel stock solution ($c = 27$ g/L) to the desired concentration of particles and salt ($c = 2.7$ g/L, $I = 15$ mM and pH $= 6$) using Milli-Q water and a solution of 15 mM of KNO$_3$ and then mixing the solution with the IL (weight ratio 9:1). In this case, mixing is done by vortexing for 30 s the two macroscopic phases in a tube. The emulsions are studied using a Zeiss Axiovert 200M confocal microscope fitted with a $100\times$ oil immersion objective.

Their stability against coalescence and Ostwald ripening is analyzed by measuring the droplet-size distribution over time using a Malvern Mastersizer 2000. The size distribution is characterized in terms of mean diameter $D_{3,2}$ defined as:

$$D_{3,2} = \frac{\sum\limits_i N_i D_i^3}{\sum\limits_i N_i D_i^2} \tag{5.1}$$

where D_i is the diameter of droplets in the class i and N_i is the number of droplets in that class.

5.3 Results and discussion

5.3.1 Emulsion stabilization

A water-in-IL emulsion prepared from the water-immiscible IL [P$_{6,6,6,14}$][NTf$_2$], stabilized by the commercial non-ionic surfactant Brij-98, shows rapid coarsening. The measured mean droplet diameter shows an order of magnitude increase over 24 hours: at $t = 0$, $D_{3,2} = 20$ μm whereas at $t = 24$ h, $D_{3,2} = 205$ μm. Clearly, simple surfactants do not effectively stabilize IL-in-water emulsions. Stability against Ostwald ripening can be improved by the formation of an elastic layer at the IL-water interface, for example by the adsorption of colloidal particles
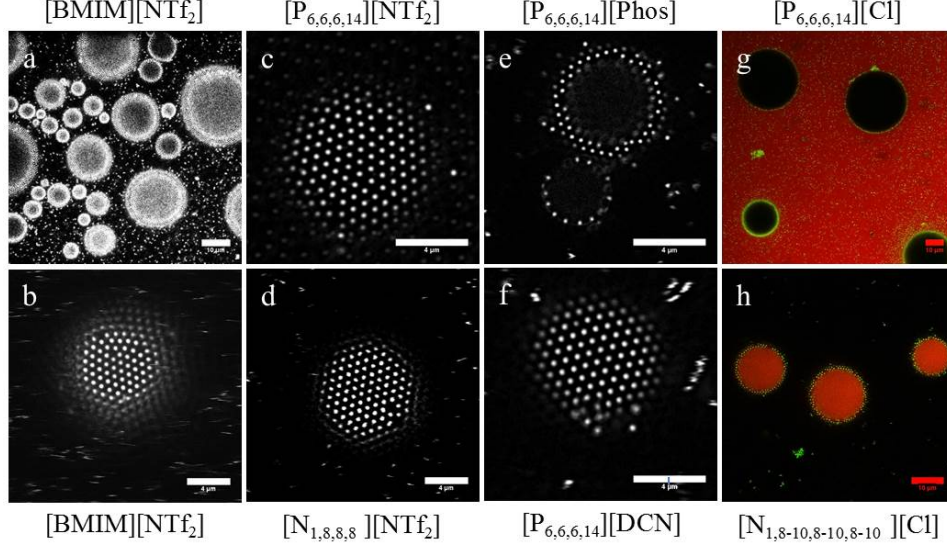
[BMIM][NTf$_2$]   [P$_{6,6,6,14}$][NTf$_2$]   [P$_{6,6,6,14}$][Phos]   [P$_{6,6,6,14}$][Cl]

[BMIM][NTf$_2$]   [N$_{1,8,8,8}$][NTf$_2$]   [P$_{6,6,6,14}$][DCN]   [N$_{1,8\text{-}10,8\text{-}10,8\text{-}10}$][Cl]

Figure 5.1: Confocal microscopy images of IL droplets in water stabilized with hexagonally packed microgels (a-f). Confocal microscopy images of emulsions of ILs containing Cl$^-$, the IL is colored red and the microgel particles green: (g) water-in-IL and (h) IL-in-water.

at the interface.[35] However, preparing well-defined and stable Pickering emulsions almost always requires careful tuning of the wettability of the particles at the liquid-liquid interface.[36–40] The microgel particles that we use in this study contain a fluorescent polystyrene core embedded into a thermoresponsive microgel shell made of poly(N-isopropylacrylamide-co-methacrylic acid) (PNIPAm-co-MA). This design allows to visualize the particles at the interface[41] while leaving the desired properties of the microgels, i.e their spontaneous adsorption and ultrastrong anchoring at liquid interfaces, intact.[42]

Upon vortexing a dispersion of these microgel particles in water with the ionic liquid [BMIM][NTf$_2$] for only 30 s, a stable and well-dispersed emulsion is created. We observe, using confocal microscopy, that almost all the interfaces are fully covered with particles, which have organized in a regular hexagonally pattern (Figures 5.1a,b). Clearly, microgel particles are able to effectively stabilize IL-water interfaces. This is corroborated by stability measurements that show no change in droplet size for several days. Therefore, we explore the universality of these particles as stabilizers by preparing emulsions from a wide variety of ILs: for different cations P$_{6,6,6,14}^+$ and N$_{1,8,8,8}^+$ while keeping the same anion NTf$_2^-$, and for different anions Phos$^-$ and DCA$^-$ while keeping the same cation P$_{6,6,6,14}^+$. For all

of these, well-stabilized droplets of IL-in-water with hexagonally-packed interfaces result (Figures 5.1c-f). Remarkably, microgel particles can stabilize a wide variety of IL-water interfaces through their spontaneous adsorption at the liquid interface. Although the exact mechanism with which microgels adsorb remains unclear, it has been established that it is significantly different from classical Pickering stabilization, and exhibits features of both particle- and polymer-adsorption.[31,42] While we observe adsorption of our microgels at all IL-water interfaces explored, for solid colloidal particles tuning the chemistry is required, for example by changing the hydrophobicity[36,37] or the charge density and species.[40] This suggests that indeed microgel adsorption and that of solid particles do not occur with the same mechanism.

In our systems, we always observe an excess of microgel particles that remain in the aqueous phase. This indicates that the emulsions are not prepared in the limited coalescence regime. However, when we combine the hydrophobic cation $P_{6,6,6,14}^{+}$ with an anion that prefers to partition into water, in this case Cl^{-}, we observe the spontaneous and full migration of all microgels into the IL. We hypothesize this is partly due to ion-exchange,[43] in which transfer of an anionically-charged microgel into the IL is accompanied by the migration of a number of chloride ions representing the same amount of negative charges into the aqueous phase, leading to a large increase in the counterion entropy. In this specific case there is a preference for forming water-in-IL instead of IL-in-water emulsions (Figure 5.1g). This illustrates how *in-situ* ion exchange can be used to tailor the emulsion type. However, when we combine Cl^{-} with another hydrophobic cation $N_{1,8-10,8-10,8-10}^{+}$, the microgels remain in the aqueous phase and the preferred emulsion type is IL-in-water (Figure 5.1h). This result suggests that not only entropic gain associated with counterion release is important but that also specific affinity between the microgels and the IL cation may play a role.[44]

5.3.2   Extraction, concentration and breaking on-demand

An important prerequisite for extractions is that the interface between IL and water remains permeable. To test this, we add β-carotene as a powder to the continuous phase of an IL-in-water emulsion prepared with [BMIM][NTf$_2$] and stabilized with microgel particles (Figure 5.2a). After only a few minutes, the pigment is found in the IL phase (Figure 5.2b). To more clearly visualize the uptake of small molecules across a microgel laden interface, we replace β-carotene by a hydrophobic fluorescent dye, pyrromethene. As far as we can observe, with confocal microscopy, all of the dye is located in the ionic liquid droplets and none is found in the water phase (Figures 5.2c,d). Despite the densely packed interface, small molecules easily
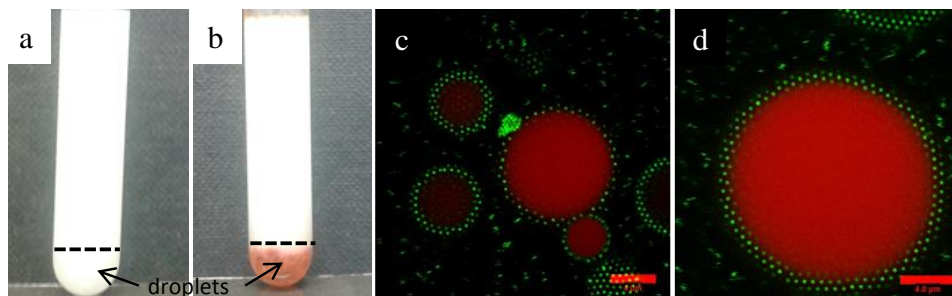
Figure 5.2: Photographs of (a) [BMIM][NTf$_2$]-in-water emulsion stabilized with microgel particles, (b) same as (a) after adding -carotene, the pigment diffused to the IL droplets. Confocal microscopy images of the successful extraction of pyrromethene by the same IL; the IL is colored red and the microgel particles green (c, d).
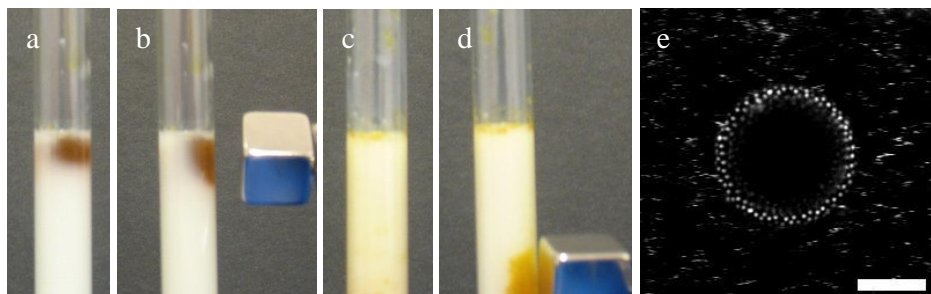

Figure 5.3: Photographs of (a) [P$_{6,6,6,14}$][FeCl$_4$] forming a two-phase system with a microgel solution, (b) distortion of [P$_{6,6,6,14}$] [FeCl$_4$] with a magnet, (c) [P$_{6,6,6,14}$][FeCl$_4$]-in-water emulsion stabilized with microgel particles, (d) concentration of the [P$_{6,6,6,14}$][FeCl$_4$] droplets; (e) confocal microscopy images illustrating the presence of microgels at the surface of the [P$_{6,6,6,14}$][FeCl$_4$] droplets

permeate the microgel layer.

To facilitate IL-emulsion based extractions, ideally the droplets should be collected with minimal energy input. To accomplish this, we render the IL magnetoresponsive by ion exchange of [P$_{6,6,6,14}$][Cl] to [P$_{6,6,6,14}$][FeCl$_4$].[34,45] The resulting paramagnetic IL is immiscible with water (Figure 5.3a). When brought in close proximity of a magnet, the liquid is attracted towards the magnet, as can be seen in Figure 5.3b. Also this IL can successfully be emulsified with microgel particles (Figures 5.3c-e). Interestingly, this results in a paramagnetic emulsion in which the droplets can be collected almost instantaneously and without energy input, with even a small magnet (Figure 5.3d). While this strategy is a promising route to stabilize emulsions and allows collecting the emulsion droplets, extractions also
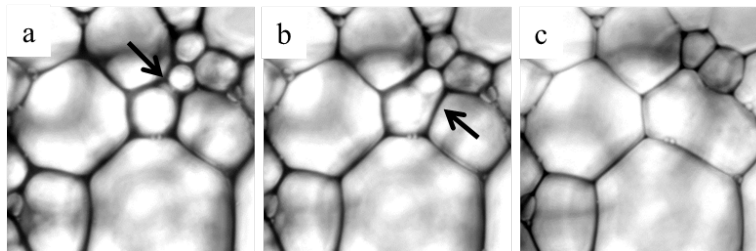
Figure 5.4: Brightfield microscopy images of the temperature triggered coalescence of a [BMIM][NTf$_2$] emulsion stabilized with microgel particles while heating the emulsion at 50°C.

need on-demand breaking of the emulsions to recover the final product. To achieve this, we use the thermoresponsive nature of the particles.

Indeed, using temperature as a trigger, oil-in-water emulsions can be broken on-demand. Particle characterization shows that the particles have a lower critical solution temperature (LCST) of 32 °C: below this temperature, the microgel particles are swollen whereas above it, the microgel particles are collapsed. When the temperature of a concentrated microgel-stabilized emulsion, prepared at room temperature, is increased above 32 °C, the emulsion becomes unstable and demixes into two macroscopic phases (Figures 5.4a-c). While the exact mechanism of this temperature-induced emulsion breaking remains speculative, we hypothesize the following: upon increasing the temperature above the LCST of the microgels, they both deswell and become adhesive. As a result, the surface coverage rapidly decreases and the two interfaces, separated by a thin film of water, become attractive. This combination simultaneously removes both the thermodynamic and kinetic barriers preventing coalescence.

To arrive to a sustainable extraction toolbox based on the system we present, this process should allow re-using of the microgel emulsifiers. To check the feasibility of this idea, we prepare an IL-in-water emulsion and break it by centrifugation at 35 °C and 200 g. The IL phase is then removed and using the same aqueous phase still containing the microgels, a new emulsion can be prepared.

5.4   Conclusion

The results presented in this chapter show that our multiresponsive system provides a comprehensive toolbox for the efficient sustainable application of ionic liquids in (bio)molecule extraction. Using the unique properties of the responsive microgel particles and through tuning the IL composition, we can prepare stable emulsions

of both water-in-IL and IL-in-water type, that can be easily concentrated using a magnetic field, that can be broken on-demand with a small temperature trigger and in which the emulsifier can be re-used for subsequent extractions. This opens up new and directly applicable avenues for the transition towards a greener (bio)chemical industry.

References

[1] X. Han and D.W. Armstrong, *Accounts Chem. Res.*, 2007, **40**, 1079–1086.

[2] Z. Du, Y.L. Yu, and J.H. Wang, *Chem.-Eur. J.*, 2007, **13**, 2130–2137.

[3] Y.C. Pei, Y.Z. Wang, K. Wu, X.P. Xuan, and X.J. Lu, *Sep. Purif. Technol.*, 2009, **64**, 288–295.

[4] E. Alvarez-Guerra and A. Irabien, *Sep. Purif. Technol.*, 2012, **98**, 432–440.

[5] X.W. Chen, Q.X. Mao, and J.H. Wang, *Prog. Chem.*, 2013, **25**, 661–668.

[6] X. Lin, Y. Wang, Q. Zeng, X. Ding, and J. Chen, *Analyst*, 2013, **138**, 6445–6453.

[7] Q. Zeng, Y. Z. Wang, N. Li, X. Huang, X.Q. Ding, X. Lin, S.Y. Huang, and X.J. Liu, *Talanta*, 2013, **116**, 409–416.

[8] R.K. Desai, M. Streefland, R.H. Wijffels, and M.H.M. Eppink, *Green Chem.*, 2014, **16**, 2670–2679.

[9] G. Young, F. Nippgen, S. Titterbrandt, and M.J. Cooney, *Sep. Purif. Technol.*, 2010, **72**, 118–121.

[10] Y.H. Kim, Y.K. Choi, J. Park, S. Lee, Y.H. Yang, H.J. Kim, T.J. Park, Y.H. Kim, and S.H. Lee, *Bioresour. Technol.*, 2012, **109**, 312–315.

[11] S.A. Choi, Y.K. Oh, M.J. Jeong, S.W. Kim, J.S. Lee, and J.Y. Park, *Renew. Energy*, 2014, **65**, 169–174.

[12] A. Soto, A. Arce, and M.K. Khoshkbarchi, *Sep. Purif. Technol.*, 2005, **44**, 242–246.

[13] Q.F. Liu, J. Yu, W.L. Li, X.S. Hu, H.S. Xia, H.Z. Liu, and P. Yang, *Sep. Sci. Technol.*, 2006, **41**, 2849–2858.

[14] C.-H. Li, J. Han, Y. Wang, Y.-S. Yan, X.-H. Xu, and J.-M. Pan, *Anal. Chim. Acta*, 2009, **653**, 178–183.

[15] Q.X. Mao, H. Wang, Y. Shu, X.W. Chen, and J.H. Wang, *RSC Adv.*, 2014, **4**, 8177–8182.

[16] T. Kakiuchi, *Anal. Chem.*, 2007, **27**, 6442–6449.

[17] T. Nakashima and N. Kimizuka, *Langmuir*, 2011, **27**, 1281–1285.

[18] Y. N. Gao, S.B. Han, B.X. Han, G.Z. Li, D. Shen, Z.H. Li, J.M. Du, W.G. Hou, and G.Y. Zhang, *Langmuir*, 2005, **21**, 5681–5684.

[19] Y. Gao, N. Li, L.Q. Zheng, X.Y. Zhao, S.H. Zhang, B.X. Han, W.G. Hou, and G.Z. Li, *Green Chem.*, 2006, **8**, 43–49.

[20] J.H. Porada, M. Mansueto, S. Laschat, and C. Stubenrauch, *Soft Matter*, 2011, **7**, 6805–6810.

[21] A. Klee, S. Prevost, W. Kunz, R. Schweins, K. Kiefer, and M. Gradzielski, *Phys. Chem. Chem. Phys.*, 2012, **14**, 15355–15360.

[22] J. Zhang and B. Han, *Acc. Chem. Res.*, 2012, **46**, 425–433.

[23] Y.C. Pei, Y.J. Huang, L. Li, and J.J. Wang, *J. Chem. Thermodyn.*, 2014, **74**, 231–237.

[24] N.V. Shvedene, S.V. Borovskaya, V.V. Sviridov, E.R. Ismailova, and I.V. Pletnev, *Anal. Bioanal. Chem.*, 2005, **381**, 427–430.

[25] M.G. Freire, C. Neves, P.J. Carvalho, R.L. Gardas, A.M. Fernandes, I.M. Marrucho, L. Santos, and J.A.P. Coutinho, *J. Phys. Chem. B*, 2007, **111**, 13082–13089.

[26] M.G. Freire, L.M.N.B.F. Santos, A.M. Fernandes, J.A.P Coutinho, and I.M. Marrucho, *Fluid Phase Equilib.*, 2007, **261**, 449–454.

[27] J. Salminem, N. Papaiconomou, R.A. Kumara, J.M. Lee, J. Kerr, J. Newman, and J.M. Prausnitz, *Fluid Phase Equilib.*, 2007, **261**, 421–426.

[28] M.G. Freire, P.J. Carvalho, R.L. Gardas, I.M. Marrucho, L. Santos, and J.A.P. Coutinho, *J. Phys. Chem. B*, 2008, **112**, 1604–1610.

[29] A. Lee, S.K.Y. Tang, C.R. Mace, and G.M. Whitesides, *Langmuir*, 2011, **27**, 11560–11574.

[30] M. Ospinal-Jimenez and D.C. Pozzo, *Langmuir*, 2012, **28**, 17749–17760.

[31] W. Richtering, *Langmuir*, 2012, **28**, 17218–17229.

[32] V. Schmitt and V. Ravaine, *Curr. Opin. Colloid Interface Sci.*, 2013, **18**, 532–541.

[33] S. Hayashi and H.O. Hamaguchi, *Chem. Lett.*, 2004, **33**, 1590–1591.

[34] R.E. Del Sesto, T.M. McCleskey, A.K. Burrell, G.A. Baker, J.D. Thompson, B.L. Scott, J.S. Wilkes, and P. Williams, *Chem. Commun.*, 2008, 447–449.

[35] D.E. Tambe and M.M. Sharma, *Adv. Colloid Interface Sci.*, 1994, **52**, 1–63.

[36] B.P. Binks, A.K.F. Dyab, and P.D.I. Fletcher, *Chem. Commun.*, 2003, 2540–2541.

[37] B.P. Binks, A.K.F. Dyab, and P.D.I. Fletcher, *Phys. Chem. Chem. Phys.*, 2007, **9**, 6391–6397.

[38] H. Ma and L.L. Dai, *Langmuir*, 2011, **27**, 508–512.

[39] D.S. Frost, M. Ngan, and L.L. Dai, *Langmuir*, 2013, **29**, 9310–9315.

[40] D.S. Frost, E.M. Nofen, and L.L. Dai, *Adv. Colloid Interface Sci.*, 2014, **206**, 92–105.

[41] D. Ershov, J. Sprakel, J. Appel, M.A. Cohen Stuart, and J. van der Gucht, *Proc. Natl. Acad. Sci.*, 2013, **110**, 9220–9224.

[42] H. Monteillet, M. Workamp, J.M. Kleijn, F.A.M. Leermakers, and J. Sprakel, *Adv. Mater. Interfaces*, 2014, **1**, 1300121.

[43] T. Nakashima, Y. Nonoguchi, and T. Kawai, *Polym. Adv. Technol.*, 2008, **19**, 1401–1405.

[44] D.S. Frost, M. Ngan, and L.L. Dai, *Langmuir*, 2013, **29**, 9310–9315.

[45] P. Brown, A. Bushmelev, C.P. Butts, J. Cheng, J. Eastoe, I. Grillo, R.K. Heenan, and A.M. Schmidt, *Angew. Chem. Int. Ed.*, 2012, **51**, 2414–2416.

Chapter 6

Microgels at solid-liquid interfaces

Previously we studied microgels at liquid-liquid interfaces, and showed how their adsorption is governed by a complex interplay between adsorption energy, elastocapillary deformation of individual particles and capillary interactions between particles. In this chapter, we investigate the case of microgel adsorption at solid-liquid interfaces, where a simpler balance between adsorption energy and particle deformability is expected to govern the adsorption. As before, our microgels are provided with a fluorescent polystyrene core to be able to visualize them using confocal microscopy; the shell consists of PNIPAm-co-MA giving the particles a pH-dependent negative charge. We explore the effects of the elasticity of the microgels and the interactions between them and solid surfaces, by varying the pH, the ionic strength and chemical modification of the surface. We determine the adsorption density from confocal microscopy experiments and use atomic force microscopy to explore the morphology and mechanical properties of these particles in their adsorbed state. We find that the adsorption density is governed by particle-particle interactions up to the point where the adsorption energy vanishes. We show that for the system explored here there is an indication of adsorption-induced particle spreading, and that the particle elasticity is of the same order of magnitude as that in bulk as determined by others.

6.1 Introduction

Microgels, solvent-swollen cross-linked polymer gels of colloidal dimensions, adsorb spontaneously to a wide variety of interfaces[1] while retaining their responsive properties.[2-4] This makes it possible to create densely packed microgel monolayers, which can be used to impart responsivity. At interfaces, microgels allow to stabilize and break on-demand emulsions and foams;[5-10] at surfaces, they allow tunable patterning[11,12] or surface functionalization.[13]

As is the case in bulk solutions,[14,15] also at interfaces microgel particles exhibit an interesting duality between polymer-like and solid colloid-like properties;[1] for example at liquid interfaces they may show rapid and barrier-free adsorption, typical for polymers, while anchoring irreversibly, typical for particles. While this offers a plethora of possibilities to tailor the structure and properties of interfaces, their behaviour is complex. For example, they may experience capillary interactions[16] leading to their deformation and exhibit supramolecular bonding.[17] As a consequence, a detailed understanding of how particle softness, adsorption energy and capillary effects interplay remains incomplete. This is exacerbated by the experimental challenge of ascertaining the conformation of these particles *in-situ*. As their refractive index contrast with the continuous phase is low by definition, optical methods appear inadequate to answer these questions; while electron microscopy[9,18,19] and x-ray microscopy[20] have been recently employed to alleviate these constraints, many aspects regarding their interfacial organization and conformation remain unclear.

At solid-liquid interfaces, capillary interactions are absent and microgel behavior is expected to be governed by particle deformation versus adsorption energy alone. In the past years, studies have shown how microgel adsorption can be controlled experimentally through active deposition methods, such as spin-coating or dip-coating.[21,22] However, these sample preparation methods required drying and rehydration of the samples prior to analysis, which induced strong convective flows and evaporative stresses that may alter the initial adsorbed state of the microgel layer. To obtain more insight into spontaneous microgel adsorption, ideally the properties are measured *in-situ* without any potentially disruptive sample treatment.

In this study, we use core-shell microgels consisting of a fluorescent polystyrene core and a PNIPAm-co-MA shell to study the adsorbed state of soft particles at solid-liquid interfaces. We first show how often used sample preparation methods, which involve a drying step, may have tremendous influence on the results obtain. Using *in-situ* liquid-state imaging, with both confocal microscopy and atomic force microscopy, we then explore how environmental conditions and surface-particle

interactions influence adsorption density and particle morphology.

6.2 Experimental details

6.2.1 Materials

N-isopropylacrylamide (NIPAm), N,N'-methylenebisacrylamide (BIS), methacrylic acid (MA), potassium persulfate (KPS), styrene, sodium dodecyl sulfate (SDS), sulphuric acid (H_2SO_4), hydrogen peroxide (H_2O_2), dimethylsulfoxide (DMSO) and 2-amino-ethanol (C_2H_7NO) were purchased from Sigma-Aldrich. The fluorescent dye Pyrromethene 605 was purchased from Exciton.

All chemicals were used as received. Milli-Q water was used for the synthesis and the characterization of the microgel particles.

6.2.2 Microgel synthesis

Core-shell microgels are synthesized in a two-step procedure. First, fluorescent cores are synthesized by emulsion polymerization. To this end, 3.75 g NIPAm, 48 g styrene, 100 mg SDS and 50 mg fluorescent dye Pyrromethene 605 are dissolved in 130 mL Milli-Q water. The mixture is stirred at 500 rpm, heated to 75 °C and purged with N_2 for 15 minutes. The reaction is initiated by the addition of 100 mg KPS dissolved in 5 mL Milli-Q water and the reaction is left to proceed overnight. The reaction mixture is filtered and the cores are cleaned by repeated centrifugation and resuspension in Milli-Q water.

Second, a shell of NIPAm, MA and BIS is grown around the cores by precipitation polymerization. 2.0 g NIPAm, 106 μL MA and 20 mg BIS are dissolved in 200 mL of Milli-Q water. Then, 1.2 g cores are added and the mixture is sonicated for 2 minutes. The mixture is stirred at 500 rpm, heated to 75 °C and purged with N_2 for 15 minutes. The reaction is initiated by the addition of 100 mg KPS dissolved in 5 mL Milli-Q water and the reaction is left to proceed for 2 hours. The reaction mixture is filtered and the composite microgels are cleaned by repeated centrifugation and resuspension in Milli-Q water.

6.2.3 Microgel characterization in bulk

The hydrodynamic radius R_h of the cores and the core-shell particles are measured using dynamic light scattering. To determine the influence of pH on the R_h, a microgel solution of pH 2 is titrated with a solution of 0.1 M NaOH. The influence of ionic strength on the R_h is determined by adding KCl in different concentrations,

10 and 50 mM, to microgel solutions of pH values 4 and 8. Results are averaged over 20 measurements for the pH experiment and 10 measurements for the salt experiment.

6.2.4   Surface preparation

Prior to any measurement or surface modification, glass slides and oxidized silicon wafers are etched with a 3:1 (v:v) solution of H_2SO_4:H_2O_2. The surfaces are then rinsed with water and ethanol and dried with N_2.

For anionic surfaces we use the cleaned substrates after drying. To obtain cationic surfaces we amino-modify the surfaces for which we adapt a protocol from Spruijt;[23] substrates are laminated by reacting them in a 2:1 solution of DMSO and C_2H_7NO, in presence of molecular sieves to maintain anhydrous conditions, for at least 16 hours. The surfaces are then rinsed with DMSO and Milli-Q water and finally dried in a stream of nitrogen.

To verify the surface has been successfully modified, we determine the contact angle between a 0.7 μL water droplet and the surface before and after modification (Kruss G10). We average the data over 5 measurements. We find a contact angle close to $40°$, comparable to what is reported in the literature for an aminopropyltriethoxysilane-modified silicon wafer.[24]

6.2.5   Confocal microscopy

Images are recorded with a Zeiss Axiovert 200M confocal laser scanning microscope fitted with a $100\times$ oil-immersion objective. A solution of microgel particles is injected into a glass sample chamber, created on a cleaned glass slide. Images are recorded at a resolution of 512×512 pixels and a pinhole of 0.5 Airy units to image a thin slice of the sample at the glass-liquid interface. The temperature is kept constant at $23°C$ during the experiment. Particles that are adsorbed onto the glass surface can be easily distinguished from those which are in close proximity of the surface but not yet attached as they appear blurred due to Brownian motion. For each experiment, 10 independent locations on the glass slide are imaged to obtain reasonable statistics. We then count the number of adsorbed particles using established 2D particle tracking algorithms,[25] from which we compute the particle density ρ as the number of adsorbed microgels per μm^2.

6.2.6   Atomic Force Microscopy

For reference images in the dry state, we deposit 20 μL of a microgel solution at the desired pH and ionic strength onto a cleaned silicon wafer with a thin oxide layer

and leave these to dry overnight. We then image the sample with atomic force microscopy (AFM), using a Multimode V Scanning Probe Microscope (Bruker), silicon nitride AFM probes (Bruker, DNP-C, nominal spring constant 0.24 N/m, tip radius 20 nm). Imaging is done in PeakForce tapping mode with a scan size of 20×20 μm^2, a resolution of 512×512 pixels and a scan rate of 2 Hz.

For imaging in the liquid state, we use a liquid cell (Bruker, MMTMEC) equipped with an O-ring seal (Bruker, FCO-10) and silicon nitride AFM probes (Bruker, DNP-D, nominal spring constant 0.06 N/m, tip radius 20 nm). The surface is first wetted with 3×1 mL water at the desired pH and ionic strength after which 0.7 mL of a microgel solution at the same pH and ionic strength is injected into the liquid cell. We allow the microgels to adsorb for 20 minutes before the liquid cell is again flushed with 3×1 mL of water at the same experimental conditions. We then allow the sample to reach thermal equilibrium for 10 minutes before commencing the measurement.

Mechanical information on the adsorbed microgels is obtained using quantitative nanomechanical mapping (QNM). This allows simultaneous mapping of the mechanical properties of a sample and topographic imaging. In this imaging mode, force distance curves are recorded at a frequency of 2 kHz while scanning, giving the adhesion force and the deformation as a function of the position. Before QNM imaging, the sensitivity of the cantilever is calibrated on a hard surface and the spring constant is determined in water using the thermal tune option of the AFM apparatus.[26] The force-curves are analysed using the Derjaguin-Muller-Toporov (DMT) model:[27,28]

$$F - F_{\mathrm{adh}} = \frac{4}{3} E^* \sqrt{R(d - d_0)^3} \qquad (6.1)$$

where R is the tip end radius, $d - d_0$ the deformation, $F - F_{adh}$ the force on the cantilever relative to the peak adhesion force and E^* the reduced Young's modulus, which is the quantity of interest. To calculate the Young's modulus E of the microgels from E^*, we assume that the modulus of the tip is much larger than that of the microgels and that ν of the microgels is 0.4:[29,30]

$$E = E^*(1 - \nu)^2 \qquad (6.2)$$

In each experiment, we record at least 3 independent images from which in total 30 particle cross-sections are taken to determine both the dimensions and elasticity of the particles. These cross-sections are selected perpendicular to the scanning direction to minimize artefacts due to scanning-induced particle deformation.
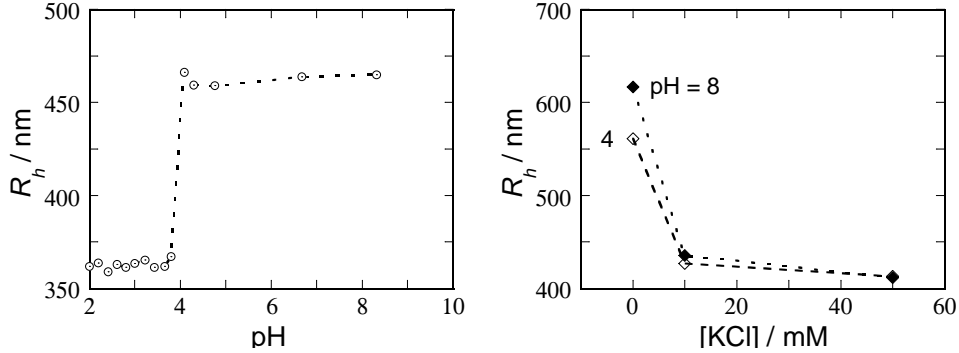
Figure 6.1: Hydrodynamic radius of the microgel particles as a function of (a) pH without added salt, (b) salt concentration at pH values of 4 and 8.

6.3   Results and discussion

We first determine the size of the particles in bulk, using dynamic light scattering. We find a hydrodynamic radius of $R_h = 124$ nm for the core particles. The shell surrounding these cores contains carboxylic acids moieties resulting in microgels which exhibit pH and ionic strength dependent swelling. Upon increasing the pH, the microgels swell from 360 nm at pH < 4 to approximately 460 nm at pH > 4 (Figure 6.1a). This is caused by deprotonation of the acidic groups, which gives rise to an electrostatic contribution to the osmotic pressure within the particle.

For pH 4 and 8, we also measure the effect of ionic strength. Upon addition of the indifferent electrolyte KCl the particles deswell due to charge screening in the microgel interior; as expected, this effect is more pronounced at higher pH (Figure 6.1b).

R_h at pH 8 in Figure 6.1a is smaller than in Figure 6.1b (at 0 mM KCl). This difference is due to the different experimental procedures. The results for the pH-dependence are obtained by acid-base titration; first, the pH of the sample is lowered to pH 2 by adding HCl and then the sample is titrated to pH 8 using NaOH while measuring R_h. As a result, the ionic strength in Figure 6.1a is about 10 mM.

6.3.1   Sample preparation: effect of drying

In several previous studies on the adsorption behaviour of microgel colloids, a drying step was applied between the particle deposition and the experimental analysis. To explore the effect this sample preparation step has on the final state, we apply a droplet of a microgel solution to a solid substrate and allow it to dry. We observe a characteristic "coffee ring" pattern, where particles have accumulated

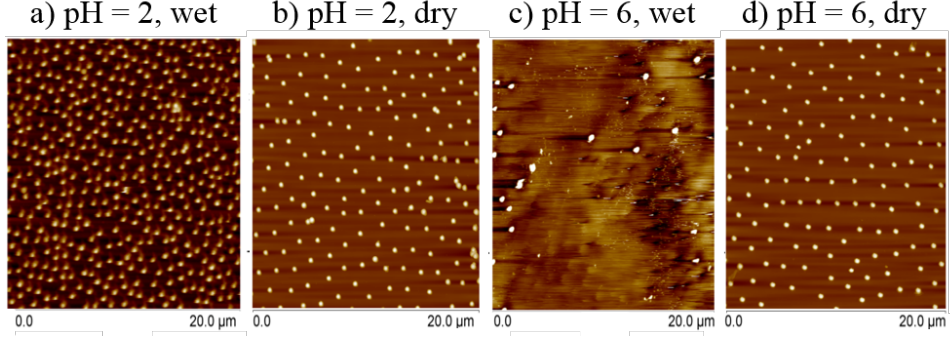a) pH = 2, wet   b) pH = 2, dry   c) pH = 6, wet   d) pH = 6, dry

Figure 6.2: AFM images of microgels deposited from solutions at pH 2 and 6 on oxidized silicon wafers without added salt.

at the droplet periphery. We compare the resulting particle patterns to images of adsorbed microgels obtained *in-situ*, i.e. without a drying step. We find that the convective flows associated with drying have a pronounced effect on the particle density and arrangement. At low pH, where both the surface and the microgels are uncharged, we find less microgels in the dried state than in the wet state (Figures 6.2a, b) whereas the opposite is observed at pH 6, where the surface and the microgels are negatively charged (Figures 6.2c, d). Moreover, for the dried sample in the areas where the microgels pack more densely, we find clearly ordered structures, while *in-situ* obtained images exhibit no pronounced ordering. This observation has also been reported in other studies;[21] the authors stated that during the drying process, a thin water film forms in which attractive capillary forces can act. It is thus important to note that the convective and capillary forces present during water evaporation may alter the configuration of the final layer. While this may be useful to obtain a specific structure of the microgel monolayer, it may hinder the interpretation of the results in terms of equilibrium adsorption properties. Therefore, all experiments presented below are obtained from *in-situ* imaging in the liquid state.

6.3.2   Adsorption density

We investigate the equilibrium adsorption density of these microgels as a function of environmental conditions by fluorescent microscopy. This is enabled by the presence of the fluorescent core, allowing accurate finding of particle positions using established algorithms. Visual inspection of the images in Figures 6.3a-f shows a decrease in the number of particles upon increasing pH. To quantify this, we compute the particle density as a function of pH (Figure 6.4). We can clearly
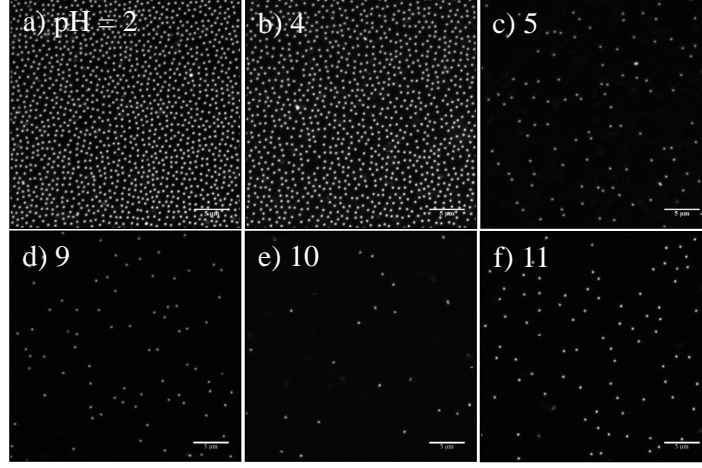
Figure 6.3: *In-situ* fluorescent microscopy images of microgel solutions deposited onto glass slides, at different pH values without added salt. Scale bar is 5 μm.
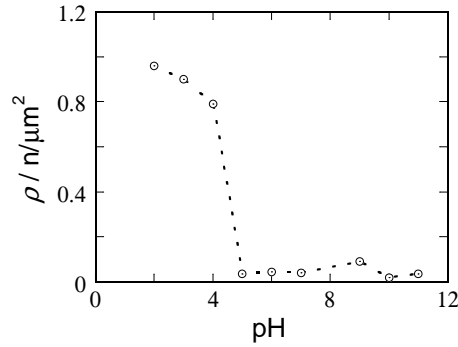

Figure 6.4: Particle density as a function of pH

distinguish two regimes. For pH < 4, less than 50% of the carboxylic groups of the microgels are dissociated and the charge density of the surface is low. In absence of strong electrostatic repulsion between surface and particles, microgels readily adsorb onto the surface and hydrogen bonds are formed between the -SiOH groups of the substrate and the -COOH groups of the microgels. Moreover, the weak particle-particle repulsion allows close-packed surfaces to form spontaneously. By contrast, for pH > 4 most acid groups of the microgels are dissociated and the negative charge density of the silica becomes higher. This leads to particle-particle and particle-surface electrostatic repulsions, resulting in a low particle density on the surface.
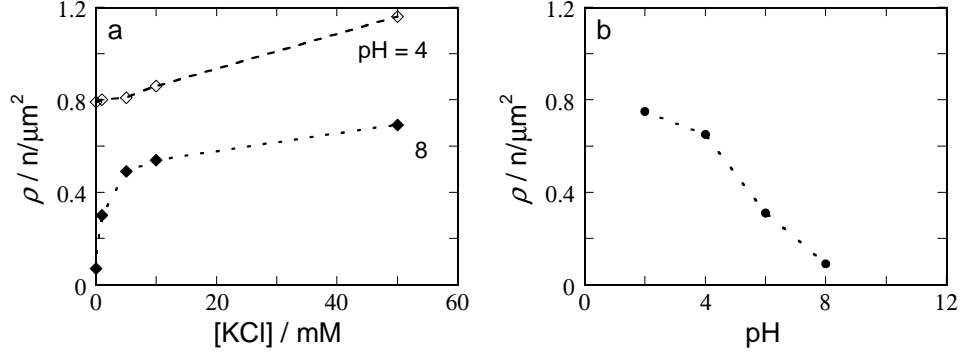
Figure 6.5: Particle density as a function of (a) the ionic strength, (b) the pH on an amino-modified wafer.

We then explore how screening the substrate-particle and inter-particle electrostatic repulsions by addition of salt influences their adsorption. As expected, the amount of particles on the surface increases with salt concentration (Figure 6.4a). The effect of salt addition is more pronounced at pH 8, where the particles and the surface are highly charged, as compared to pH 4, where only half of the acidic groups are charged; this confirms that the increase in adsorbed amount is due to charge screening.

Finally, we investigate the effect of surface charge on the amount of adsorbed microgels by using a surface in which the silanol groups have been reacted into primary amines (Figure 6.5b). This results in a positive charge for the surface at pH < 3.3 while the microgels are uncharged. With increasing pH, the microgels obtain a negative charge whereas the cationic surface charge reduces. If the particle-surface interaction controls the adsorption, we should expect a high density under conditions where the microgels and the surface are oppositely charged. Interestingly, we observe an adsorption density that decays monotonically with increasing pH. This suggests that rather repulsive particle-particle interactions govern the final density of adsorption. This is corroborated by comparing the densities obtained for anionic and cationic surfaces at the same solution conditions, where we find a marginal difference, with $\rho = 0.79$ for anionic substrates and $\rho = 0.65$ particles / μm^2 for amino-modified surfaces, which is within experimental error. Instead, adsorption appears governed by other interactions such as hydrogen bonding; indeed, the highest adsorption density is observed for microgels deposited on bare silicon wafer at pH 2.
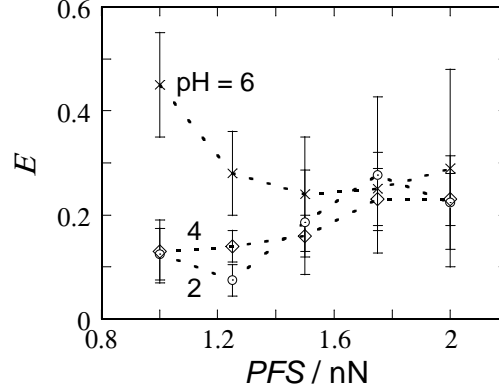
117

Figure 6.6: Modulus of the shell, normalized with respect to the center of the particle, as a function of the peak force setpoint for different pH values.

6.3.3 Microgel deformation

In previous studies attempting to evaluate the conformation of microgels adsorbed at a solid-liquid interfaces, focus was on isolated particles. However, in dense adsorbed layers, lateral interactions between microgels can affect their shape. We explore this using quantitative nanomechanical mapping (QNM) AFM. To obtain accurate information on the properties and configuration of these soft particles in their liquid state, it is important to verify that the imaging procedure does not significantly deform the particles at the surface. We therefore determine the effect of changing the peak force setpoint (PFS), which sets the maximum force exerted by the AFM tip on the sample. If the PFS is too large, the tip compresses the shell and only the core is measured. However, if the PFS is too low, accurate imaging is compromised. In Figure 6.6 we show that for PFS > 1.6 nN, the differences between the elastic modulus of the microgels at different degrees of charging vanish, suggesting that above this threshold no relevant data can be obtained. We therefore use a peak force setpoint of 1.2 nN for the experiments below.

To evaluate if the microgels deform significantly upon adsorption at a solid-liquid interface, we investigate the topographic cross-sections, averaged over 30 individual particles, as shown in Figure 6.7. In all cases, the cross-sections have a Gaussian shape. Because of the possible convolution of the shape of the particle and the tip, we extract two main features: the height of the particle at the center h_0 and their width w; w is determined by the elasticity going up, which means that the tip hits either the surface or another microgel particle. From this their apparent aspect ratio h_0/w is calculated; the results are summarised in Table 6.1.
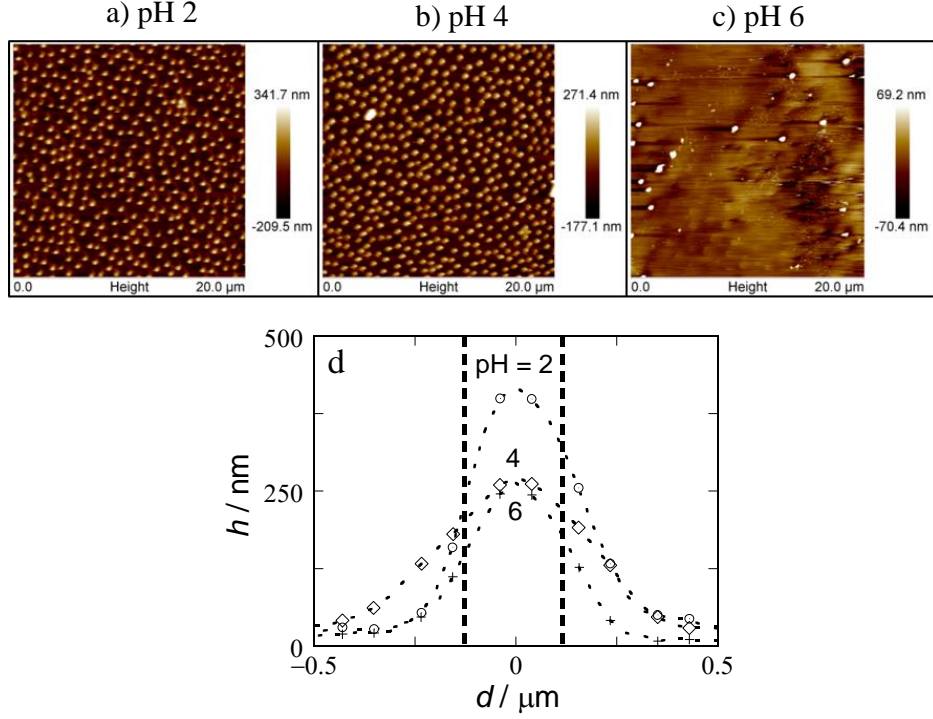
Figure 6.7: Atomic force microscopy on microgels in water deposited on silica wafer (a) topographic images as a function of pH, (b) cross-section profiles of height as a function of pH. The dashed lines indicate the position of the polystyrene core.

We observe that variations in size occur with solution conditions and surface properties, both in the lateral and in the vertical directions. We calculate the height:width ratio, which gives an indication of the degree of microgel deformation at the surface; a small height:width ratio signifies flattening of the microgels upon spreading at the solid surface. It appears that microgels at pH 2 are less spread than pH values of 4 and 6. With changes in ionic strength at pH 4, the dimensions of the particles change but their degree of conformation remains constant. Finally, we see that the deformation on an amino-modified surface is less than that of the same particles on an unmodified-silica surface. We speculate that this is due to a reduction in the adsorption energy, since as we argued above the adsorption on silica is promoted by hydrogen bonding, which does not occur at the amino-modified surface.

Table 6.1: Dimensions and aspect ratio of microgels deposited onto solid surfaces. The abbreviations h_0 and w correspond respectively to the height at the center of the particle and the width of the particle on the substrate. The values are averaged over 30 particles.

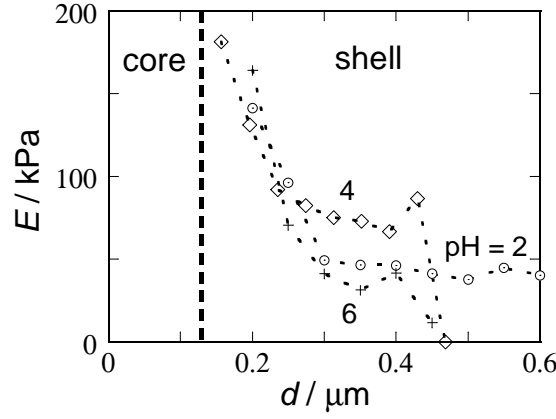| pH	[KCl] (mM)	Surface type	h_0 (nm)	w (nm)	h_0/w
2	0	silica	418	980	0.43
4	0	silica	273	900	0.30
6	0	silica	263	1060	0.25
4	0	silica	273	900	0.30
4	10	silica	246	740	0.33
4	50	silica	180	660	0.27
4	0	silica	273	900	0.30
4	0	amino	467	900	0.52

Figure 6.8: Cross-section profiles of elasticity as a function of pH obtained from atomic force microscopy. The dashed line indicates the position of the polystyrene core.

6.3.4 Microgel elasticity

The microgels we use for this study consist of a hard polystyrene core, with a modulus of the order of a few MPa, embedded within a soft hydrogel shell, with typical moduli of several tens to hundreds of kPa. This becomes evident from elasticity cross sections which show two distinct regimes reflecting core and shell regions respectively.

In Figure 6.8 we show the modulus of the microgel shell as a function of the distance from the core, at different pH values. Independently of pH, we observe a decrease in the shell modulus with increasing distance from the core. However, we

notice that the moduli for pH 4 and 6 fall off to zero at a smaller distance than at pH 2 (0.45 μm compared to 0.75 μm). This suggests that the microgels are softer at pH 4 and 6 than at pH 2 and this may be the origin of the larger degree of deformation at high pH.

6.4   Conclusion

In this work we studied the adsorption of microgel particles at solid-liquid interfaces. We first highlight how important it is to measure *in-situ* the adsorbed state (particle densities and shapes) to avoid artefacts due to drying steps. At the oxidized silicon surface, particle adsorption appears to be governed by hydrogen bonding interactions between the surface silanol groups and the carboxylic acid groups of the particles. Also repulsive electrostatic interactions between the particles influence the final packing density at the surface. Adsorption is almost entirely suppressed at pH > 4-5, when both the surface and the particles are negatively charged. Moreover, we show how these particles spread upon adsorption, using atomic force microscopy. The spreading of the microgels is higher at pH 4 and 6 than at pH 2 and is rather independent of the salt concentration. On an amino-modified surface the degree of spreading is lower than on an oxidized silicon surface. Nanomechanical AFM measurements highlight that the modulus of the microgels is lower at pH 4 and 6 than at pH 2. All together, the deformation of the particles under different conditions can be explained by a balance between the adsorption energy, promoting spreading, and the elasticity modulus, inhibiting deformation.

References

[1] H. Monteillet, M. Workamp, J.M. Kleijn, F.A.M. Leermakers, and J. Sprakel, *Adv. Mater. Interfaces*, 2014, **1**, 1300121.

[2] V. Nerapusri, J.L. Keddie, B. Vincent, and I.A. Bushnak, *Langmuir*, 2006, **22**, 5036–5041.

[3] S. Hofl, L. Zitzler, T. Hellweg, S. Herminghaus, and F. Mugele, *Polymer*, 2007, **48**, 245–254.

[4] S. Schmidt, H. Motschmann, T. Hellweg, and R. von Klitzing, *Polymer*, 2008, **49**, 749–756.

[5] S. Brugger and W. Richtering, *Langmuir*, 2008, **24**, 7769–7777.

[6] S. Brugger, B.A. Rosen, and W. Richtering, *Langmuir*, 2008, **24**, 12202–12208.

[7] S. Tsuji and H. Kawaguchi, *Langmuir*, 2008, **24**, 3300–3305.

[8] S. Brugger, S. Ruetten, K.-H. Phan, M. Moeller, and W. Richtering, *Angew. Chem. Int. Ed.*, 2009, **48**, 3978–3981.

[9] M. Destribats, V. Lapeyre, M. Wolfs, E. Sellier, F. Leal-Calderon, V. Ravaine, and V. Schmitt, *Soft Matter*, 2011, **7**, 7689–7698.

[10] T. Liu, S. Seiffert, J. Thiele, A.R. Abate, D.A. Weitz, and W. Richtering, *Proc. Natl. Acad. Sci.*, 2012, **109**, 384.

[11] J. Kim, M.J. Serpe, and L.A. Lyon, *J. Am. Chem. Soc.*, 2004, **126**, 9512–9513.

[12] M. Horecha, V. Senkovskyy, A. Synytska, M. Stamm, and A.I. Chervanyov, *Soft Matter*, 2010, **6**, 5980–5992.

[13] L.V. Sigolaeva, S.Y. Gladyr, A.P.H. Gelissen, O. Mergel, D.V. Pergushov, I.N. Kurochkin, F.A. Plamper, and W. Richtering, *Biomacromolecules*, 2014, **15**, 3735–3745.

[14] M. Stieger, J.S. Pedersen, P. Lindner, and W. Richtering, *Langmuir*, 2004, **20**, 7283–7292.

[15] L.A. Lyon and A. Fernandez-Nieves, 2012, pp. 25–43.

[16] D. Ershov, J. Sprakel, J. Appel, M.A. Cohen Stuart, and J. van der Gucht, *Proc. Natl. Acad. Sci.*, 2013, **110**, 9220–9224.

[17] J.K. Cho, Z. Meng, L. Andrew Lyon, and V. Breedveld, *Soft Matter*, 2008, **5**, 3599–3602.

[18] S. Berger, H.P. Zhang, and A. Pich, *Adv. Funct. Mater.*, 2009, **19**, 554–559.

[19] K. Geisel, L. Isa, and W. Richtering, *Langmuir*, 2012, **28**, 15770–15776.

[20] K. I. Geisel, K. Henzler, P. Guttmann, and W. Richtering, *Langmuir*, 2015, **31**, 83–89.

[21] S. Schmidt, T. Hellweg, and R. von Klitzing, *Langmuir*, 2008, **24**, 12595–12602.

[22] A. Burmistrova, R. Steitz, and R. von Klitzing, *ChemPhysChem*, 2010, **11**, 3571–3579.

[23] E. Spruijt, S.A. van den Berg, M.A. Cohen Stuart, and J. van der Gucht, *ACS Nano*, 2012, **6**, 5297–5303.

[24] Y. An, M. Chen, Q. Xue, and W. Liu, *J. Colloid Interface Sci.*, 2007, **311**, 507–513.

[25] Y.X. Gao and M.L. Kilfoil, *Optics Express*, 2009, **17**, 4685–4704.

[26] J.L. Hutter and J. Bechhoefer, *Rev. Sci. Instrum.*, 1993, **64**, 1868–1873.

[27] B. Derjaguin, V. Muller, and Y.P. Toporov, *J. Colloid Interface Sci.*, 1975, **53**, 314–326.

[28] X. Shi and Y.-P. Zhao, *J. Adhes. Sci. Technol.*, 2004, **18**, 55–68.

[29] S. Hirotsu, *J. Chem. Phys.*, 1991, **94**, 3949–3957.

[30] P. Voudouris, D. Florea, P. van dere Schoot, and H.M. Wyss, *Soft Matter*, 2013, **9**, 7158–7166.

Chapter 7

General Discussion

While in the previous chapters we answered some of the questions we addressed, our study also raised many new ones that could form the basis for future scientific research. In the following, we will highlight the questions emerged, discuss why they are important and we suggest some possible approaches, which may be valuable to tackle these questions in the future.

For both systems, complex coacervates and microgels, we demonstrated that their adsorption is spontaneous and their anchoring strong and irreversible, until the adsorption energy is reduced using an external trigger. These properties are essential in the development of sustainable extraction processes using emulsions. It is clear from the proof-of-concept of a sustainable extraction process presented in Chapter 5 why our interest involved the study of microgels as stabilizers; perhaps less evident is the choice to investigate complex coacervates. Polyelectrolytes find widespread use in the preparation or functionalization of separation membranes. Often, these layers are prepared using layer-by-layer assembly, a time-consuming process whose drawbacks have been summarised in Chapter 1. From a sustainability point-of-view, layer-by-layer deposition is undesired, as it requires numerous rinsing steps, producing large wastewater streams that must be treated or recycled. Our exploration into methods to form spontaneously dense and thick coacervate layers in a single and continuous process, resulting in the approach presented in Chapter 2, circumvents these issues. However, for both systems around which this thesis revolves, future work is required to arrive at both a complete understanding of how they work, and to translate our results to an industrial application. In the following, we will discuss our results in this context and define the steps still missing to fulfill the ultimate aims outlined at the start of this thesis.

7.1 Stabilizer design

The polyelectrolyte pair we chose to investigate in Chapter 2 consists of a home-designed and synthesized oil-soluble polyelectrolyte and commercially available water-soluble polyelectrolytes. Although the oil-soluble polyelectrolyte we used offers the advantage that it is auto fluorescent due to its conjugated structure, enabling its visualisation with fluorescence microscopy, such a complex structure is not required for more practical applications. Polyelectrolytes with a high charge density are typically well-soluble in water, due to charge hydration and dissociation. However, if the charge density is kept low, and the charge type is compatible with apolar solvents, for example carboxylic acids or amines, simpler designs for the oil-soluble species should be easily accessible. One interesting avenue would be to use polymerized ionic liquids, or poly(ionic liquids), which can be made oil-soluble by choosing the appropriate anion-cation pair. Further tuning of the properties of the spontaneously formed coacervate film, for example to go towards its use in membrane processes, would require an in-depth study of the effects of internal and environmental parameters such as molecular weight, charge density, ionic strength, pH, etc. Moreover, while complex coacervation typically refers to the electrostatic complexation between polyelectrolytes, the strategy we have developed may in
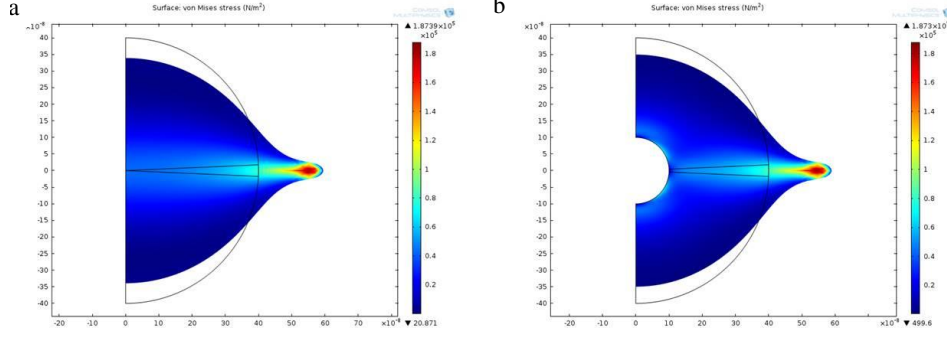
Figure 7.1: Finite-element calculation of the deformation of a spherical microgel, a) with core, b) without core, which experiences a line force at its equator, mimicking the deformation that it would experience due to elastocapillarity at a liquid interface. Calculations are conducted using the following parameters: relative density $\Delta\rho = 10$ kg/m^3, Young's modulus $E = 100$ kPa, Poisson's ratio $\nu = 0.4$, contact angle $\theta = 90°$ and interfacial tension between the two liquids $\gamma = 50$ mN/m.
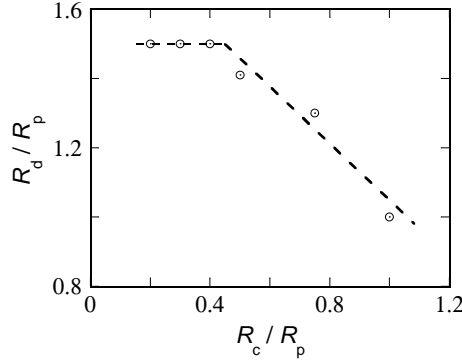

Figure 7.2: Ratio between the radius of the deformed particle over the radius of the undeformed particle versus the ratio of the radius of the core versus the radius of the particle, parameterised as in Figure 7.1.

principle be extended to particle-polyelectrolyte or polyelectrolyte-surfactant complexes as well. For Pickering stabilization, it is well known that mechanical energy is required to force particles across the energy barrier to rupture the thin film separating particles in bulk from their equilibrium position at the interface. We can imagine that attractive electrostatic interactions across the interface may lower the energy barrier, allowing spontaneous Pickering emulsification for a wide variety of particles and not only for microgels.

As mentioned, we have worked with systems, which are fluorescently labelled

to enable their study using fluorescence microscopy techniques. For the microgels, this involves the use of core-shell microgels in which a solid and undeformable core is embedded in a soft microgel shell (Chapters 4, 5 and 6). In our experiments we tuned the size ratio of core and shell such that the core is always much smaller than the shell thickness, to maintain as much as possible the softness and deformability unique to microgel colloids. To confirm the effects of the presence of a solid core on the deformability of these composite particles, we have performed some preliminary finite-element calculations. To mimic the elastocapillary force a microgel would experience at the oil-water-microgel contact line, we subject a homogeneous and a core-shell type spheres to a line force at the particle equator, thus simulating a particle that adsorbs with a contact angle $\theta = 90\,^\circ$. For the core-shell ratio used in our experiments we find no difference in deformation between the homogeneous and core-shell architectures, as shown in Figure 7.1. Indeed, the stiffening effect of a solid core only becomes significant when the core diameter becomes larger then the shell thickness (Figure 7.2). Also the exact configuration of microgels, both homogeneous and core-shell type, at liquid interfaces remains a topic of debate in literature;[1] while this is difficult to answer experimentally due to the wide range in length scales, ranging from the polymer mesh size on the order of nanometers, the dimensions of the microgels and their interactions, at micrometer scales, these issues may be answered using computer simulations, which thus forms an interesting avenue for future research.

7.2 Emulsion stability

As outlined in the introduction, emulsion stabilizers are expected to prevent a variety of mechanisms in which an initially stable and homogeneous emulsion can disproportionate and phase separate. Effective stabilizers do not only decrease the oil-water surface tension, to reduce the driving forces for coalescence and Ostwald ripening, but they also provide the interface with some elasticity, which in some cases can drastically slow down, or completely prevent, destabilization from occurring. For both complex coacervates and microgels it is well known and studied that viscoelastic phases are formed in the bulk at sufficient polymer concentration; the structure, dynamics and mechanics of their interfacial layers however is much less understood.

For the complex coacervate film, ideally one would start by ascertaining the organization of the polyelectrolytes in the film. Are they intermixed and entangled as in the bulk or in weak layer-by-layer films, or does a significant charge gradient develop, as suggested by our self-consistent field calculations? While the spontaneously formed coacervate layer proved too thin to investigate in detail using
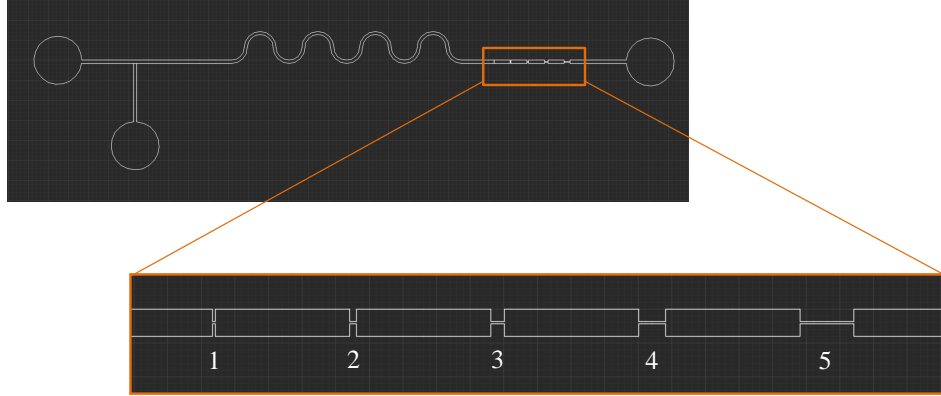
Figure 7.3: Microfluidic device designed to study the relaxation time of droplets. Length of the constrictions: No. 1: 75.0 μm, No. 2: 112.5 μm, No. 3: 150.0 μm, No. 4: 187.5 μm, No. 5: 225.0 μm.

conventional confocal microscopy, with a lateral resolution of ≈ 300 nm, the advent of superresolution techniques, which offer an order-of-magnitude reduction in resolution, may allow resolving the finer structure of these thin films. Simultaneously, the internal dynamics of the layers could be studied *in-situ* using Fluorescence Recovery After Photobleaching (FRAP), which could allow the differentiation between liquid- and solid-like films. This information may also be obtained using shear- or dilatational interfacial rheometry, even though these experiments are known to be challenging experimentally, and probe dynamics at time- and length scales much larger than those relevant in various applications. This suggests a clear need for the development of new experimental tools to probe surface properties of micronsized droplets *in-situ*. This is possible with new microfluidic methods, which have already proven valuable in for example measuring dynamic surface tensions [2] and droplet stability and coalescence. [3,4]

To take this one step further, we have started the design and testing of a microfluidic device that allows the fabrication and characterization of droplets in a single stream. The microfluidic device as illustrated in Figure 7.3 consists of two parts. In the first part, a T-junction produces a continuous stream of droplets, whose size can be tuned by the relative flow rates of disperse and continuous phases. After formation and incubation to allow the interface to become saturated with stabilizer, the droplets pass through a sequence of constrictions of different lengths in the second part. These constrictions impose a deformation of the droplet (Figure 7.4), but are designed in such a way that the droplets do not break-up and split
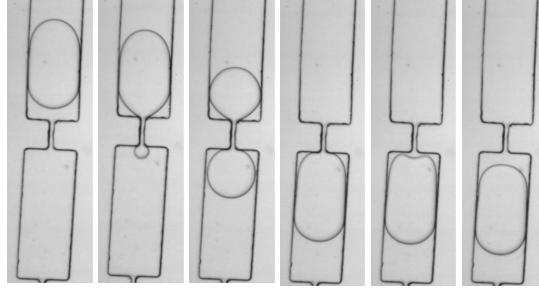
Figure 7.4: Image sequence of a MG1-stabilized droplet, which is deformed in a constriction and then relaxes back to its original shape.
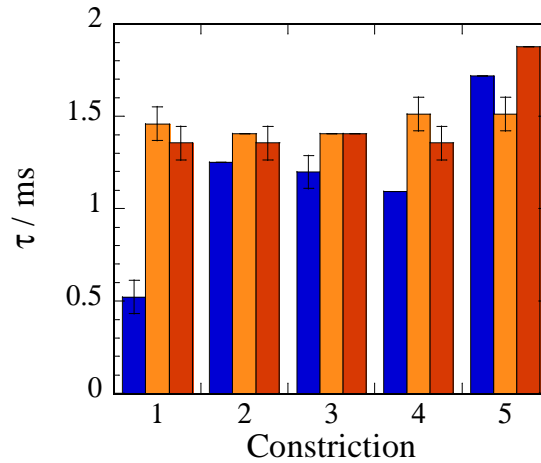

Figure 7.5: Relaxation time of the droplets in milliseconds as a function of the number of the constriction. Droplets were stabilised by 0.01 mol/L SDS, 9.37 g/L MG1 and 10.21 g/L MG20 respectively. Plotted is the mean relaxation time of three droplets and the standard deviation. Columns without visible standard deviation, exhibit a standard deviation below the detection limit.

due to a Rayleigh-Plateau instability. [5,6] By quantifying droplet relaxation after deformation, using image processing of microscopy pictures obtained using a high-speed camera, direct information about interfacial properties can be determined. [7]

We investigated the potential of this approach with three stabilizers, the surfactant sodium dodecyl sulfate (SDS), loosely-crosslinked soft microgels (MG1) and highly crosslinked hard microgels (MG20) (Figure 7.5). For surfactant-stabilized
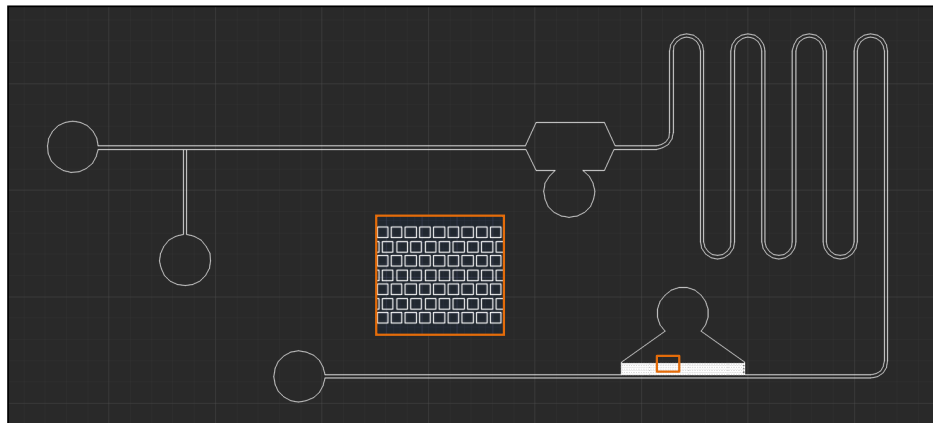
Figure 7.6: Microfluidic device for a continuous process of extraction using IL-in-water emulsions stabilized by microgels.

droplets, we observe an increased relaxation time with increasing constriction length. When the interface of a SDS-stabilized droplet is deformed, the emulsifier molecules spread out to the depleted regions and lower the gradient of the interfacial tension. Due to the interfacial mobility of small surfactant molecules, droplet deformation is easier as compared to slow interfaces laden with micronsized microgel particles. In other words, the elastic interface of microgels provides higher resistance to deformation than interfaces of surfactant-stabilized droplets; surprisingly however, no difference between soft and hard microgels was observed in our preliminary experiments. While these highly preliminary results confirm the potential of such an approach, future work is required to establish the relations between droplet relaxation processes and interfacial elasticity.

7.3 Liquid-liquid extractions

Many lab-scale extraction processes are designed at first, by convenience, to operate on a batch scale. For industrial application it is however preferred to perform large scale extractions in a continuous manner, to increase throughput efficiency. In Chapter 5 we provided the proof-of-concept for a new batch-based process for sustainable extractions, using thermoresponsive microgels as stabilizers for ionic liquid-in-water emulsions. However, the toolbox we developed consists of a series of subsequent batch processes; we therefore explored the possibility of using this strategy in a continuous processing design.

Also here, microfluidic chips offer a cheap, easy and versatile method to proto-

type a fully continuous extraction process. Our very preliminary work has focussed on the design shown in Figure 7.6. The device consists of a T-junction to create IL droplets in water, an inlet to inject the mixture of (bio)molecules for extraction, a "snake" to incubate droplets and continuous phase to allow mass exchange to occur. Finally, the continuous phase is siphoned off a side channel, to concentrate the IL droplets where a heat trigger may be applied to separate the ionic liquid and water phases again. We used soft lithography to fabricate this device and preliminary experiments show that the single components work as predicted, but experiments on the integrated device are topic for future research. Interestingly, microfluidic devices also allow the integration of various detection methods, which could allow *in-situ* monitoring of extraction processes with high temporal resolution and with easy fluidic methods to screen a wide variety of ionic liquids or solvent conditions. Especial focus in future research into this topic should go towards the design of chips and surface modification protocols, which prevent the corrosive action of many ionic liquids to occur.

7.4 Academic questions and directions

In addition to the practical issues discussed above that need to be resolved before the work presented in this thesis may lead to industrial application, our work has also revealed some interesting and unexplained observations, and academic questions, which are worth pursuing.

We have shown that the ion pair of the IL plays an important role in the type of emulsion formed and the partitioning and adsorption behaviour of charged microgels. For strongly hydrophobic ion pairs, the microgels remain in the aqueous phase and oil-in-water emulsions are preferred. By contrast, if one of the ions is made more water-soluble, for example using chloride ions, a spontaneous transfer of the microgels into the ionic liquid was observed, and a reverse water-in-oil type emulsion formed. Interestingly, for the water-in-IL emulsions we observed the spontaneous recruitment of particles at the perifery of the droplet, as shown in Figure 7.7. This "microgel cloud" grows in time but was confirmed free of particle aggregation. The formation of this particle-rich zone is possibly due to ion exchange effects, where the ionic liquid-water interface acts as an effective ion exchange resin. The formation of long-ranged structures in charged suspensions in proximity to an ion exchange resin, due to the establishment of ion strength gradients, was recently reported and explained for solid ion exchange resins due to a process coined "diffusiophoresis".[8] It is imaginable that a similar process occurs in these mixtures of water droplets and charged particles immersed in an ionic liquid.

The spontaneous anchoring of microgels at liquid interfaces, and the tunability
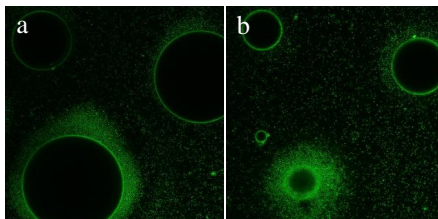
Figure 7.7: Formation of particle clouds in proximity to the interface between a water droplet in an ionic liquid.
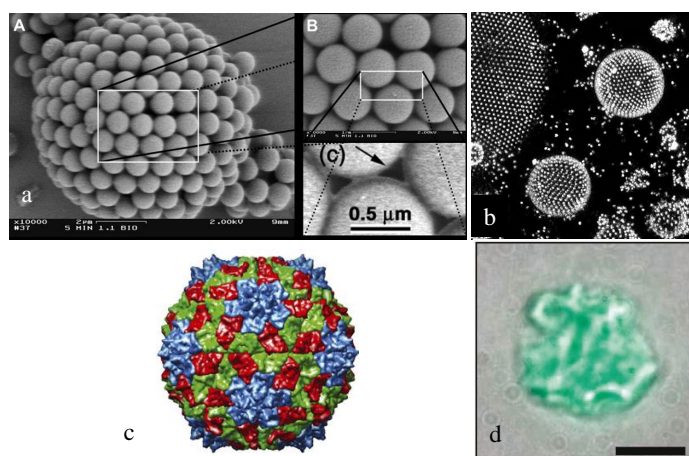

Figure 7.8: (a) Colloidosome made from hard particles. [9] (b) Decane droplets in water stabilized by composite microgels (see Chapter 4). (c) Illustration of simulation result for a spherical virus capsid. [10] (d) Crumpled Pickering droplet. [11] Reprinted with permission from the different editors.

of their softness and resulting particle-particle interactions, makes them an interesting platform to explore self-assembly processes in two dimensions. For example, work from our group has shown that these microgels can be made to interact anisotropically simply by manipulating the curvature of the oil-water interface. [12] Perhaps, they are also a useful experimental tool to explore how defects form and diffuse in curved crystals (Figures 7.8a-b), which is not only interesting academically, but relevant to understand the self-assembly of soft and shapable building blocks, such as proteins, into curved elastic sheets in for example viral capsids (Figure 7.8c) and pollen grains. [13] The soft but densely-packed interfaces formed by adsorbing microgels may also be used to explore the mechanical stability of elastic sheets assembled from discrete building blocks, which are known to undergo

a variety of buckling and crumpling instabilities (Figure 7.8d).

7.5   Outlook

Ionic liquids became a hot research topic in the last 10 years and this in a wide variety of domains such as synthesis and separations. Over the past 4 years we have made some significant steps in developing IL-based sustainable extraction processes. We hope these steps will inspire people to take the next ones to reach a fully sustainable and continuous process of extraction based on IL-emulsions.

References

[1] S. Schmidt, T.T. Liu, S. Rutten, K.H. Phan, M. Moller, and W. Richtering, *Langmuir*, 2011, **27**, 9801–9806.

[2] M.L.J. Steegmans, Warmerdanm A., K. Schroën, and R.M. Boom, *Langmuir*, 2009, **25**, 9751–9758.

[3] T. Krebs, K. Schroën, and R. Boom, *Soft Matter*, 2012, **8**, 10650–10657.

[4] H. Feng, D. Ershov, T. Krebs, K. Schroën, M.A. Cohen Stuart, J. van der Gucht, and J. Sprakel, *Lab on a Chip*, 2015, **15**, 188–194.

[5] L. Rayleigh, *Proc. R. Soc. London*, 1879, **29**, 71–97.

[6] S.D. Geschiere, I. Ziemecka, V. van Steijn, G.J.M. Koper, J.H. van Esch, and M.T. Kreutzer, *Biomicrofluidics*, 2012, **6**,.

[7] E. Scholten, L.M.C. Sagis, and E. van der Linden, *J. Phys. Chem. B*, 2006, **110**, 3250–3256.

[8] D. Florea, S. Musa, J.M.R. Huyghe, and H.M. Wyss, *Proc. Natl. Acad. Sci.*, 2014, **111**, 6554–6559.

[9] A.D. Dinsmore, M.F. Hsu, M.G. Nikolaides, M. Marquez, A.R. Bausch, and D.A. Weitz, *Science*, 2002, **298**, 1006–1009.

[10] E.R. May, *Mol. Simul.*, 2014, **40**, 878–888.

[11] S.S. Datta, H. Cheung Shum, and D.A. Weitz, *Langmuir*, 2010, **26**, 18612–18616.

[12] D. Ershov, J. Sprakel, J. Appel, M.A. Cohen Stuart, and J. van der Gucht, *Proc. Natl. Acad. Sci.*, 2013, **110**, 9220–9224.

[13] E. Katifori, S. Alben, E. Cerda, D.R. Nelson, and J. Dumais, *Proc. Natl. Acad. Sci.*, 2010, **107**, 7635–7639.

Chapter 8

Summary

The use of ionic liquids (ILs) as replacement of organic solvents in liquid-liquid extractions has shown great promise due to their low volatility, flammability and toxicity, tunable solvency to a wide variety of extractable compounds and mildness to delicate compounds such as biomolecules for pharmaceutical applications. However, the efficiency of extractions using ionic liquids is limited as the inherently high viscosity of ILs slows down the mass transfer. Increasing the interfacial area between the immiscible phases is an efficient way to increase the efficiency of liquid extractions; typically done by formulating emulsions, dispersions of fluid droplets suspended in a second immiscible continuous phase. While strategies to formulate stable emulsions from conventional apolar solvents, such as aliphatic or halogenated oils, in water are abundant, the peculiar properties of ionic liquids requires the exploration of new strategies to formulate stable emulsions; for example, common surfactant stabilization leads to rapid Ostwald ripening due to the inherent water solubility of many ionic liquids. Moreover, while the intended ionic liquid-in-water emulsions must be stable at operating temperatures for prolonged times, it should be possible to break the emulsion on-demand to recover the extracted product. Also, the interfacial layer used for stabilization should not hinder the transfer of the intended product to the droplet phase. To increase the sustainability of extraction processes, recovery of both ionic liquid and stabilizer for re-use in a subsequent extraction step is highly desired. Aimed to establish new ways of stabilizing emulsions in general, and ionic liquid emulsions in specific, this thesis describes investigations into two novel stabilizers: interfacial electrostatic complexes and soft colloidal microgels.

In **Part I**, we focussed on how oppositely charged polyelectrolytes interact and form complexes across an oil-water interface. In **Chapter 2**, we demonstrated a new method for emulsion stabilization, in which electrostatic complexes formed across a liquid interface between two polyelectrolytes, one dissolved in the aqueous phase, the other in the oil phase. Using tensiometry we followed the polyelectrolyte adsorption at the oil-water interface; while the presence of either polyelectrolyte alone leads to interfacial depletion, the presence of both species leads to strong adsorption at the interface. This was further confirmed using confocal fluorescence microscopy where the colocalization of both species at the interface was observed; the strong overlap of peak intensities at the interface suggests a strongly intermixed layer. Using this approach, we prepared stable emulsions, which could be reversibly broken and reformed by simple pH and salt triggers. Interestingly, oil-in-water but also water-in-oil emulsions could be produced. This is the first demonstration of using selective associative phase separation to stabilize a segregating system.

The experimental results triggered questions on the nature of the interfacial layer, which was too thin to be ascertained in detail using microscopy. Therefore,

we turned to self-consistent field (SCF) modelling to develop a deeper understanding of the structure and thermodynamics of this interfacially-templated complexation, as presented in **Chapter 3**. In analogy with our experiments, we use the Scheutjens-Fleer lattice method to consider mixtures of two solvents, an anionic oil-soluble polyelectrolyte, a cationic water-soluble polyelectrolyte, their counterions and additional indifferent monomeric electrolyte. We first considered a two-phase system with only one polyelectrolyte and salt. We found that the polyelectrolyte adsorption depends on its concentration. For polyelectrolyte concentrations lower than the salt concentration, the polyelectrolyte is depleted from the oil-water interface while for polyelectrolyte concentrations higher than the salt concentration, the polyelectrolyte adsorbs at this interface. This transition from depletion to adsorption originates from a competition between small ion and macroion adsorption, governed by the overall ionic strength. Upon introducing a second polyelectrolyte in the immiscible second solvent, a new phase spontaneously formed at the interface between oil and water. Surprisingly, our calculations showed that ion release entropy is not the driving force for complexation, as it often is in bulk complex coacervation; co-assembly is governed by enthalpic contributions. This is due to the solvent-selectivity of the polyelectrolytes in this scenario, which leads to low solvent content in the coacervate layer, hence close approach of the opposite charges resulting in a relatively large Coulombic enthalpy. Finally, we examined systems with asymmetric composition of the two polyelectrolytes within the same theoretical approach. This revealed an unusual pseudo-partial wetting scenario, due to interactions occurring at different length scales. When the electrostatic interactions are short ranged, the microscopically thin wetting film transitions to a mesoscopic thin film. However, charges built up on either side of the coacervate layer restrict the growth of the film to macroscopic dimensions. In our experiments we observe that the coacervate layer becomes turbid over time, suggesting structures on optical length scales, much larger than the typical dimensions of the polymer coils. This may be explained by the pseudo-partial wetting scenario due to the coexistence of a mesoscopic film with interfacial liquid droplets nucleating due to thermal fluctuations.

In the second part of this thesis, **Part II**, we studied the adsorption and organization of colloidal microgels at a variety of liquid interfaces. These soft and deformable hydrogel colloids have gained a lot of interest in recent years due to their excellent ability to stabilize emulsions. As a result of their polymeric nature and osmotic equilibrium with the bulk solution, microgels exhibit an interesting duality between colloidal properties and polymeric behaviour. Microscopic research into their interfacial behaviour is often made difficult as they offer little refractive index contrast to the continuous phase and covalent attachment of fluorophores is known

135

to drastically alter their interactions. To overcome this problem, in **Chapter 4** we introduce composite microgels, in which a solid fluorescent core is embedded in the centre of a soft and tunable hydrogel shell, thereby decoupling the imaging features of these microgels with the tunability of their softness, size, solvent-responsivity and interactions. We surprisingly find that while these microgels adsorb spontaneously, without any energy barrier which is usual for the Pickering adsorption of micron-sized colloids, their anchoring at the liquid interface is irreversibly strong. Due to the high adsorption energy, saturated interfacial layers of these microgels show mild compression of the particles, increasing their packing density at the cost of elastic deformation. Moreover, we showed that these particles are able to stabilize a wide variety of oil-water interfaces and due to their spontaneous adsorption allow the fabrication of Pickering droplets using microfluidics, which is usually hindered by the adsorption barrier for solid particles.

In **Chapter 5**, we arrive at the ultimate aim of this thesis, i.e. to provide proof-of-concept for a fully sustainable extraction process based on IL-in-water emulsions. We first show how microgels are able to create emulsions of a wide variety of ILs in water and prevent their Ostwald ripening, resulting in extended stability at room temperature. Upon heating and applying centrifugal compression, the emulsion can be rapidly broken, with all of the microgels returning the aqueous phase which can then be re-used in a secondary extraction step. Finally, we demonstrated that through the use of a paramagnetic ionic liquid, the concentration and breaking step can be performed without energy input with a simple permanent magnet, rendering the process sustainable from start to end.

Finally, in **Chapter 6**, we studied the adsorption and conformation of these composite microgels at solid-liquid interfaces. We first demonstrate how conventional sample preparation for studying microgels at solid interfaces, often involving a drying step, induces strong sample artefacts. We therefore developed a method to study the adsorption and conformation of microgels *in-situ* using liquid-state confocal and atomic force microscopy. Our results showed how the packing density for particle adsorption is governed by particle-particle repulsion, as adsorption energies are typically very high. Using Quantitative Nanomechanical Mapping, the spatially-resolved mechanical analysis of surfaces using atomic force microscopy, we find that the degree of spreading of microgels during adsorption at a solid interface is governed by adsorption energy and particle softness as expected. This leads us to conclude that the unique properties of microgels at interfaces results from a subtle interplay between adsorption energy and internal elasticity.

Samenvatting

Het gebruik van ionische vloeistoffen als vervanging voor organische oplosmiddelen in vloeistof-vloeistof extracties is veelbelovend vanwege hun lage vluchtigheid, ontvlambaarheid en giftigheid, terwijl een grote verscheidenheid van extraheerbare componenten oplosbaar is in deze vloeistoffen; verder zijn ze niet agressief voor delicate verbindingen zoals biomoleculen voor farmaceutische toepassingen. Echter, de efficintie van extracties met ionische vloeistoffen is gelimiteerd doordat hun inherente hoge viscositeit het massatransport verlaagt. Een doeltreffende manier om de efficintie van vloeistofextracties te verhogen is het vergroten van het contactoppervlak tussen de onmengbare fases en dit gebeurt typisch door het maken van emulsies: dispersies van vloeistofdruppels in een tweede niet mengbare continue fase. Hoewel er veel strategien bekend zijn om stabiele emulsies van conventionele apolaire oplosmiddelen, zoals alifatische of gehalogeneerde olin, in water te vormen, vereisen de specifieke eigenschappen van ionische vloeistoffen onderzoek naar alternatieve manieren om stabiele emulsies te formuleren; bijvoorbeeld de algemeen bekende stabilisatiemethode met oppervlakteactieve stoffen leidt bij ionische vloeistoffen snel tot Ostwald rijping doordat ze beter oplossen in water dan conventionele oplosmiddelen. Een vereiste voor extractie is dat de emulsie voor lange tijd stabiel moet zijn bij werktemperaturen, maar toch on demand moet kunnen worden gebroken om het extract te isoleren. Daarnaast mag de stabilisatie van het grensvlak tussen water en ionische vloeistof de overdracht van het product naar de gedispergeerde fase niet hinderen. Voor een duurzaam extractieproces is hergebruik van de ionische vloeistof en stabilisator in latere extractiestappen een groot voordeel. Met het doel om alternatieve methoden te ontwikkelen voor het stabiliseren van emulsies in het algemeen, en meer specifiek voor het stabiliseren van ionische vloeistof-in-water emulsies, beschrijft dit proefschrift het onderzoek naar twee nieuwe mechanismen voor stabilisatie: de vorming van elektrostatische complexen in het vloeistof-vloeistofgrensvlak en de adsorptie aan dit grensvlak van zachte microgeldeeltjes.

Deel I van het proefschrift beschrijft de manier waarop tegengesteld geladen polyelektrolyten wisselwerking met elkaar hebben en complexen vormen in een olie-water grensvlak. In **Hoofdstuk 2**, demonstreren we een nieuwe methode voor de stabilisatie van emulsies, waarbij in het grensvlak een elektrostatisch complex gevormd wordt tussen twee polyelektrolyten, de ene opgelost in de waterige fase

en de andere in de oliefase. Door het meten van de grensvlakspanning volgden we de adsorptie van de polyelektrolyten aan het olie-water grensoppervlak; terwijl elk van de polyelektrolyten apart depletie aan het grensvlak vertoont, zorgt de aanwezigheid van beide juist voor een sterke adsorptie. De vorming van een elektrostatisch complex in het grensvlak werd bevestigd door confocale fluorescentie microscopie; de ruime overlap in de fluorescentieprofielen van de twee polyelektrolyten aan het grensvlak wijst op een sterk gemengde laag. Door van deze complexvorming gebruik te maken, konden we stabiele emulsies maken die omkeerbaar kunnen worden gebroken en hersteld door variatie van de zoutconcentratie of de pH. Interessant is dat niet alleen olie-in-water maar ook water-in-olie emulsies gevormd kunnen worden. Dit is de eerste demonstratie van het gebruik van selectieve, associatieve fasescheiding om een segregerend systeem te stabiliseren.

De experimentele resultaten wierpen vragen op wat betreft de eigenschappen van de coacervaatlaag, die te dun was om met behulp van microscopie in detail te onderzoeken. Daarom richtten we ons op moleculaire zelf-consistent veldmodellering om inzicht te krijgen in de structuur en thermodynamica van deze grensvlak-georinteerde complexvorming. De resultaten daarvan zijn beschreven in **Hoofdstuk 3**. In analogie met onze experimenten beschouwen we olie-water systemen met een negatief geladen olie-oplosbaar polyelektrolyt, een positief water-oplosbaar polyelektrolyt, hun tegenionen en kleine zoutionen. Als eerste stap modelleerden we een tweefasen-systeem met slechts n polyelektrolyt en zout. De adsorptie van het polyelektrolyt hangt af van zijn concentratie; voor concentraties die lager zijn dan de zoutconcentratie, bleek het polyelektrolyt het olie-water grensvlak te mijden, maar als de concentratie van het polyelektrolyt hoger is dan die van het zout, adsorbeert aan het grensoppervlak. Deze overgang van depletie naar adsorptie is het gevolg van competitie tussen de adsorptie van kleine ionen en macro-ionen en wordt bepaald wordt door de totale ionsterkte. Bij introductie van het tweede polyelektrolyt in het systeem, ontstaat spontaan een nieuwe fase in het grensvlak tussen water en olie. Tot onze verrassing toonden onze berekeningen aan dat de drijvende kracht voor de complexering in het grensvlak niet de entropiewinst ten gevolge van het vrijkomen van tegenionen is, zoals vaak wel het geval bij complexcoacervatie in oplossing, maar is de vorming van het complex vooral enthalpisch gedreven. Dit komt door de voorkeur van elk van de polyelektrolyten voor slechts een van de oplosmiddelen, waardoor er uiteindelijk weinig oplosmiddel in de coacervaatlaag terecht komt en de tegengesteld geladen groepen dicht bij elkaar kunnen komen; dit levert relatief veel Coulomb energy op. Tenslotte bestudeerden we systemen waarbij de concentraties van de polyelektrolyten in de twee fasen verschilden. Dit bracht een ongewoon pseudo-partieel bevochtigingsscenario aan het licht, veroorzaakt door interacties op verschillende lengteschalen. Op moleculaire schaal is het

gunstig dat het grensvlak bevochtigd wordt door de coacervaatfilm en daardoor gaat de microscopisch dunne bevochtigingsfilm over naar een mesoscopische dunne film. Een ladingsoverschot aan beide kanten van de coacervaatlaag voorkomt dat de filmdikte toeneemt tot macroscopische omvang. Het pseudo-partieel bevochtigingsscenario zou onze experimentele observatie dat de coacervaatlaag troebel werd, kunnen verklaren. Zon vertroebeling wijst op het ontstaan van structuren met lengtes in de orde van de golflengte van het licht, zoals een mesoscopische film in het grensvlak met daarin coacervaatdruppeltjes die ontstaan door temperatuurschommelingen.

Deel II van het proefschrift gaat over de adsorptie en organisatie van collodale microgels in verschillende typen vloeistof-vloeistof grensvlakken. Deze zachte en vervormbare hydrogeldeeltjes staan de laatste jaren in de belangstelling dankzij hun capaciteit om emulsies te stabiliseren. Microgeldeeltjes vertonen een interessante dualiteit in hun gedrag dat kenmerken vertoont van zowel (harde) deeltjes als polymeren. Microscopisch onderzoek naar microgels in grensvlakken wordt bemoeilijkt door hun lage brekingsindex ten opzichte van de continue fase. Covalent binden van een (fluorescente) kleurstof in de gelmatrix zou helpen, maar zou ook de interacties van de deeltjes benvloeden. Om dit laatste probleem te omzeilen, introduceren we in **Hoofdstuk 4** samengestelde microgels, waarin een vaste fluorescerende kern vastzit in een zacht hydrogel-omhulsel; hiervoor is het mogelijk de deeltjes microscopisch in beeld te krijgen zonder hun interacties te benvloeden, terwijl we controle houden over hun grootte en mechanische eigenschappen. Heel verrassend bleken deze microgels spontaan te adsorberen in allerlei olie-water grensvlakken, zonder dat er een energiebarrire overwonnen hoeft te worden, zoals wel het geval is bij Pickering-adsorptie van deeltjes met micrometeromvang, terwijl hun verankering in het vloeistofgrensoppervlak heel sterk is. Door de hoge adsorptie-energie worden de deeltjes een klein beetje samengedrukt in het grensvlak als dit vol raakt, zodat de pakkingsdichtheid toeneemt ten koste van elastische vervorming.

In **Hoofdstuk 5** bereiken we het uiteindelijke doel van deze thesis, het leveren van een proof-of-concept voor een volledig duurzaam extractieproces gebaseerd op ionische vloeistof-in-water emulsies. We lieten eerst zien dat microgels een grote verscheidenheid van ionische vloeistoffen kunnen emulgeren in water en Ostwald rijping kunnen voorkomen, resulterend in een grote emulsiestabiliteit bij kamertemperatuur. Door verwarmen en gebruik te maken van centrifugale compressie kunnen de emulsies snel worden gebroken waarbij microgels terugkeren naar de waterfase en deze opnieuw kan worden gebruikt in een tweede extractiestap. Tot slot toonden we aan dat door toepassing van paramagnetische ionische vloeistoffen, het concentreren van de emulsiedruppeltjes en het breken van de emulsie kan worden uitgevoerd met een eenvoudige permanente magneet, zonder toevoer van energie,

wat het proces van begin tot eind duurzaam maakt.

Tenslotte, in **Hoofdstuk 6**, bestudeerden we de adsorptie en vervorming van samengestelde microgels aan een vast-vloeibaar grensvlak. We lieten eerst zien hoe de conventionele monstervoorbereiding voor het bestuderen van microgeldeeltjes op vaste oppervlakken, vaak gecombineerd met een droogstap, artefacten veroorzaken. Om zulke artefacten te voorkomen, bestudeerden we de adsorptie aan het vast-vloeistof oppervlak in situ met confocale en atomic force microscopie. Door ook de elastische eigenschappen van de deeltjes op het oppervlak in beeld te brengen, ontdekten we dat de mate van spreiding van de microgels tijdens adsorptie bepaald wordt door de adsorptie-energie en de zachtheid van de deeltjes. Dit leidt tot de conclusie dat de unieke eigenschappen van microgels aan grensoppervlakken het resultaat is van een delicate wisselwerking tussen adsorptie-energie en interne elasticiteit.

List of publications

- H. Monteillet, F. Hagemans, J. Sprakel, Charge-driven co-assembly of poly-electrolytes across oil-water interfaces, *Soft Matter* **9** (2013), 11270-11275, doi 10.1039/C3SM52241E (Chapter 2).

- H. Monteillet, J. M. Kleijn, J. Sprakel, F. A. M. Leermakers, Complex coac-ervates at liquid interfaces: a self-consistent field analysis, *Manuscript in preparation* (Chapter 3).

- H. Monteillet, M. Workamp, J. Appel, J. M. Kleijn, F. A. M. Leermakers, J. Sprakel, Ultrastrong Anchoring et Barrier-Free Adsorption of Compo-site Microgels at Liquid Interfaces, *Adv. Mater. Interfaces* **1** (2014), doi 10.1002/admi.201300121 (Chapter 4).

- H. Monteillet, M. Workamp, X. Li, B. Schuur, J. M. Kleijn, F. A. M. Leermakers, J. Sprakel, Multi-responsive ionic liquid emulsions stabilized by microgels, *Chem. Commun.* **50** (2014), 12197-12200, doi 10.1039/C4CC04990J (Chapter 5).

- H. Monteillet, M. Brouwer, J. M. Kleijn, F. A. M. Leermakers, J. Sprakel, Microgels at solid-liquid interfaces, *Manuscript in preparation* (Chapter 6).

Acknowledgements

Almost four years ago, I remember applying to the following job description: "We are looking for a PhD student interested in making emulsions of ionic liquids in water for separation purposes ... Molecular modelling may be part of your activities". Four years later, here we are at the end of my thesis and with one chapter on modelling!

Frans, Martien, I would like to thank you both for giving me the opportunity to do my thesis at Fysko. Frans, thank you for your involvement in the project; your 'I have an idea' will stay embedded in my memory. You even managed to make me work with the scf box and thanks to your patience, we could write the third chapter of this thesis. Mieke, you welcomed me the first day when I arrived at Fysko. You were very approachable and gave me a lot of freedom even at the beginning of the project. I enjoyed your valuable critics on my manuscripts, thesis and presentations. Joris, I remember how it all started: I was working in the lab and you were quite curious about my work. You gave me some suggestions and after few weeks you became naturally one of my supervisors. I am very grateful you joined the project. Your guidance helped me to find my way in the project and your insights were very useful at all stages of the project. Frans, Mieke and Joris what a team we formed! I will always remember our very lively meetings. Thanks for helping me to grow as a scientist and as a person.

Joshua, Hans, Herman, Marleen, Renko, I appreciated the ease I could talk to all of you and ask for suggestions/advice.

Special thanks to the students who worked with me on this project Andrea, Erik, Fabian, Marcel and Max. I enjoyed having you around. You were so enthusiast and worked so hard that we could achieve a lot. I appreciated that even after you left, you were still willing to help me while I was going through your data.

I would like to thank to present and past members of the lab: Anita, Anton, Antsje, Bert, Céline, Christian, Diane, Dmitry, Gosia B., Gosia W., Hande, Hanne, Hannie, Harke, Huanhuan, Ilse, Inge, Evan, Kamuran, Jacob, Jan Bart, Jan Maarten, Jeroen, Joanne, Johan, Josie, Juan, Junyou, Katarzyna, Lennart, Liyakat, Mara, Marcel, Maria, Maarten, Merve, Monika, Nadia, Natalia, Lione, Remco, Ronald, Ruben, Rui, Sabine, Soumi, Surender, Ties, Tingting, Thao, Yunus, Vittorio, Wolf. You all contributed to this thesis and supported me in one way or the other during these four years by creating a nice atmosphere in the

lab, having stimulating discussions, helping me with my experiments, solving my issues (diploma, Latex, etc). Good luck to all of you for the future.

Hande, Marcel, thank you for agreeing to be my paranymphs. I did not have to think very long to decide that you would be standing with me on the stage on this special day.

I would like to thank the jury members for accepting to read my thesis: Dr Duits, Prof. Dr Eppink, Dr Kraft and Prof. Dr Schroën.

My time was also enjoyable due to the many friends that are/became part of my life. Eric, Fabien, Lorinne, Rémi, Sabine, Vincent, Yann, on dit souvent que la distance est un bon test pour l'amitié, je crois pouvoir dire que nous avons passé ce test haut la main. Vous n'avez pas hésité à braver le froid et venir dans le Nord pour nous rendre visite, merci. Ellen, Erik, Hande, Robert Jan, Niels thank you for all the great moments spent together.

Je terminerai avec les personnes les plus importantes pour moi. Maman, papa, ces quelques lignes ne suffiront pas à exprimer combien je vous suis reconnaissante de tout ce que vous avez fait pour moi durant toutes ces années. Vous m'avez toujours soutenue dans mes choix même si cela impliquait de m'éloigner de vous. Merci d'avoir été et d'être toujours là.

Kevin, nous savons tous les deux que sans toi je ne serai pas là aujourd'hui. J'avais des doutes sur mes capacités à faire une thèse mais toi tu n'en avais pas et tu as finis par me convaincre de me lancer dans ce projet. Cela n'a pas été facile tous les jours et c'est ensemble que nous y sommes arrivés. Mille mercis pour ton amour, ton soutien indéfectible, tes encouragements permanents.

It is time to turn this page and open a new chapter ...

Hélène

144

About the author

Hélène was born the 27th of July 1985 in Rodez, France. After getting her baccalaureat, she went to the university of Albi where she studied physics and chemistry. She obtained her Bachelor diploma in 2007. After that, she moved to Lyon to start her chemical engineering studies with a focus on physico-chemistry and formulation. As part of her studies, she carried out two projects. As a gap-year, she spent one year at the Machine Dishwash Group in Unilever Vlaardingen, The Netherlands. There she worked on formulation of detergents. As her final-year project, she spent six months in the Emulsion Group of Dow Corning in Seneffe, Belgium. She studied elastomer film-forming emulsions. She graduated from CPE with an engineer diploma, equivalent to a MSc. In October 2011, she started as a PhD on an STW project "Smart separations" at the Physical Chemistry and Soft Matter Group of Wageningen University, under the supersivion of Prof. Dr Frans Leermakers, Dr Mieke Kleijn and Dr Joris Sprakel. This thesis is the result of that 4-year research project.

Overview of completed activities

Discipline specific

Winter school	Han sur Lesse (Belgium)	2012
ECIS Training Course	Malmö (Sweden)	2012
ECIS ‡	Malmö (Sweden)	2012
Advanced Soft Matter	Wageningen	2012
Soft Matter Day †	Wageningen	2012
Soft Matter Day	Twente	2013
FOM ‡	Veldhoven	2013
Rheology School	Leuven (Belgium)	2013
ISMC ‡	Rome (Italy)	2013
COMSOL	Wageningen	2014
NWO Meeting *	Veldhoven	2014
Gordon Research Seminar *	Ventura (USA)	2014
Gordon Research Conference ‡	Ventura (USA)	2014
SoftCom Meeting *	Heraklion (Greece)	2014
STW Smart Separation Meeting ‡	Utrecht	2014
Workshop Bubbles and Droplets †	Wageningen	2015
IACIS *	Mainz (Germany)	2015

General

Teaching and supervising thesis students	Wageningen	2013
Scientific Writing	Wageningen	2013
Efficient Writing Strategies	Wageningen	2014
Voice and Presentation Skills Training	Wageningen	2014
Career Perspectives	Wageningen	2014

Optionals

Preparation of research proposal	Wageningen	2011
Research Methods	Wageningen	2012
PhD study tour **	USA	2013
Group meetings and colloquia *	Wageningen	2011-2015

Notes: ∗ oral presentation, † soundbite, ‡ poster presentation